Metabolomics using dissolution DNP-NMR

Frahm, Anne

Publication date:
2021

Document Version
Publisher's PDF, also known as Version of record

Technical University of Denmark

Anne B. Frahm

METABOLOMICS USING DISSOLUTION DNP-NMR

PhD Thesis, June 2021

DTU Health Tech
Department of Health Technology

Metabolomics using
dissolution DNP-NMR

PhD dissertation by:
Anne B. Frahm

Main Supervisor:
Mathilde Hauge Lerche, Senior researcher, DTU Health Technology

Co-supervisor:
Pernille Rose Jensen, Associate Professor, DTU Health Technology

DTU Health Technology
Center for Hyperpolarization in Magnetic Resonance
Technical University of Denmark
Ørsteds Plads 349, 1st floor
2800 Kgs. Lyngby
Denmark
Tel: +45 4525 3518

Project period:	January 2018 – June 2021
Class:	Public
Edition:	1st Edition
Remarks:	This thesis is submitted as partial fulfilment of the requirements for the degree of Doctor of Philosophy in Engineering at the Technical University of Denmark.

ABSTRACT

Dissolution Dynamic Nuclear Polarization (dDNP), a hyperpolarization technique, offers a way to dramatically enhance the signals in Nuclear Magnetic Resonance (NMR) experiments, by transferring spin polarization from electrons to nuclei like carbon-13 (^{13}C). With a more than 10.000 fold increase in the signal-to-noise ratio (SNR), on a very short time scale, dDNP has opened up the possibilities of directly monitoring metabolism in an organism. Such real-time metabolism is measured by injecting a hyperpolarized ^{13}C-labelled tracer into the subject and measuring the biochemical transformations through changes in hyperpolarized NMR signals as a function of time. The first real-time experiment performed clinically was done in 2013, studying tumours in prostate cancer patients. Since then, hundreds of real-time studies have been performed, elucidating metabolic flux in different types of organs and organisms.

Besides such real-time studies, with narrow focus on the immediate metabolic products of a tracer, the field of metabolomics studied through dDNP NMR remains relatively unexplored. Newer studies using hyperpolarized NMR on natural abundance ^{13}C samples from tomato extracts, show that the method is highly repeatable and yields easily interpretable spectra with the information necessary for biological classification.

The focus of this thesis is metabolomics performed by combining metabolic fingerprints obtained with dDNP NMR with the tracer based method of Stable Isotope Resolved Metabolomics (SIRM). In this combined methodology a biological system is injected with a ^{13}C labelled tracer and, after an incubation period, the resulting metabolic products are harvested to be analysed in a single dDNP enhanced NMR spectrum (dDNP SIRM fingerprint). This approach has been shown to have potential for insight into metabolic pathways in the cancer cell, useful for classification of cancer and for identification of the biomarkers of cancer.

Specifically, this thesis explores the potential for dDNP SIRM fingerprints to contain the information needed to classify between prostate cancer samples of different aggressivity. Two studies were conducted as part of this thesis, one on prostate cancer cell lines and one on tissue samples from Transgenic Adenocarcinoma of Mouse Prostate (TRAMP) mice. The process from production of the metabolite samples, to the acquisition of the dDNP NMR spectra and subsequent data analysis is described. Statistical analysis was performed with a combination of Random Forest (RF) and Support Vector Machines (SVM), to obtain both feature importance and classification. The goal in the statistical analysis was both to use the dDNP SIRM fingerprints to classify between samples of different cancer types, and to use the highly resolved data to pinpoint which metabolites support such a classification. The latter has the potential to enable selection and evaluation of potential biomarkers of aggressivity in prostate cancer.

RESUMÉ (IN DANISH)

Hyperpolariseringsteknikken dissolution Dynamic Nuclear Polarization (dDNP) giver en metode til drastisk at højne signalet i kernemagnetisk resonans (NMR) forsøg, ved overføring af spin-polarisering fra elektroner til atomkerner som carbon-13 (^{13}C). Med en mere end 10.000 folds forøgelse i ratioen mellem signal og støj (SNR), på en meget kort tidsskala, har dDNP åbnet muligheden for direkte at observere metabolismen i en organisme. Metabolisme er målt i realtid ved at injicere et hyperpolariseret, ^{13}C-mærket sporstof ind i forsøgsorganismen og derefter måle på de kemiske transformationer, via forandringer i hyperpolariserede NMR signaler som en funktion af tid. Det første kliniske forsøg i realtid blev udført i 2013, på tumorer i prostatakræftpatienter. Siden er hundredevis af forsøg i realtid blevet udført, og har givet indsigt i metabolsk flux i forskellige organer og organismer.

Udover eksperimenterne i realtid, med deres snævre fokus på de umiddelbare metabolske produkter af sporstoffet, har feltet af metabolomics studeret gennem dDNP NMR, været relativt uudforsket. Nyere studier af hyperpolariseret NMR med prøver fra tomatekstrakter med naturlig isotophyppighed af ^{13}C, viser at metoden er repeterbar i høj grad, og giver let tolkelige spektra, med den nødvendige information for biologisk klassificering.

Fokus i denne afhandling er på metabolomics udført med en kombination af metabolske "fingerprints" optaget med dDNP NMR, sammen med den sporstofbaserede metode Stable Isotope Resolved Metabolomics (SIRM). Med denne kombinerede metode, bliver et biologisk system injiceret med et ^{13}C-mærket sporstof og efter en inkubationsperiode, høstes de fremkomne metabolske produkter, som så analyseres med et enkelt, dDNP forstærket NMR spektrum (dDNP SIRM fingerprint). Denne tilgangsvinkel er blevet vist til at have potentiale til at give indsigt i de metabolske reaktionsveje i kræftceller, og være brugbar for klassifikation af kræft og identifikation af biomarkører for kræft.

Specifikt, undersøger denne afhandling dDNP SIRM fingerprints potentiale for at have den nødvendige information for klassification mellem prostatakræftprøver med forskellig aggresivitet. To studier blev udført som del af denne afhandling, et på cellelinjer af prostatakræft og et med vævsprøver fra Transgenic Adenocarcinoma of Mouse Prostrate (TRAMP) mus. Processen er beskrevet, fra produktionen af metabolske prøver, til optagelsen af dDNP NMR spektra og den viderede dataanalyse. Statistisk analyse blev udført med en kombination af Random Forest (RF) og Support Vector Machines (SVM), for opnå både rangering af de metabolske komponenter og en klassifikation af prøverne. Formålet med analysen var både at bruge dDNP SIRM fingerprints til at klassificere mellem prøver med forskellige kræfttyper, og at bruge den høje opløsning i dataen til at fastslå hvilke metabolitter der understøtter denne klassifikation. Sidstnævnte har potentialet til at gøre os i stand til at selektere og evaluere potentielle biomarkører af aggressivitet i prostatakræft.

PREFACE

This PhD thesis presents research conducted from January 2018 to May 2021 with affiliation to the Center for Hyperpolarization in Magnetic Resonance (HYPERMAG), at the department of Health Technology (originally at the department of Electrical Engineering until January 2019) of the Technical University of Denmark (DTU), in Kongens Lyngby, Denmark.

The PhD project period included a six month research stay at the MR Cancer group in the Department of Circulation and Medical Imaging, Faculty of Medicine and Health Sciences, at the Norwegian University of Science and Technology (NTNU), in Trondheim, Norway. The collaboration with NTNU facilitated a large part of the experimental work, presented in this thesis.

This thesis is submitted as partial fulfilment of the requirements for the degree of Doctor of Philosophy in Engineering at the Technical University of Denmark.

The research was partly funded by the Danish National Research Foundation (DNRF124). Mouse breeding, housing, and genotyping for the animal experiments was provided by the Comparative medicine Core Facility (CoMed), NTNU. CoMed is funded by the Faculty of Medicine at NTNU and Central Norway Regional Health Authority. Travel grants for the external research stay was awarded by the Danish Cancer Society (R235-A14222-19-S44), the Otto Mønsted foundation (19-70-0763) and the Knud Højgaard foundation (19-02-0683).

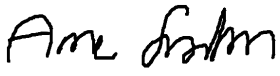

Anne Birk Frahm, 2021

LIST OF PUBLICATIONS

Paper 1

Anne Birk Frahm, Pernille Rose Jensen, Jan Henrik Ardenkjær-Larsen, Demet Yigit, and Mathilde Hauge Lerche. **Stable isotope resolved metabolomics classification of prostate cancer cells using hyperpolarized NMR data**. *Journal of Magnetic Resonance*, 316:106750, 2020.

Paper 2

Anne Birk Frahm, Deborah Hill, Sotirios Katsikis, Trygve Andreassen, Jan Henrik Ardenkjær-Larsen, Tone Frost Bathen, Siver Andreas Moestue, Pernille Rose Jensen, and Mathilde Hauge Lerche. **Classification and biomarker identification of prostate tissue from TRAMP mice with hyperpolarized 13C-SIRA** Manuscript submitted for publication to *Talanta*, 2021.

ACKNOWLEDGEMENTS

I want to thank my advisors, Senior Researcher Mathilde Hauge Lerche and Associate Professor Pernille Rose Jensen very much. I feel so privileged to have gotten the opportunity to do this project under your competent supervision. You have created a space for me to use and develop my skills as broadly as possible, while encouraging me to take ownership of the project and engage myself both in laboratory work, data analysis and dissemination. I feel like I have grown so much in the years we have worked together, both professionally and personally. Mathilde, every time I have felt frustrated or like a challenge was too great, you have always had time to talk it through with me, and afterwards I would always leave with the needed knowledge and a confidence that I could get it done. Pernille, your rational feed-back and guidance have been invaluable in keeping me focused and my research as thorough as possible. I admire you both immensely.

I want to thank all my colleagues at HYPERMAG. It has been fantastic to work with such skilled researchers, with such diverse areas of expertise as you guys. I especially want to mention Postdoc Sotirios Katsikis for your fantastic work with the construction of the transfer line between the magnets, I cannot understate the impact that has had on the quality of my data. Laboratory Manager Demet Yigit, you have my thanks for your excellent work with the cell lines. I want to thank Senior Researcher Magnus Karlsson for always being there when I had a problem in the lab, or just when I had questions. I want to thank Center Administrator Signe Rømer Holm and Laboratory Manager Anne Egholm Høgh for helping me with any administrative problem I have encountered and for keeping me well provided in tea. I also want mention the students I have worked with during their bachelor projects, Emma Lundsgaard, Amalia Matei and Helena Bugge Nicolaisen; it has been a pleasure learning alongside you. Finally my fantastic office-buddies PhD Student Christine Pepke Gunnarsson, PhD Student Tine Kliim Nydahl and Postdoc Ke-Chuan Wang; I have really enjoyed your company.

My secondment at NTNU in Trondheim, was a fantastic experience for me, both professionally and personally. I want to thank Professor Tone Frost Bathen for welcoming me into your group. Special thanks to Senior Engineer Deborah Hill for your fantastic work in planning and executing the TRAMP mouse study with me, and for all the good conversations we had while working in the lab; they are certainly one of the reasons I still miss Trondheim. I also want to thank Professor Siver Andreas Moestue for your great work with the mice and Senior Engineer Trygve Andreassen for your great work with the NMR recording. Lastly, I want to mention Senior Engineer Torill Eidhammer Sjøbakk, for helping me with all my practical questions and helping me settle in at NTNU.

Finally, a big thank you to my friends, family and loved ones, for keeping me fed and taking care of me. I am so lucky to have you in my life and I could not have done this work without you! I want to especially thank Adam Svane Pedersen, Michael Spange Olsen, Hans-Henrikk Kjøller and Jacob Bundgaard Nielsen, for keeping my mood up while I wrote the thesis and for helping me proofread. You guys are the best!

TABLE OF CONTENTS

LIST OF FIGURES

LIST OF TABLES

NOMENCLATURE

3PG	3-Phosphoglycerate
^{13}C	Carbon-13
ANOVA	Analysis Of Variance
C	Soft margin parameter for SVM analysis
dDNP	dissolution Dynamic Nuclear Polarization
DHAP	Dihydroxyacetone phosphate
DU-145	Prostate cancer cell line, aggressive
G3P	Glyceraldehyde 3-phosphate
HSQC	Heteronuclear Single Quantum Correlation
IP	Intraperitoneal
IV	Intravenous
KOH	Potassium hydroxide
LDA	Linear Discriminant Analysis
LNCaP	Prostate cancer cell line, early metastatic
NMR	Nuclear Magnetic Resonance
NOESY	Nuclear Overhauser Effect Spectroscopy
PC-DFA	Principal Components - Discriminant Function Analysis
PC3	Prostate cancer cell line, aggressive
PCA	Perchloric Acid
PCA	Principal Components Analysis
PEP	Phosphoenolpyruvate
PLS-DA	Partial Least Squares-Discriminant Analysis
PNT1a	Prostate cell line, immortalized
RF	Random Forest

SEM	Standard Error of the Mean
SIRM	Stable Isotope Resolve Metabolomics
SNR	Signal-to-Noise Ratio
SVM	Support Vector Machines
T1	Spin-Lattice relaxation time
TCA	Tricarboxylic acid cycle
TRAMP	Transgenic Adenocarcinoma of Mouse Prostate

1 INTRODUCTION

Real-time dissolution Dynamic Nuclear Polarization (dDNP) Nuclear Magnetic Resonance (NMR) has opened up the possibilities for directly measuring carbon metabolism non-invasively in living systems. By transferring spin polarization from electrons to nuclei like Carbon-13 (^{13}C), dDNP offers a way to dramatically enhance the ^{13}C signals (hyperpolarize) with a more than 10.000 fold increase in the signal-to-noise ratio (SNR) compared to thermal NMR but only on a very limited time scale.[1] Such hyperpolarization of a ^{13}C labelled tracer allows it to be injected into a biological system and measuring signal changes over time as the tracer undergo metabolic transformations, figure 1.1, A. The measurable metabolic changes can establish the presence or severity of disease and e.g enable identification of metabolic biomarkers of cancer. Real-time dDNP NMR experiments on cancer cells grown *in vitro* have successfully been performed to measure flux in the glycolysis,[2, 3] and to observe treatment response.[4] The first *in vivo* real-time dDNP NMR experiment performed clinically was done in 2013, studying tumours in prostate cancer patients[5]. Since then, hundreds of real-time studies have been performed, elucidating metabolic flux in different tissues.[6]

The classification of prostate cancer in terms of its aggressivity, has been a focus in several dDNP NMR studies.[7–9] Over-diagnosis of prostate cancer is suspected to be a vast problem, with a rate estimated to be up to 67%, depending on the population and method used for calculation.[10] With over-diagnosis, patients undergo unnecessary treatments, which can lower life spans and life quality, as well as be costly for society. A better understanding of metabolic changes with disease progression and precise measurement methods of such metabolic change, both when normal prostate tissue grows cancerous and when the cancerous tissue grows malignant would be valuable. With such knowledge and tools at hand, we could stop operating on men who only have low risk of their cancer developing to become life threatening.

A main drawback of the real-time dDNP NMR method, is that the sensitivity boost from the hyperpolarization is short lived. The experiment has to take place on a time scale ~ 1 minute, which severely limits the reactions that can be monitored. For a ^{13}C tracer to be useful it has to have a long relaxation time, to allow measurements before the signal has disappeared, and a high cellular up-take and metabolism rate to allow metabolic products to reach measurable quantities during the experiment. 1-^{13}C labelled Pyruvate is currently the most widely used tracer,[11] and the only compound approved for clinical use. Pyruvate is attractive as a real-time metabolic tracer, due to both its biological relevance in cancer metabolism and its longer relaxation time, compared to compounds such as glucose.[12] Thus, real-time dDNP NMR metabolic studies *in vivo* are limited to a few tracers, and a narrow focus on the immediate metabolic products of the tracer.

The scope of the dDNP NMR method has recently been broadened, with the method being evaluated for its use in the field of metabolomics. Studies on natural abundance carbon, have showed that the method is highly repeatable and yields easily interpretable spectra with the

information available needed for biological classification.[13–15] Further to this, we have developed an assay in which we combine Stable Isotope Resolved Metabolomics (SIRM) with dDNP enhanced NMR, to gain a single snap-shot of the metabolites produced in a fixed time frame.[16]. With this combined dDNP SIRM fingerprint method, the time restraints of the of the real-time experiment is gone. It is in this assay possible to choose tracers with shorter relaxation times and to use a longer incubation period to allow for a broader range of metabolic products to be measured. This method, which is the method explored and developed through this thesis, can be described as a reversal of the real-time dDNP experiment, as illustrated in 1.1, B.

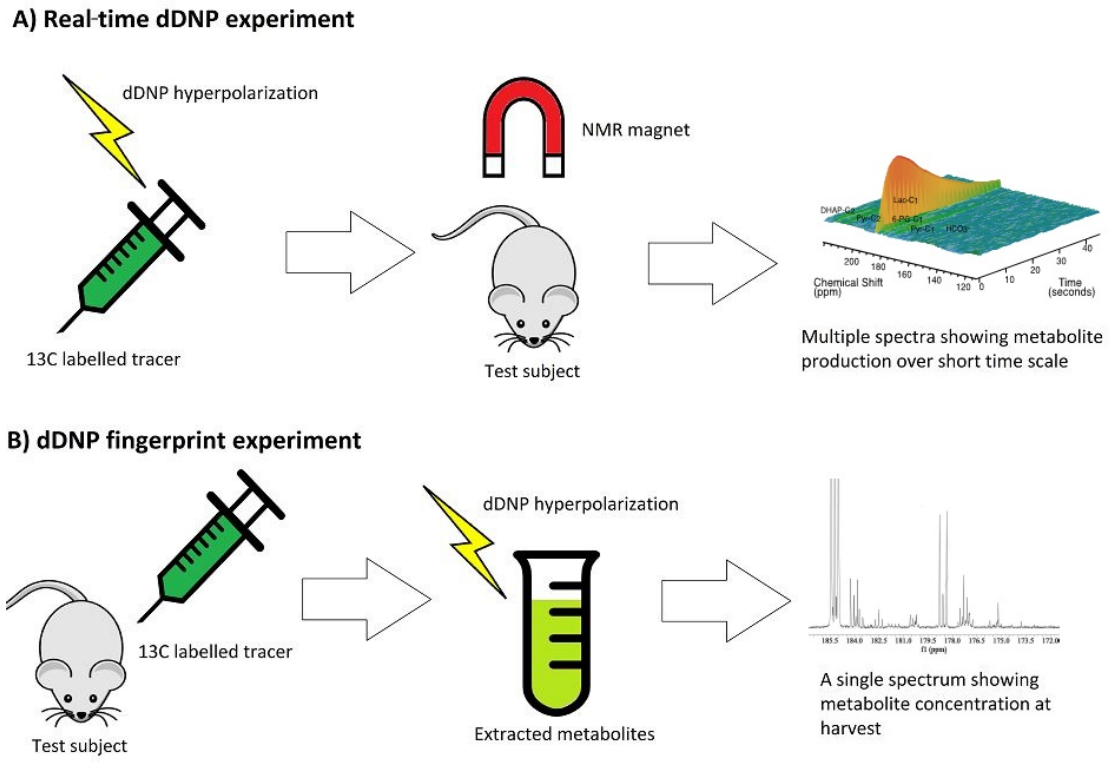

Figure 1.1: An illustration of the two different approaches to a tracer based dDNP study. A: The real-time dDNP experiment where the ^{13}C labelled tracer is hyperpolarized, injected into the system and metabolite production is measured over time. B: The dDNP fingerprint experiment, where the ^{13}C labelled tracer is injected into the system, and metabolites produced are then harvested and hyperpolarized.

The goal with the work presented in this thesis, has been to develop a methodology capable of identifying potential metabolic biomarkers of aggressivity in prostate cancer, on the basis of the dDNP SIRM fingerprint assay and further development of if. We wanted to construct a methodology that would enable the discovery of metabolic compounds and reactions of interest in further real-time dDNP studies of clinical relevance for prostate cancer diagnosis. This was done specifically by measuring the broadest possible range of tracer produced metabolites in dDNP SIRM fngerprints, and utilizing machine learning methods to compare samples of different aggressivity.

1.1 THESIS OVERVIEW

This thesis concerns both the experimental part of producing the dDNP SIRM fingerprint spectra from the living system and the analysis of the data, particularly how a combination of Random Forest (RF) and Support Vector Machines (SVM) can be useful for feature ranking and classification. The thesis is structured into four main chapters:

- Chapter 2 serves to provide the prerequisite knowledge of the main subjects of the thesis: Metabolomics with a focus on NMR and SIRM; dDNP; and some of the most relevant machine learning algorithms to analyse metabolomics data.
- Chapter 3 concerns the performed experimental work behind the two studies in this thesis. It includes the production of metabolite extracts from isolated cells and from tissue harvested from mice, and the acquisition of NMR spectra, to be analysed in the later chapters.
- Chapter 4 contains a deeper discussion of the analysis and results on the cell line study, published in the paper included in appendix A. With a particular emphasis on the set-up of the RF+SVM method for feature ranking and classification.
- Chapter 5 is similarly a deeper discussion of the data and results of the mouse tissue study, presented in the manuscript included in appendix B. This manuscript is submitted to and in review in the journal Talanta. In this chapter the limits of the RF+SVM method is explored and it is discussed how to best construct a data matrix to gain the most interpretable results.

2 BACKGROUND

This chapter is an introduction to the research topics relevant for this thesis. Metabolomics is described, with a focus on NMR metabomolics. A fundamental understanding of NMR is considered a prerequisite for this thesis, and will not be covered. The principles behind dDNP hyperpolarization is introduced, and their role in metabolomics is discussed. Finally benefits and drawbacks of selected classification algorithms most relevant for and commonly used in metabolomics is discussed.

2.1 METABOLOMICS

Metabolomics, often used interchangeably with metabonomics,[17, 18] is the complete study of the metabolites in a biological system - metabolites being the small molecules involved in the metabolism, as intermediates or end products. Compared with other -omics disciplines, metabolomics is more closely related to biochemical activity and biological phenotype, as the metabolome is constantly responding to environmental factors. In contrast the genome is relatively static for the organism and the transcriptome and proteome are changing on a slower scale and are subject to post-translational modification.[19] In this way, metabolomics is down-stream to genomics, transcriptomics and proteomics, as the metabolites of a system are a function of both the genetics of the system, its protein activity and its current environment.[20]

Metabolic studies are often set up as either targeted or untargeted.[21] In a targeted study, specific predefined metabolites are investigated, to challenge a specific hypothesis. The targeted approach is useful for intervention studies, where a hypothesis is formed on how a drug studied might affects certain metabolites in a specific pathway. Untargeted metabolomics aims to study as many metabolites as can be measured at once. This is a more holistic approach to get information about the system, to help build hypotheses and to connect phenotypes to genotypes.[19] An additional approach, the semi-targeted analysis, involves a defined set of metabolites, but a less defined hypothesis, allowing for description of metabolic pathways and the discovery of new biomarkers of disease.[22]

Nuclear Magnetic Resonance (NMR) spectroscopy, is one of the principal analytic techniques used for metabolomics.[23, 24] In the NMR experiment, the sample is placed in a strong magnetic field and the nuclear property of spin is utilised to make the nucleus absorb and then emit a radio frequency radiation. This emitted frequency varies depending on the local chemical environment of the nucleus, giving rise to a frequency spectrum in which metabolites can be identified.[25] Compared with mass spectrometry, the other main technique for studying metabolomics, NMR have the benefit of high reproducibility and quantitativeness, while being generally non-selective in metabolite detection.[23]

In a so-called NMR metabolic fingerprint, the current metabolic state of the studied system,

is captured in a single NMR spectrum. The signals recorded in this "snapshot" can be analysed using multivariate statistics, to describe or classify groups in the metabolic data, which can be useful for screening between healthy and diseased subjects for instance.[26] 1D-proton NMR spectroscopy is frequently used for metabolic fingerprinting. Proton NMR has the benefit of high signal intensity compared to NMR of other nuclei, and as protons are found in almost all possible metabolites, this gives proton NMR a wide scope. 1D-proton NMR is efficient as it is highly automatable and reliable, and can be recorded in minutes, allowing for a high through-put of samples.[23] Different pulse sequences for generating the 1D-proton NMR spectra exists, but one widely used for metabolic fingerprinting is the Nuclear Overhauser Effect Spectroscopy (NOESY) sequence. The NOESY contains an easily applied, high quality water suppression sequence, which keeps the spectrum from being overpowered by the signal from the solvent, which otherwise will be much larger than the metabolite signals of interest.[27]

A great challenge with the use of 1D-proton NMR for metabolomics is spectral overlap. With an abundance of signals and a narrow spectral dispersion, many metabolite signals will be overlapping, making it difficult to identify and quantify metabolites from the spectra. An alternative could be ^{13}C-NMR. The spectral dispersion for ^{13}C is 20 times larger compared to that of the proton spectrum, and carbon is, like protons, also universally present in metabolites.[23, 28] The drawbacks of ^{13}C-NMR is its much lower sensitivity, compared to proton-NMR, exacerbated by the fact that only 1.1% of natural abundance carbon is in the form of ^{13}C.[28] 2D techniques like Heteronuclear Single Quantum Correlation Spectroscopy (HSQC) does exist, where the ^{13}C signal is detected through bonds to proton, thus benefiting from the greater sensitivity of proton NMR. These techniques are most often used for signal assignment, as running high resolution HSQC is more time extensive.[23]

2.1.1 *Stable Isotope Resolved Metabolomics*

Measuring and comparing metabolite concentrations in static metabolomic fingerprints, does not give a complete picture of the metabolic state of the studied system. The organism controls metabolic pool sizes to maintain homoeostasis, as larger deviations could result in lethal changes in its temperature or blood composition for instance.[29, 30] Thus an increase of production of metabolite A, may not necessarily lead to a measurable increase in the concentration of A, if a pathway downstream from A is also simultaneously up-regulated. On the flip side, if we do see a difference in concentration of metabolite A between two samples, we might not be able to infer anything on the biological change leading to the difference, as the metabolic pathways are inter-connectively linked with the metabolites utilized in a vast array of processes.

Stable Isotope Resolved Metabolomics (SIRM) is a method for indirectly tracking metabolic pathways and measuring the turn-over rate of metabolites (the flux). In SIRM, a tracer labelled with an NMR active isotope, like ^{13}C is injected into the studied system, and measurements of the metabolic products are then made, either over time or in a fingerprint after a harvest period.[31] Multiple measurements over a short time provides information to determine flux, while incubation until after metabolic steady state has been reached gives information about pathway activity.[32] SIRM has the benefits of being non-toxic, and it utilizes the low natural abundance of ^{13}C to its

favour, as this means that the "background" metabolites, already present in the system before the injection of the tracer, will provide 100 times less signal strength compared to a product of the tracer in the same concentration. NMR analysis works well with SIRM, as different isotopomers gives rise to different spin-spin couplings in the NMR spectrum, making it possible to utilize strategic labelling schemes to elucidate specific metabolic pathways.[33]

As cells undergo metabolic reprogramming, SIRM has been found to be an excellent tool for identifying biomarkers of cancer, by giving insight into the changes in energy metabolism.[34] One of the most generally observed hall-marks of the cancer cell is the Warburg-effect. Here glucose uptake is increased, but the normal mitochondrial break down of glucose is down-regulated in favour of an increased glycolysis, even in the presence of oxygen.[35] This effect is not always that apparent. In prostate cancer for instance, it has been observed that the Warburg-effect does not set in before the cancer reaches a late stage. In contrast to most other healthy tissue, the prostate normally depend on glycolysis for energy production, and when it begins to grow cancerous it typically decreases the glycolysis and increases the mitochondrial energy production. Only in the aggressive and late stage, it turns back and rely again on a drastically unregulated glycolysis for energy production.[36] Many of the specific metabolic changes related to prostate cancer are still not well understood.[37] Research utilizing SIRM can aid in elucidating pathway changes and identifying therapeutic targets.[38]

2.2 DISSOLUTION DYNAMIC NUCLEAR POLARIZATION

2.2.1 *The NMR sensitivity problem*

NMR suffer from relatively low sensitivity compared to mass spectrometry, the other main method used for metabolomics.[39] This, in part, stems from the fact that a spin-1/2 nucleus (like ^{1}H or ^{13}C) can be in two different states of spin (denoted as up or down), and it is only the difference in spin populations that will give rise to a detectable signal. At equilibrium the ratio between the spin populations is given by the Boltzmann distribution:

$$\frac{N_{up}}{N_{down}} = e^{-\Delta E/k_B T} \quad \text{with} \quad \Delta E = \hbar \cdot \gamma B_0 \tag{2.1}$$

Where k_B is the Boltzmann constant, T is the temperature, $\hbar$ is the reduced Planck constant, γ is the gyromagnetic ratio, specific for the nucleus, and B_0 is the strength of the magnetic field.[40, 41] From this, the polarization is defined as:[42]

$$P = \frac{N_{up} - N_{down}}{N_{up} + N_{down}} = tanh\left(\frac{\Delta E}{2k_B T}\right) \tag{2.2}$$

The polarization can be increased by "brute force" by increasing the B_0 magnetic field or lowering the temperature. Some nuclei have a higher (more favourable) γ than others; γ for ^{1}H is for instance four times larger than γ for ^{13}C. For ^{13}C in a 9.4 T magnet at 298 K (room temperature), the equilibrium ratio of spin populations comes out to 99.9984% meaning that only 16 out of 2 million nuclei gives rise to detectable signal. The same calculation made for a 11.7 T

magnet gives a 99.9979% ratio; we now get a signal from 21 out of the 2 million nuclei - increasing field strength does help, but a lot of power is needed for relative small improvements.

The measures attempting to raise this polarization fraction are collectively known as hyperpolarization techniques. Of these techniques, dissolution Dynamic Nuclear Polarization (dDNP) have been described as the most versatile.[43]

2.2.2 *DNP*

The concept of Dynamic Nuclear Polarization(DNP) was first described by Overhauser in 1953,[44] and proven to work during the late nineteen fifties.[45] DNP achieves hyperpolarization by the transfer of polarization from electrons to nuclei.

As seen in the plot to the left in figure 2.1, the polarization equilibrium of all particles goes to unity as the temperature approaches zero, but this happens at much higher temperature for electrons, compared to ^{13}C and protons. At the temperature (1.4 K) and field strength (3.3 T) where the polarizer used in the studies included in this thesis is operating (marked in the plot with the vertical line), the equilibrium polarization of electrons is at 92.3%, while its only 0.24% and 0.06% for protons and ^{13}C respectively.

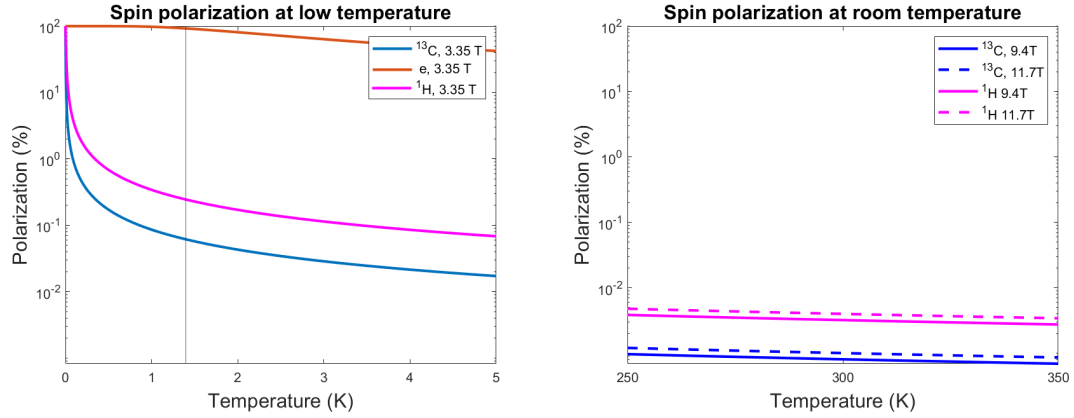

Figure 2.1: Semi-log plots showing the relationship between temperature and polarization equilibrium. To the left: Polarization of electrons, ^{13}C and protons in a 3.35 T polarizer near absolute zero temperature. To the right: Equilibrium polarization of ^{13}C nuclei and protons, at room temperature, shown for a 9.4 T and a 11.7 T magnet.

In preparation for the DNP process, a sample is mixed with a polarization medium. This medium should contain both a free radical, as a source of electrons from which polarization can be transferred, and a glassing agent, like glycerol, that ensures a non-clustering distribution of the radical in the sample when frozen.[46] The addition of a low concentration of a gadolinium containing complex to the polarization medium, further enhances the polarization process, by shortening the solid state relaxation of the electrons.[47]

The sample mixed with the polarization medium, is placed in the polarizer, were the magnetic field and the low temperature ensures the high equilibrium polarization of the electrons. The spin polarization transfer from electrons to nuclei is then induced by microwave irradiation with

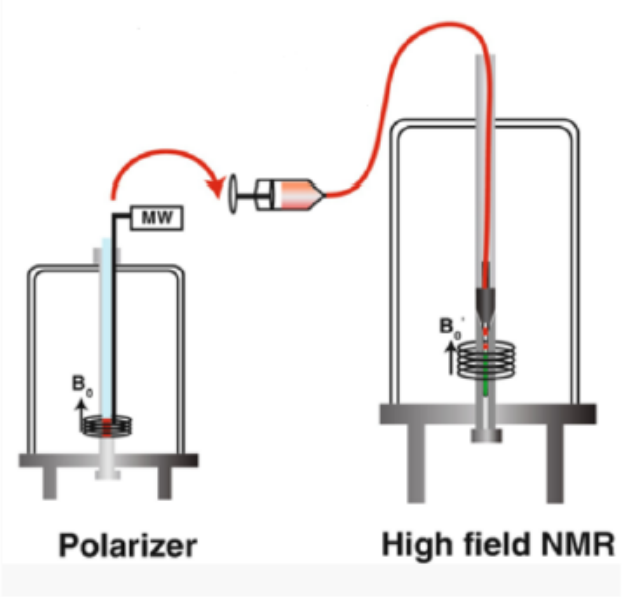

Figure 2.2: Illustration of the polarizer and NMR magnet set-up with transfer line. Illustrations reproduced from Lerche et al.[46] with permission.

a frequency that induces transitions in the spin state of the electrons, causing nearby nuclei to also transition. Over time, the altered spin states diffuse through the nuclei in the sample and the electron returns to their high equilibrium polarization, ready for the next microwave surge to again transfer the spin state to the nuclei. In this way, the polarization of the nuclei is enhanced over time, until a plateau of maximum polarization is reached.[48]

2.2.3 *Dissolution DNP*

In 2003 Ardenkjær-Larsen et al.[1] published the invention of dissolution DNP: A method to rapidly dissolve the frozen, hyperpolarized sample, while conserving the gained polarization. With this, dDNP can be used with liquid-state NMR opening up the possibilities of a broad range of applications. An illustration of the dDNP set up is shown in Figure 2.2: After the DNP process has taken place in the core of the polarizer, a heated dissolution liquid is injected to dissolve the sample, which is then collected and transferred to the NMR spectrometer.

With dDNP a gain in signal strength of four orders of magnitudes can be achieved, but as soon as the dissolution starts and the sample is removed from the polarizer, a relaxation process sets in that eventually brings the polarization level back to the non-hyperpolarized level. Figure 2.1 on the right shows the low equilibrium polarization levels of ^{13}C and protons in the NMR magnet where the signal acquisition takes place at room temperature. How quickly the polarization reaches equilibrium, depends on the chemical environment of the nucleus and on magnetic effects from its surroundings. This relaxation is described through the spin-lattice relaxation time constant $T1$. $T1$ varies for ^{13}C on a scale of ~1 minute for a carbonyl carbon, down to a few seconds for methyl carbon.[1] This also means that dDNP NMR is not directly quantitative, as

signals from different molecules (and different nuclei in the same molecules) will have different relaxation constants and thus have a different degree of polarization at the time of recording, due to transfer time between polarizer and NMR spectrometer.

2.3 MACHINE LEARNING FOR CLASSIFICATION IN METABOLOMICS

When studying the production of a small number of metabolites, the relationship between a metabolite and classes of the data (such as healthy/diseased or cell line of origin) can easily be examined through univariate statistical tools, such as t-test or Analysis Of Variance (ANOVA). But as metabolomic datasets can contain tens or even hundreds of features, in the form of specific measured metabolite concentration in the targeted studies or as binned spectral data in untargeted studies, such statistical tools become insufficient for examining the complex relationships between the features and how they relate to classification.

When working with metabolic fingerprints, machine learning can be incredibly useful both for classifying data points and for revealing the features in the data that support the classification. Since datasets often suffer from "the curse of dimensionality" where more features than data points exist in the dataset, the choice of a robust, cross-validated classification algorithm is essential to ensure a non-overfitted model.[49]

2.3.1 *Partial Least-Squares Discriminant Analysis*

Partial Least-Squares Discriminant Analysis (PLS-DA) is one of the most widely used machine learning models, for discriminating between classes in metabolomics.[50] PLS-DA, works as an extension on a supervised regression algorithm, where a linear relationship between the features in the data and the target output variable (class membership) is assumed. This relationship is reduced to a set of latent variables, built from the original variables.[51] There are many benefits of PLS-DA as a tool for analysing metabolomic data. This algorithm handles noisy data and data with a high collinearity between features well. It produces both a classification and a variable ranking, with easily interpretable visualizations, and it is easy to implement, with only one variable (the number of included latent variables) to be optimized. Also, the popularity of PLS-DA for metabolomics has lead it to be included in many statistical packages, further making it a household algorithm.[52]

Figure 2.3 shows plots from a PLS-DA performed on artificial data. The data was created with n = 150 data points, and three classes (named "blue", "purple" and "red") each assigned 50 data points. The dataset had eight features, with values randomly generated from Gaussian distributions. Four of the features (named "a" through "d") were signal features. These were generated with different means and standard deviation for each of the classes. Four features ("e" through "h") were noise features, made from the same distribution for all classes. The score plot to the left in figure 2.3, shows how the first two PLS-DA constructed components separates the "purple" class of points well from the rest, whereas there is some overlap between the "red" and "blue" classes. The loading plots to the right shows, with the high absolute values assigned to the first four features, that the algorithm has succeeded in recognising that these features contain

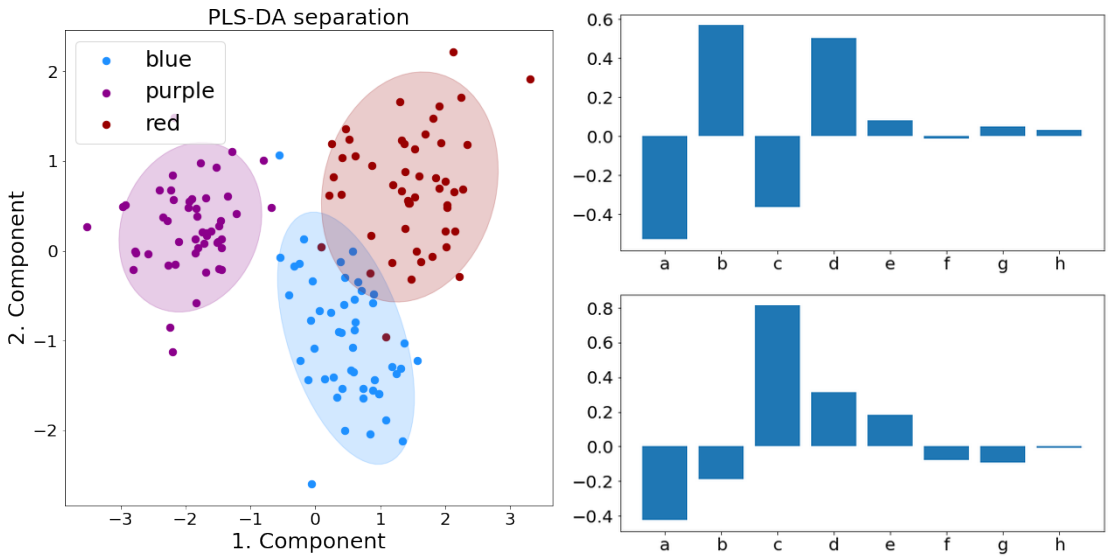

Figure 2.3: PLS-DA results of a classification of artificial data. On the left: Score plot with the first two components plotted against each other, illustrating the separation of the data points. Coloured ellipses show 2 standard deviations of each point cloud. On the right: Loading plots for each of the components (1. on top, second on bottom), illustrating their composition from the features of the data.

the signal relevant for the separation. The classification success rate, with leave-one-out cross validation was 94.7%.

However, despite the attractive qualities, PLS-DA analysis for metabolomics has attracted criticism.[52, 53] PLS-DA requires rigorous validation to not overfit, and as this requires a large amount of data points, such validation is often not applied diligently.[50, 54] The score plots, illustrating good separation between classes in data, can be misleading as similar results can be obtained on randomized data.[55] Especially, when working on a dataset with a reduced number of features, PLS-DA is shown to underperform compared to other machine learning algorithms, making it less suited for variable ranking.[56, 57] PLS-DA requires features to be on the same scale to be unbiased. This can be a problem in studies using binned spectral data, where scaling is either not used or where alternative scaling methods to unit-variance scaling are used, to avoid scaling up noise. In these cases PLS-DA is biased towards the larger features.[58]

2.3.2 *Principal Component-Discriminant Function Analysis*

A lesser known alternative to PLS-DA, which offers some of the same benefits, is the algorithm Principal Component-Discriminant Function Analysis (PC-DFA). DFA (also known as Canonical Variates Analysis or Linear Discriminant Analysis (LDA)), is a supervised algorithm that generates a vector in the feature-space of a dataset, which maximizes between-class variance, while minimizing within-class variance, for a specified target class.[59] LDA by itself is very sensitive to the collinearity that exists between features in metabolomic data. To eliminate this source of overfitting, it is combined with a Principal Component Analysis (PCA), forming the full

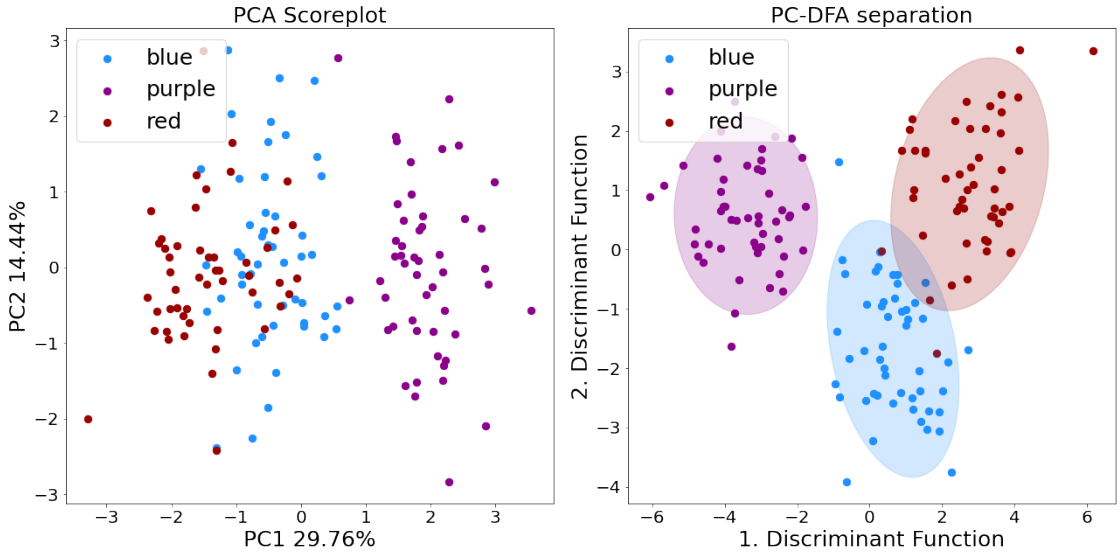

Figure 2.4: PC-DFA results of a classification of artificial data. On the left: Score plot of the first two components of the unsupervised PCA, plotted against each other. To the right: Score plot of the two discriminant functions generated from the PCA components.

PC-DFA.[60]

PCA is in itself an unsupervised, pattern recognition technique, widely used in metabolomics for dimension reduction and data visualization.[58] PCA works by transforming the original features of the data into in a set of new features - the principal components. In the new, transformed set of data the first component is constructed to capture as much of the variance of the data as possible, and the the second component is constructed to be orthonormal to the first while capturing as much of the remaining variance as possible and so on.[61] As the last components often will contain only a slim fraction of the full variance in data, these can be discarded in a reduced set of features.

Figure 2.4 shows the results of a PC-DFA analysis applied to the artificially generated data used also in the PLS-DA illustration above. The PCA score plot shows that the component, which accounts for 29.76% of the variance in the data, separates the "purple" data points, from the rest, even though the algorithm is unsupervised and no information on class is given at this points. The "red" and "blue" data points are tangled together in the PCA plot, but separates with a little overlap in the plot of PC-DFA discriminant functions. The leave-one-out cross-validated success rate of this classification was 96.7%.

PC-DFA has some of the same benefits as PLS-DA: It handles noisy data well, and it is easy to implement. The only parameter to be optimized is the number of PCA components that should be included in the LDA. For multiclass problems, the first two discriminant functions can be plotted against each other, to give a good illustration of success of separation. PC-DFA has been shown to perform as well as a classifier as PLS-DA, and outperform it in some cases, especially when the feature set is small. [53, 52]

A drawback of PC-DFA is that it is a parametric function, meaning that it is only completely

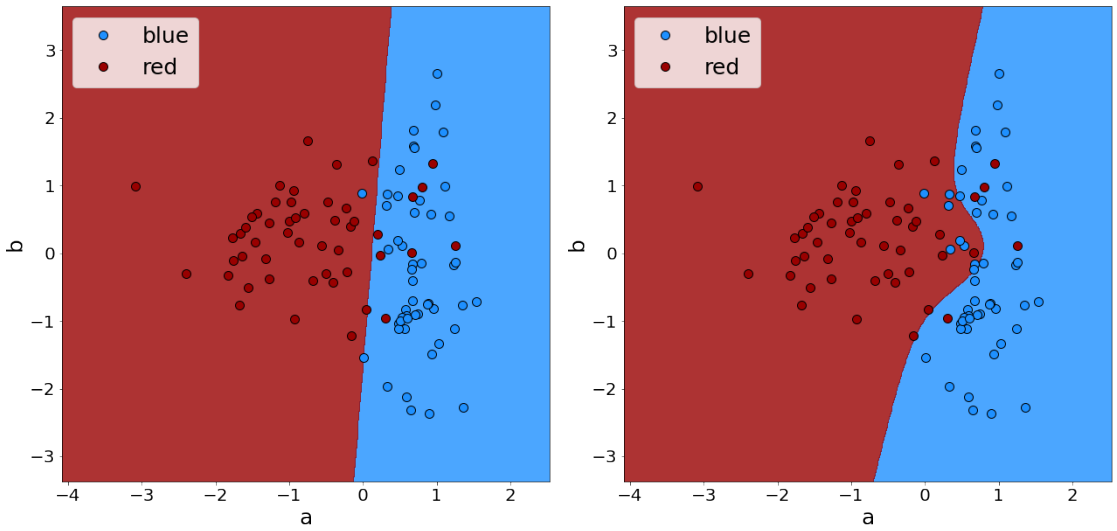

Figure 2.5: SVM separations of artificial data, plotted for the features "a" and "b". Coloured background shows how the algorithm would classify a point with those values for the two features. On the left: A linear classification. To the right: A separation with a polynomial kernel.

reliable when its inherent assumption that the data is Gaussian distributed is met. This means that additional data transformations can be necessary to apply before the analysis. Since PC-DFA generates a number of discriminant functions, always one less than the number of classes it is separating, this means that there is no straight-forward visualization for binary classification problems with PC-DFA.[52]

2.3.3 *Support Vector Machines*

Support Vector Machines (SVM) is a non-parametric algorithm, where a hyperplane is constructed in feature-space of the data, to best separate the specified classes. The separating plane is adjusted to maximize the margins between the plane and the groups of data points and a soft margin parameter (C) is introduced to allow some misclassification when training, for the benefit of a simpler non-overfitted model. SVM can be based on different kernel functions, to allow separations based on more complicated models than just a linear one.[62]

Figure 2.5 shows examples of SVM separation made on the "red" and "blue" data points from the artificial dataset described above. The plot for linear separation shows how the algorithm has optimized a straight line through the "a"-"b" feature space, to best make the binary separation between the classes. The separation made with the polynomial kernel, uses linear and higher level combinations of the features to create the separation, creating the curved line in the feature space. Of course, these 2-dimensional plots can only show the separation based on values in two of the eight features in the full dataset. The leave-one-out cross-validated success rate (using all features) was 97% for linear kernel and 94% for the polynomial. It makes sense that the polynomial kernel would overfit for this dataset; since the data was specifically created to be linearly separable, and thus no higher order relationship between the features should exist.

SVM has been found to outperform LDA in most cases,[63] and PLS-DA both in terms of prediction accuracy and ability to select features, when its run together with feature selection algorithms.[64, 57] It is a robust classifier, less likely to overfit compared with others.[52]

The drawbacks of SVM are, that its parameters are not predefined: The kernel function and value of C has to be optimized for the specific test, along with other parameters for non-linear kernels. While the separation made by SVM can be plotted if it is based on only two features (or three if plotted in a 3D diagram), visualization for higher dimensions is not possible, as no feature reduction is applied. The important features in a classification made with SVM is not directly measurable, why additional techniques are needed if a feature ranking is desired. Also: SVM was designed to handle binary classification problems, and while solutions like testing the classes one-against-all (thereby viewing multiclass problems as a series of binary problems), these requires additional time and work.[52]

2.3.4 *Random Forest*

Random Forest (RF), is a decision tree-based classification algorithm, where the final classification model is based on the combined prediction of a large number of constructed classification trees. Each tree is built on the basis of how to sort a selection of samples in the data, randomly chosen from the full training data, with replacement. Each node in a tree sorts the data based on a small subset of the variables in the data, which are randomly selected from the full feature set. The criterion for how to split the data at each node, can be made on a principle of minimizing entropy with each split, or by minimizing gini impurity, which is a computational effective measure of entropy.[65] The prediction success rate can be measured from testing on the data points not included in building the tree, this is termed the out-of-bag score.[66] The process of building each tree on part of the data and testing on the rest, essentially works as an internal cross-validation and the repeated process of building trees, means that the algorithm converges into a robust model unlikely to overfit.[67]

Figure 2.6 shows an example of one of the decision trees made as part of the RF algorithm, for classification of the artificial dataset described above. For simplicity, the illustrative tree was made using only 12 data points, four in each class. For each node in the tree, the algorithm chooses from a subset of the features, and makes a split in the features that results in the lowest possible gini-measurement in the two resulting groups. In the first node on the graph the group with all points in the data (gini = 0.667) could be split using feature "d", in a way that the "purple" data points were separated in one node (gini = 0) and one node with the non-purple data points (gini = 0.5), which then in turn could be separated further using other features. A full RF analysis on the full dataset, built with 500 trees, had a 94.7% classification success rate, using the out-of-bag score.

RF is non-parametric and unlike all other methods discussed here, requires no scaling, meaning that the preprocessing of data before the application of RF is minimal. The main drawbacks of RF is that no visualizations are possible. Single trees can be shown, but this does not give an overview of the whole forest, and in some cases parameters such as tree-depth or minimum splits at each node have to be limited to avoid overfitting.[52]

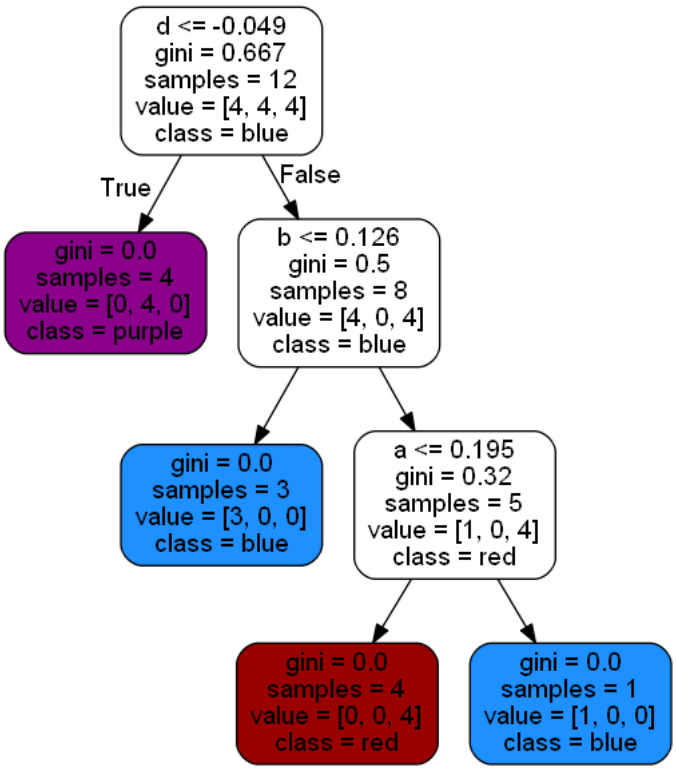

Figure 2.6: Graph of a single decision tree, made with 12 data points of artificially created data.

For spectral data specifically, PLS-DA has been shown to outperform RF in terms of success rate for classification, but RF is much better at feature ranking.[65] Combined with the fact that SVM classification benefits from feature reduction,[68] this means that a combination of RF for feature reduction before applying SVM for classification on a reduced dataset, could give better results than each of the algorithms alone.[68–71]

DEVELOPMENT OF THE dDNP SIRM ASSAY: FROM LIVING SYSTEM TO NMR SPECTRUM

3

This chapter is a walk-through of the experimental developments and procedures involved in obtaining the dDNP SIRM fingerprint spectra from cell and tissue extracts, as they have been used in the studies in this thesis (chapters 4 and 5). Both the handling of in vitro cell lines and in vivo TRAMP mice is described and discussed, detailing tracer incubation, metabolite harvest and the dDNP NMR experiment. Further details and discussion on the background of the cell line experiment and its results can be found in chapter 4 and on the mouse experiment in chapter 5. The chapter ends with a description and discussion of the data obtained for each study.

The basic steps of the dDNP SIRM fingerprint experiment, encompasses the introduction of ^{13}C-labelled tracer into the biological system of interest, the extraction of the metabolic products after a period of incubation, and then the dDNP NMR recording. The obtained spectra can be analysed to gain insight into which metabolites were produced from the tracer, and machine learning can be applied for classification of groups in the data. An overview of the protocol for the full experiment is shown in Figure 3.1.

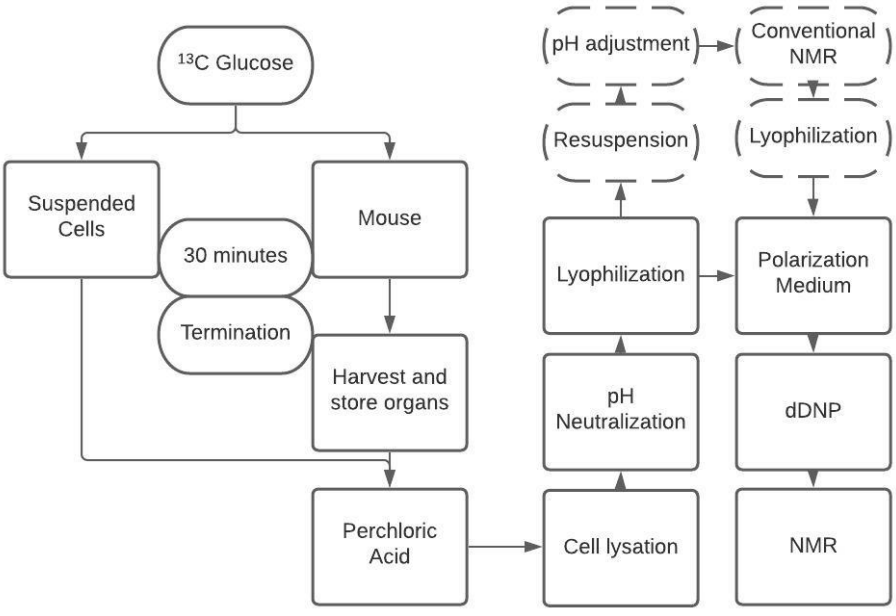

Figure 3.1: Flow chart illustrating the main points of the dDNP SIRM fingerprint experiment. The procedure from the injection of the tracer up to the dDNP process, as it was performed in the described studies. The stippled boxes, show the steps that were only done in the mouse tissue experiment.

Optimizations have to be made for the incubation, harvest and NMR procedures, to secure the most robust data, so that the relevant biological process - in our case, the metabolism in prostate cancers of differing aggressivity - can be explored with minimal interference from other biological or technical factors. What is most beneficial will of course change, depending on the system and the exact metabolic process to be explored.

3.1 METABOLISM UNDER INCUBATION

At the start of the SIRM experiment, when the labelled tracer is introduced to the cells or animal, ideally, it should be instantaneously distributed in the system. Then after incubation, the metabolism should be instantly quenched, to make for the most repeatable and precise fingerprint of the metabolic production during the incubation. With cell line experiments, this ideal is easy to approach, since the tracer can reach each cell by diffusion. In animal studies it becomes more difficult, as the tracer has to be distributed by the animals blood system and organs. Also, cells growing in vitro can be washed, removing external metabolites already produced by the system before introducing the tracer, whereas in the animal, a larger background of metabolites will be present. The type of tracer has to be matched with the incubation time and the method of harvesting the metabolic products, to insure that relevant metabolites are obtained in quantities measurable with dDNP.

3.1.1 *Choice of tracer*

When choosing a tracer to inject into our model systems, our primary considerations were that the metabolism of the chosen tracer should be expected to change as a cell grows more cancerous and that the tracer and its products will be measurable with dDNP NMR.

As we wanted to study the changes in energy metabolism described by the Warburg effect,[35] where cancer cells increase their glucose uptake and the tricarboxylic acid (TCA) cycle is inhibited in favour of anaerobic glycolysis; glucose was a natural tracer choice. Glucose is the first substrate in the glycolysis, and metabolic products from glucose is used in both the TCA and the pentose phosphate pathway. Products from a glucose tracer can therefore report on cancer related changes to many different pathways, and glucose is therefore widely used for metabolic flux analysis.[72] To get the largest range of metabolic products, we therefore chose to use full labelled ^{13}C-glucose as our tracer.

In the cell-line study we used fully deuterated ^{13}C-glucose. We wanted to preserve as much polarization during the transfer as possible and ^{13}C nuclei bound to deuterium have a longer relaxation time, compared to nuclei bound to protons.[12] For the mouse study, we also wanted to acquire proton NMR spectra from the samples, so we chose protonated ^{13}C-glucose as the tracer.

3.1.2 *Cell incubation*

When working with cell lines, the incubation and metabolic quenching were relatively easy: The cells were grown to 90% confluence in culture flasks. Before collection, the cells were washed

with a phosphate buffer, to remove the growth medium and dead cells. Cells were then harvested by trypsinization, spun down and resuspended in phosphate buffer in a concentration of either 20 or 40 million cells/mL. Each sample was made with 500 μL of cell suspension for at total of either 10 or 20 million living cells for the incubation.

The fully deuterated ^{13}C-glucose tracer was added to each sample, and the cells metabolized the glucose for 30 minutes while kept at 37 °C on a shaking thermostat to allow for the most ideal conditions for the cell metabolism. From our previously published work[16], we knew that 30 minutes of incubation time gives rise to a metabolic fingerprint with multiple quantifiable metabolites. In this previous study, the rate of lactate production was found to change significantly between the first minute of incubation and the full 30 minutes,[16] and we wanted to capture a image of the production more akin to the steady state.[72]

A longer incubation time could have been considered, but as the cells do not thrive suspended in the buffer and without an oxygen supply, we did not want to take the risk of having the metabolism change during the experiment, to that of a distressed system. As the glycolysis is a fast responding process, an incubation that is as short as possible, with the metabolic products in measurable quantities is desirable.

After precisely 30 minutes, ice cold perchloric acid (PCA) was added to the samples, which were then placed on ice, to quickly kill the cells and halt any further metabolism as quickly and thoroughly as possible.

3.1.3 *Mouse incubation*

Our first concern regarding tracer incubation in the mice, was how to get the tracer distributed to the tissue of interest. SIRM literature recommends administrating the tracer with a intravenous (IV) injection through the tail vein.[73] However, an IV injection is challenging, in such a small animal. Intraperitoneal (IP) injections of labelled glucose for flux measurements have been shown to be useful, but with a lower degree of enrichment for time points below 45 minutes, compared with IV injections.[74]

Based on these concerns we chose to make a small pilot study.

Pilot study I, injection method

Two mice were used: one IV injected and one IP injected with uniformly ^{13}C-labelled glucose in a 150 mg/ml solution. It was possible to use a larger bolus of 1666 μmol in the IP injection, compared to 166 μmol in the IV. The IP mouse was terminated after 30 minutes, and the IV mouse after 15 minutes. Metabolic extracts were made, following the protocol described below, from the prostate, kidney, heart and brain of each mouse, and relative signals from metabolites were measured with HSQC NMR. Results are presented in figure 3.2. We found that for all measured metabolites (lactate, glutamate and alanine), signal were higher in the IP injected mouse, compared to the IV injected, in the prostate, kidney and heart, but much lower in the brain. Comparison on the measurements on the glucose, showed a higher concentration in all samples from the IP mouse. This difference was much higher for the brain, than the other tissues. This could suggest

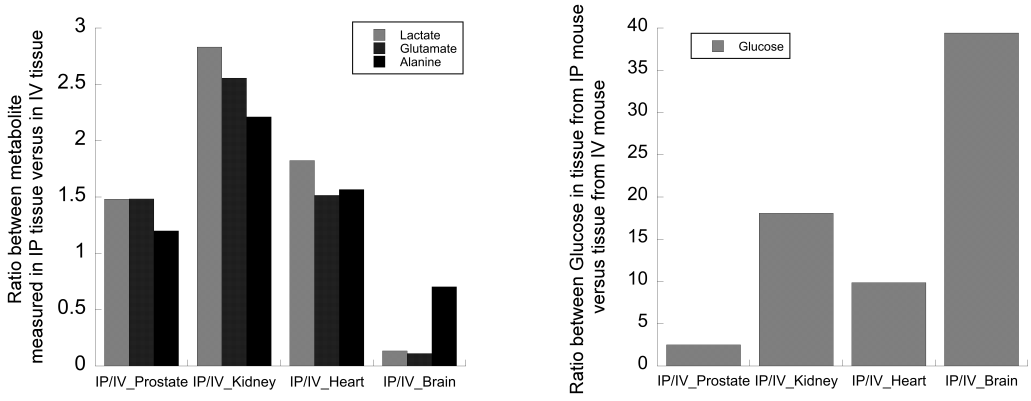

Figure 3.2: Metabolite concentration ratios between IP and IV injected mice, measured in prostate, kidney, heart and brain tissue extracts. On the left: For the metabolic products lactate, glutamate and alanine. On the right: For the glucose tracer.

that the tracer glucose up-take in the brain is significantly slower with the IV injection compared to IP, as we saw a comparatively higher tracer but lower product concentration in the IP injected mouse brain. If further studies wish to use this protocol for studies on the mouse brain, they should consider using IV injection or a longer incubation time. Of course with results based on data from only two mice, this is merely a suggestion. As our focus in this study is the prostate, we chose to use IP injections, where a larger bolus size resulted in higher metabolite signals in this tissue compared to the IV.

Pilot study II, incubation time

Next, to determine the optimal incubation time, we performed a second pilot study including three mice, all IP injected, incubated for 15, 30 or 45 minutes respectively. We saw that the metabolite signals were generally much lower in the 15 minute samples, and that after 45 minutes the glucose signals were very low. We concluded that 30 minutes was the optimal time window for the up-take of the tracer and production of measurable products, while not depleting the tracer, ensuring steady state conditions throughout the experiment, and leaving some glucose to be quantified.

Main mouse tissue study

With injection method and incubation time established, we conducted the main experiment. Each mouse was first sedated with a strong dose of isoflurane gas in a small chamber. When the mouse was asleep, it was removed from the chamber and injected with the protonated uniformly labelled ^{13}C-tracer. The mouse was then placed in a anaesthetic mask distributing a lower dose of isoflurane gas, keeping the mouse asleep. The mouse was placed on a heating pad to aid blood circulation. A picture of a mouse in the mask is shown to the left on figure 3.3.

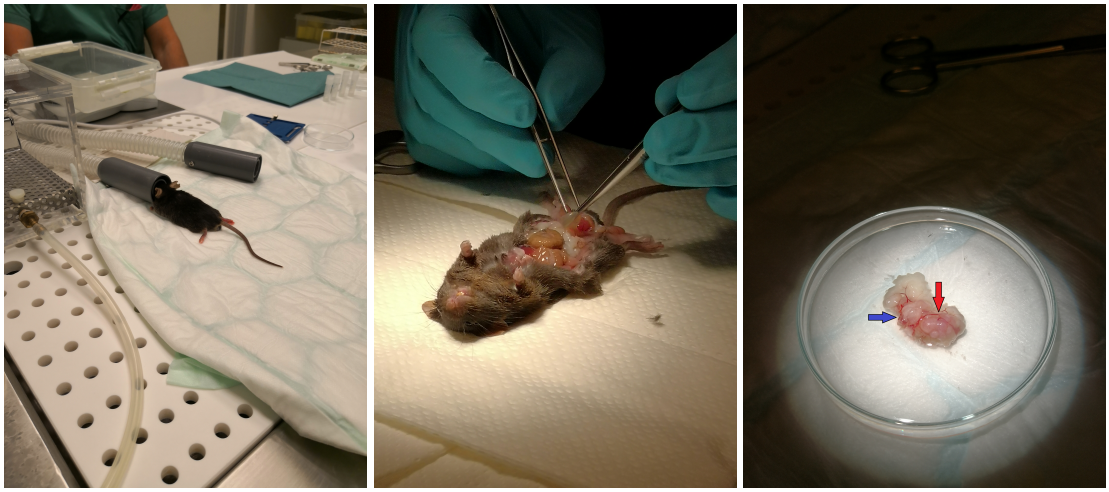

Figure 3.3: Illustrations from the mouse experiment. On the left: Sedated mouse during incubation. Middle: Dissection of the mouse, right before removal of the prostate complex. On the right: The prostate complex before micro-dissection, with the prostate indicated by the blue arrow and a large tumour growing in the seminal vesicle indicated by the red arrow.

During the second pilot study, we experimented with waking one of the mice, after the injection was administered. The reason was that the isoflurane gas might have a metabolic effect, and that the energy metabolism of a sleeping animal is lowered compared to an active one. The awakened mouse was placed back inside its cage with the other mice, but it was visibly uncomfortable; its hairs were standing up and its breathing was heavy. After some minutes, where the mouse showed no signs of getting less uncomfortable and did not move about in the cage, we chose to sedate the mouse again. We concluded that the large volume of liquid in the intraperitoneal cavity from the bolus, was unpleasant for the mouse and we decided against waking any other mice, both to make the experiment as painless as possible and not to stress the mice awaiting injection in the cage unnecessarily.

After the 30 minutes of incubation, the mouse was terminated by cervical dislocation. The mouse was then dissected as shown in the middle picture in figure 3.3. First, the prostate complex, composed of the prostate, the much larger seminal vesicles, and the bladder, was removed for micro-dissection. The prostate complex is shown to the right in figure 3.3. Each lobe of the prostate was carefully removed and placed together in a single sample tube. Tumours found on the prostate and in the seminal vesicles, were collected as separate samples. The seminal vesicles and the bladder were discarded. Other tissue was collected from the rest of the mouse; the brain, the liver and the kidneys, but they were not used any further in this study. Dissection was done as quickly as possible and the samples were immediately snap-frozen in liquid nitrogen to halt metabolic activity. The samples were kept frozen until metabolic extraction.

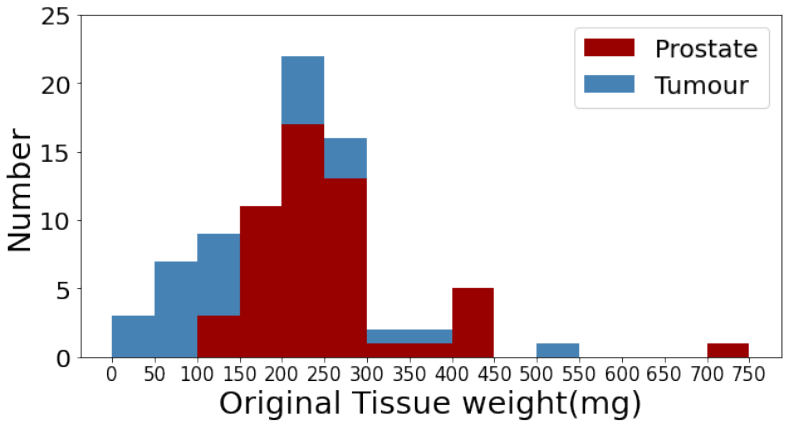

Figure 3.4: Stacked histogram plot showing the measured weight (in milligrams) before metabolite extraction, of all prostate and tumour tissue samples.

3.2 METABOLITE HARVEST AND PREPARATION FOR THERMAL NMR

When the incubation is over and the metabolism quenched, the next step in the experiment is the extraction of the metabolites from the cells or the tissue.

With the cell line samples, cell debris and larger molecules like protein was removed by centrifugation after PCA was added to the samples. The use of PCA is well described for metabolic extraction. [75] By extracting this way, the total of metabolites, both internal and external from the cell, is included in the samples.

For the mouse study, metabolite extracts were made from each tumour sample and for all collected prostate tissue for each mouse. Only parts of the largest tumours were used for extraction, to keep a more uniform sample size and keep the samples easy to work with. From the smaller tumour, a sliver was removed for possible histology. A chart of the weight of the tissue used for extraction is shown in figure 3.4. The weight of the tumour samples had a large variation, with the smallest being only 36 mg (this sample was removed from the final dataset, as it was too small to produce measurable signals in the dDNP experiment) and largest being more than 1000 mg before it was reduced. PCA was added to each sample and the largest samples were first homogenized manually in a glass mortar, before all samples were mechanically homogenized with a Precellys machine. Then, as with the cell line samples, cell debris could be removed with centrifugation.

For both cell line and mouse tissue samples, the supernatant containing the metabolites were then neutralized with potassium hydroxide (KOH). The formed salt precipitates and can be removed by centrifugation, leaving the extracted metabolites in the supernatant. The pH was estimated by an universal indicator added to each sample. This is an important step, as changes in pH-level between samples, causes some signals in the spectra to shift in position.[76]

After, neutralization the samples were lyophilized to a powder. The cell line samples were kept lyophilized until dDNP, but for the mouse tissue study we had decided to perform traditional NMR on the samples as well.

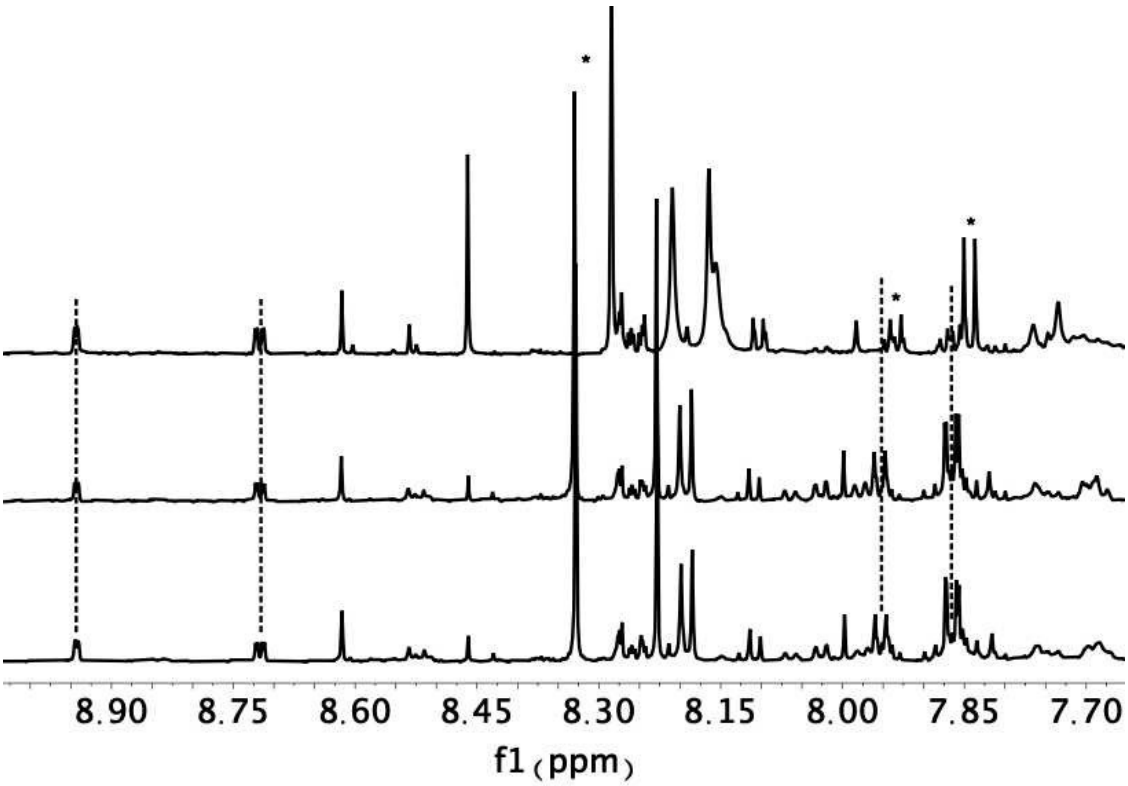

Figure 3.5: Proton spectrum with failed pH-adjustment compared with well shifted ones. The asterisks indicate where signals in the badly aligned spectra (on top) has shifted to no longer be aligned with the comparable signals in the well-alligned spectra (middle and bottom).

In preparation for the thermal ^{1}H NMR experiments, the samples were resuspended in a deuterium based phosphate buffer with DSS added as a standard. Each sample was then more precisely pH-adjusted using a pH-meter for measurements, to 7.5 ± 0.05 pH, before being transferred to the 5 mm NMR tubes. This process revealed some problems with the previous neutralization before lyophilization: Some samples had pH-values way out of the expected range, most often much higher. This seemed to correlate somewhat with sample size, with the larger samples apparently being harder to adjust correctly. Even with the pH-level adjusted after re-suspension, some spectra had peaks shifted to a point beyond possible re-alignment with the other spectra. An example of this is seen in figure 3.5, showing the 1D NOESY spectra from three samples, the one on top having a very high pH-value before the final adjustment. The spectrum at the top, has the singlet placed at 8.33 ppm in the well aligned spectra, shifted up with about 0.03 ppm, making it overlap with other peaks. Similarly at around 7.87 ppm, some peaks that are overlapping in the well adjusted spectra, have moved apart in the badly aligned ones. Because of these kinds of spectral shifts, some samples had to be removed from the final dataset.

Thermal NMR was performed on a 600 MHz Bruker spectrometer, equiped with a a cryoprobe and an autosampler. The spectra were recorded with a 20 ppm spectral width and 128 scans.

After thermal NMR, the samples were re-lyophilized.

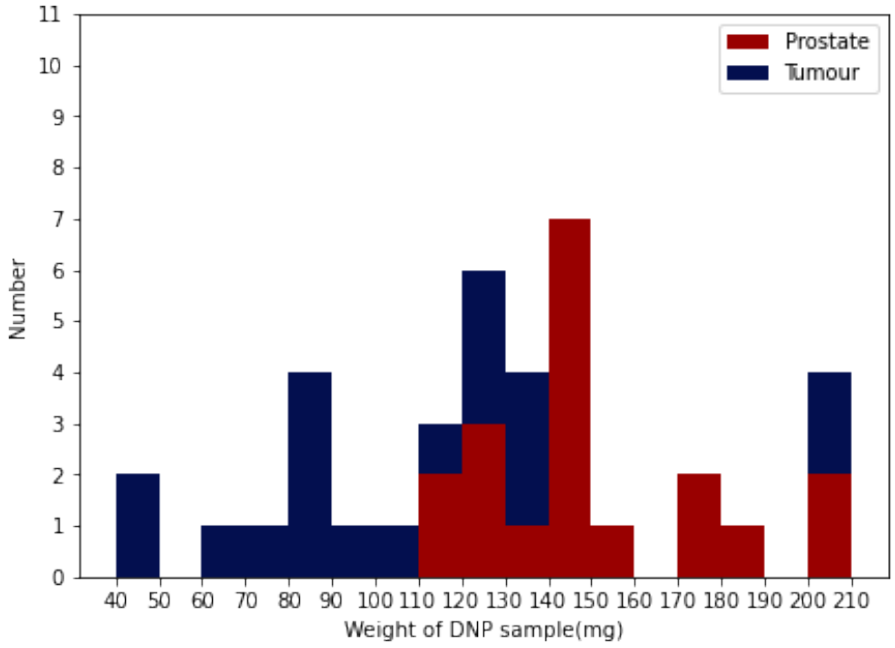

Figure 3.6: Stacked histogram plot showing the calculated weight (in milligrams) for samples prepared for dDNP, of each mouse tissue sample included in the final study.

3.3 THE DDNP EXPERIMENT

For the dDNP experiment, each sample was dissolved in the polarization medium, prepared as described in Lerche et. al[16], consisting of a mixture of glycerol, water, trityl radical OX063 and Gadoteridol. The water/glycerol mixture forms a glass when frozen, allowing for homogeneous spin exchange between the electrons in the radical and the ^{13}C in the sample. The addition of Gadoteridol shortens the $T1$ relaxation time of the electrons, allowing for a more effective polarization.[77] 150 μl of the polarization medium was used for each cell line samples, and 50 μl for each mouse tissue sample. A larger volume was needed for the cell extracts, as the phosphate buffer used for cell suspension caused salts to form in the samples, making them harder to dissolve. 5 μl of the reference compound HP001 (1.1-bis (hydroxymethyl)-[1-^{13}C]cyclopropane), was also added to each sample. HP001 is attractive as an internal standard, as its carbon signal lies isolated in the spectrum and it has a long $T1$.

Due to concerns on whether the largest of the mouse tissue samples, could dissolve into the small volume of polarization medium used, we chose to re-suspended every sample from the study and split those from tissue larger than 215 mg up, before again lyophilizing them. A plot of the calculation of the final weight is shown in figure 3.6.

The samples were polarized in a HyperSense polarizer at 3.35 T and 1.4 K for 90 minutes and then rapidly dissolved in 5 ml hot phosphate buffer, and then transfered to the NMR magnet, where a 1D ^{13}C-spectrum was obtained from a single scan with 90° pulse.

In the study on cell line extracts, the transfer between polarizer and NMR magnet was done manually, where a scientist would collect the dissolved sample in a syringe and walk across the

lab to the NMR magnet and inject the sample into a line connected to the NMR tube placed in the magnet. This process would take approximately 12 seconds from dissolution until the start of the recording, with a couple of seconds in variation between the samples.

For the study on the mouse tissue, an automatic transfer line had been installed, connecting the polarizer and the NMR magnet. This offered several benefits: The most apparent benefit was a decrease in transfer time; the automated transfer was done in less than a second, with a three second delay added, to let the sample settle in the NMR tube. This change from 12 to 4 seconds of time between dissolution and spectral recording gives a large boost to signals with a short $T1$, making it possible to measure a lot more signals outside of the carboxyl area of the spectra. With the automated transfer, the human introduced variation in transfer time was also removed, making the transfer time virtually constant. This benefits the repeatability of the measurements. The other main benefit of the automated transfer was that the volume of the transferred sample could now be kept constant, making much more precise shimming possible, greatly improving the line width and signal-to-noise ratio (SNR) in the data.

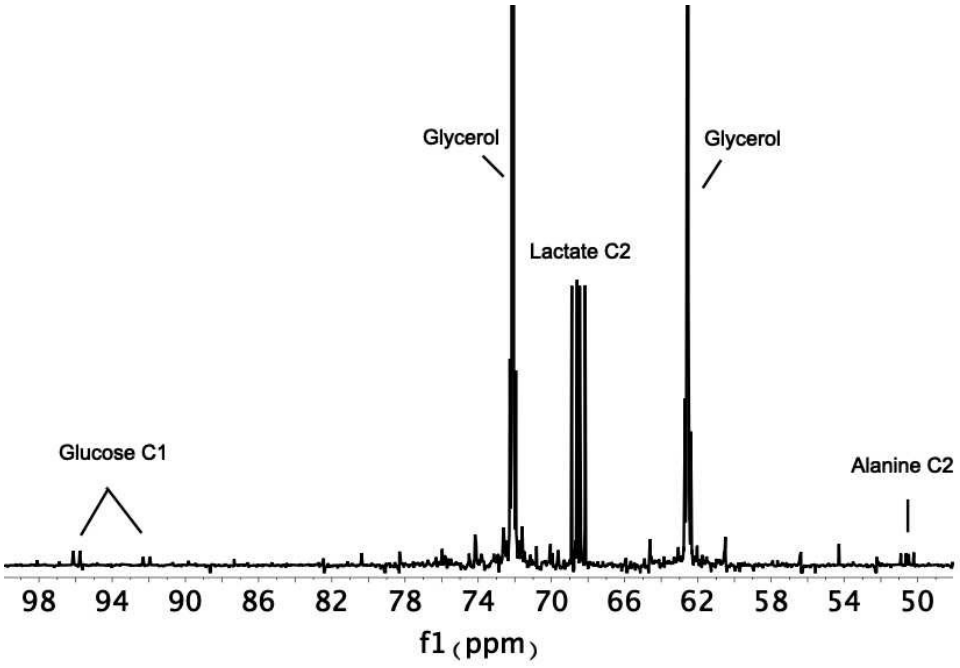

Figure 3.7: Zoom on a dDNP spectrum of a test sample, showing the problem with spikes, caused by proton-decoupling on the too large glycerol peaks.

Apart from the installation of the automated transfer line, we also worked with a 11.7 T Bruker magnet with a cryo-probe, compared to the 9.4 T Varian magnet used in the cell line study, which greatly increased the sensitivity of the NMR experiment. But with great signal strength, comes new challenges: In tests runs with the transfer line, we discovered that the the signals from the natural abundance ^{13}C in the glycerol, were so large that the proton de-coupling failed on them, creating spectral artefacts, in the form of "spikes" around the signals. An illustration of this can be seen in figure 3.7. The presence of the spikes would make all signals between ~ 25 and 120 ppm unusable for data analysis, as the spike would make metabolite identification

difficult and relative quantification impossible. After some experimentation we discovered that using deuterated glycerol in the polarization medium removed the spikes from the spectra.

3.4 FINAL DATASETS PRODUCED FOR FURTHER ANALYSIS

A summary of the cell line data from the first study is shown in table 3.1. 8 samples from each cell line were made for a total of 32 samples.

Table 3.1: Overview of samples in cell line study.

Cell line	Aggresivity	Number of samples
PC3	Aggresive	8
DU145	Aggresive	8
PNT	Indolent	8
LNCaP	Indolent	8
Total		**32**

A summary of the mouse tissue data from the second study is shown in table 3.2. 53 mice were originally included in the study, giving a total of 79 prostate and tumour samples. Some samples were chosen to be removed based on biological reason: 51 of the mice had well differentiated (WD) cancerous prostate tissue, and the last two had poorly differentiated (PD) cancerous prostate tissue (the concept of PD vs. WD is described in more detail in chapter 5). We chose to focus our model on tissue from WD mice so on this ground one prostate and two tumour samples were removed from the data - one of the PD mice only had a large tumour and no identifiable prostate. Additionally, one mouse had a tumour on its liver and one on its kidney. As these tumours were the only one of their kind - all other tumours were found on the prostate and seminal vesicles - these two samples were also removed from the dataset to make the tumour samples more statistically comparable. Three samples were removed from the dataset for technical reasons based on the appearance of their NOESY spectra: For one sample the water suppression in the spectrum had failed, leaving some signals on the side of the water peak affected, and two samples were removed due to peak shifting from failure in pH-adjustments, as described above. Removal of these samples left us with 22 tumour samples, and to make a balanced dataset we chose to include 22 prostate samples. The samples were as far as possible chosen from the same mice that had provided the tumours, but as some mice had grown more than one tumour, and no mouse had more than one prostate, this was not entirely possible. Six samples had to be removed after the dDNP experiment: One was too small to give measurable signal, in one case the dDNP procedure had failed to run spilling the sample, and four had had shimming problems, making the spectra impossible to compare with the others. This left us with a balanced dataset with a total of 38 samples from 23 different mice for further data analysis.

Table 3.2: Overview of samples in mouse tissue study.

	Prostates	**Tumours**	**total**
Mice sacrificed	-	-	53
Samples total	52	27	79
Samples removed on biological basis	*1*	*4*	*5*
Samples removed based on NOESY spectrum	*2*	*1*	*3*
Samples chosen for dDNP	22	22	44
Samples removed based on dDNP spectrum	*3*	*3*	*6*
Total samples in study	**19**	**19**	**38**

3.5 DISCUSSION AND CONCLUSION

The protocol for metabolite harvest and dDNP NMR recording, as described in this chapter, was successfully established. The differences made between the first and the second study are summarized in figure 3.8.

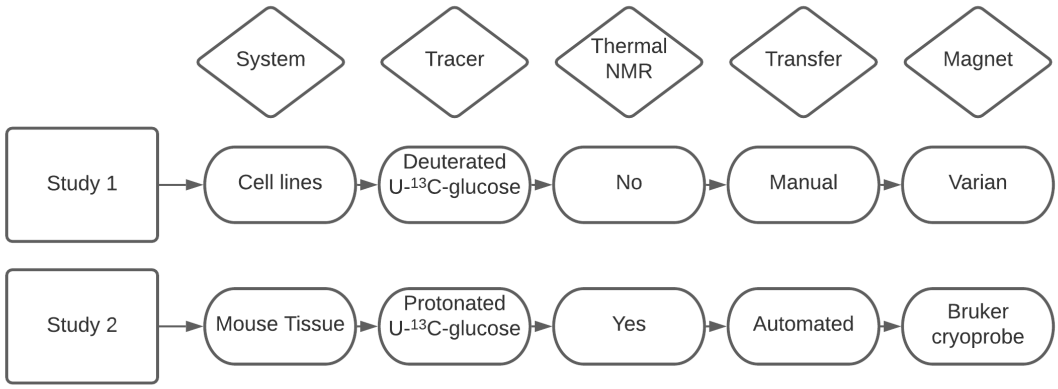

Figure 3.8: General overview summarizing the differences between the first and the second study.

The metabolite extraction done with PCA posed problems in the second study, but not in the first. This seems related to the varying sizes of the tissue samples, where the largest of the prostate and tumours extracted, were hard to pH-neutralize, compared with the smaller tissue samples and the uniformly sized cell extracts. As we did not do proton NMR on the samples in the cell line study, it could also be that some problems would have shown up in that case too. It has been documented that PCA extractions causes metabolite instability, which makes the data obtained less reproducible.[78] Further studies wishing to do both proton and dDNP NMR on the same samples, should consider other extraction procedures.

Studying metabolic flux through ^{13}C labelled glucose with 1D proton NMR, has been shown possible.[79] Some metabolite signals are isolated in the spectra, making it possible to identify and quantify both the signals arising from protons coupled to ^{12}C in unlabelled compounds and from the ^{13}C labelled tracer. The latter shows up as side-bands around the first signal, due to the

spin-coupling between the ^{13}C and proton. This approach gets the advantages from 1D proton NMR; fast acquisition times and readily quantifiable signals, but the drawbacks are there too; the chemical shift range of the proton spectrum is narrow, and the inherent crowding problem is made worse, with the additional peaks from the ^{13}C couplings, limiting the range of metabolites that can be measured, relative to the dDNP spectra.

dDNP fingerprint experiments on metabolite extracts, measuring natural abundance ^{13}C, have been shown to have a high repeatability and contain the information needed for biological classification.[14, 15] With transfer times on scale with ours in the cell line experiment, they show that it is possible measure up to 40 different signals, and use this information on metabolic pool sizes in the biological system for un-targeted metabolomics.

Figure 3.9 shows a representative spectrum from the cell line study, a spectrum from a sample from the pilot study done with mouse tissue, performed with the same NMR set-up as the first study (no transfer line, 9.4 T Varian magnet without cryoprobe) and a representative spectrum from the mouse tissue study. Especially the addition of the pressurized transfer line system with the benefits of lowered transfer time, and volume control, has had a large impact on the sensitivity and spectral resolution.[80] If not for the updates on the hardware, we would not have been able to get the same amount of measurable spectral features in the mouse tissue study, as we did in the cell line study. The more difficult incubation conditions from working with a living animal and the protonated tracer, makes conditions for the NMR study much worse. With the cryoprobe and the transfer line, however we got a much higher sensitivity in the second study and were able to detect a wider range of metabolites, despite the difficulties in working with tissue compared to cell extracts.

Further improvements to the dDNP process could be made, for an even higher sensitivity gain; coating the NMR tube with Hellmanex solution, has been shown to reduce micro bubbles in the sample, improving the line width of the spectral peaks.[15] As the majority of the 4 second transfer time, when using the automated transfer line, was a 3 second delay to allow the sample to settle into the tube, less micro bubbles could mean a shorter delay needed, increasing our ability to measure signals from low $T1$ ^{13}C. Improvements on retaining polarization levels during transfer could also be made by adding magnetic tunnel around the transfer line, as the polarization rapidly decreases when passing through areas of low magnetization between the polarizer and the NMR magnet.[81]

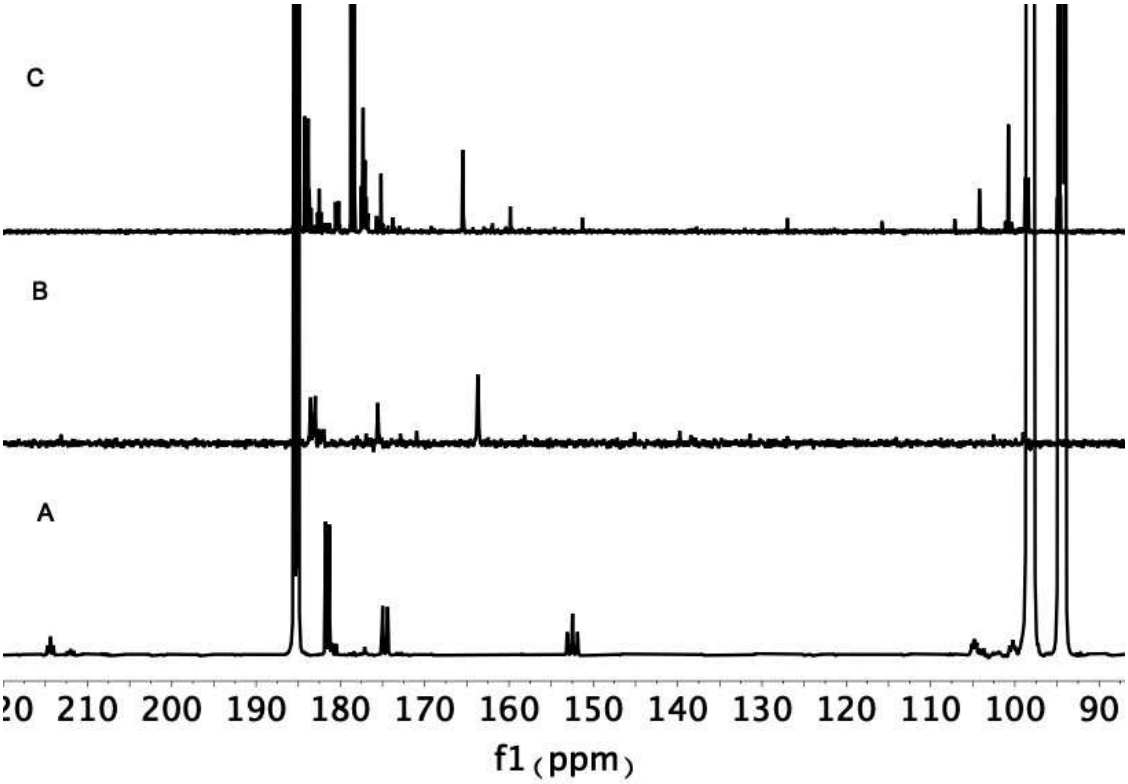

Figure 3.9: Comparison of spectra between the studies. Bottom spectrum is a representative spectrum from the cell line study. Middle from the first pilot study with mouse tissue. Top a representative spectrum from the mouse tissue study.

ARTICLE 1: METABOLOMICS WITH A SMALL FEATURE SET

4

Compared with other spectral methods utilized for metabolomics, the dDNP SIRM fingerprint spectrum offers a sparse spectrum with easily identifiable features. In the study published in the article included in appendix A, we explored dDNP SIRM as a tool for classifying prostate cancer cell line data. This chapter will explore the background of the study; how we chose to utilize the information in the spectra and the choices made for the machine learning methods to work with this information.

To study the possibilities of using SIRM fingerprints made with dDNP NMR, as a tool for research in prostate cancer, we chose to focus our first study on prostate cancer cell lines. Using cell lines as a model for cancer in humans, offers the benefits of limiting individual variation across samples. They are easier to manage and being less expensive, compared to tissue samples from humans or animal models.[82] We worked with samples from four different human derived cell lines: DU-145[83] (isolated from a brain metastatic tumour), PC3[84] (isolated from a vertebral metastatic tumour), LNCaP (isolated from a lymph node metastatic tumour), and PNT1a[85] (immortalized cells from a healthy prostate).

There were three goals with studying the obtained fingerprints: First to determine if we had sufficient information captured in the spectra to distinguish the four cell lines from each other. Secondly to make a robust, binary classification between aggressive (PC3 and DU-145) and indolent (PNT1a and LNCaP) cell line samples. Thirdly to perform a feature analysis, to investigate which metabolic signals contributes positively to such a binary classification.

4.1 THE DDNP SIRM FINGERPRINT SPECTRUM

With the metabolite extract samples created and the dDNP NMR spectra recorded, there is still the challenge of how to generate the data matrix, and determining what pre-processing steps should be applied to the data, to prepare it for the application of classification algorithms. These choices have to be carefully optimized, to ensure an unbiased model with interpretable results without over-fitting to the data.

Figure 4.1 shows a representative dDNP fingerprint from this study. The spectrum is sparse, with a small number of mostly well separated signals. The middle region of the spectra, around 60-100 ppm, is not sparse however, because of the many, signals from the ^{13}C labelled glucose tracer. As the tracer was fully labelled, the couplings between the ^{13}C nuclei, and to the deuterium nuclei in the molecule, make the glucose peaks split into complex patterns. Most of the clearly visible signals are found in the carbonyle region of the spectrum, as shown in the zoomed in region in figure 4.1. This is as we expected, since the carbonyle carbons have the longest $T1$s and

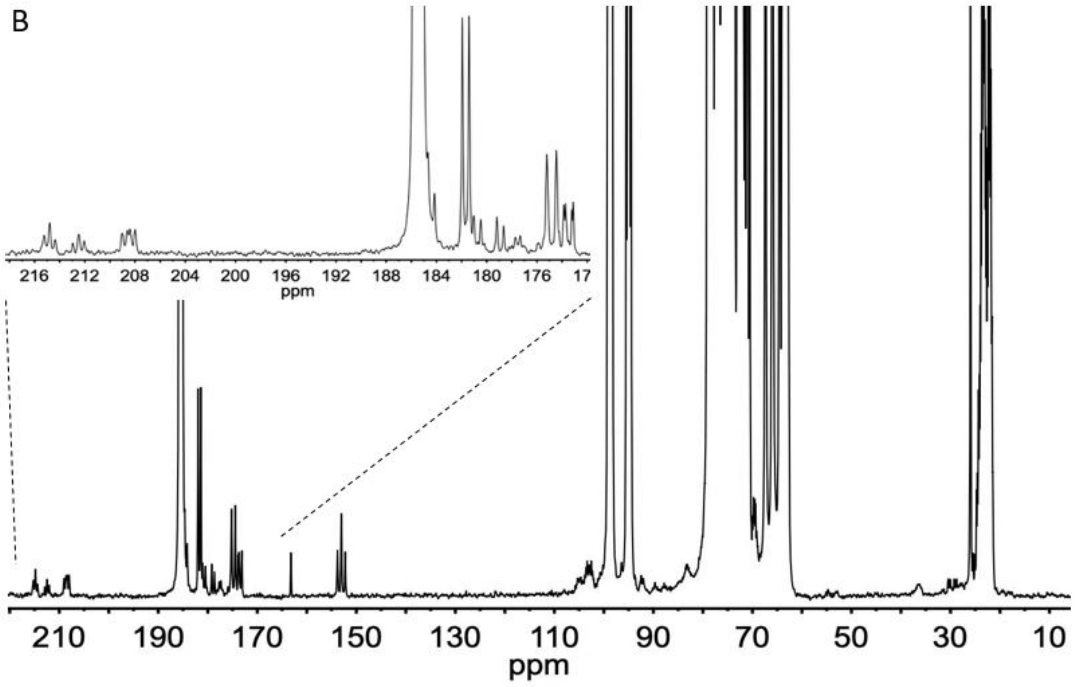

Figure 4.1: A representative dDNP NMR fingerpint spectrum from the study, made from a 10 million DU145 extract. The zoomed excerpt shows the carbonyle area.

therefore more of their polarization remains after the transfer to the NMR magnet, compared to the proton or deuterium bound carbons. For some of the most abundant metabolites, like lactate and alanine, signals from several carbons are clearly seen. Most notable, all three signals from lactate is clearly visible as large signals at around 23, 71 and 185 ppm.

Table 4.1: List of metabolite signals used for statistical analysis. C-[n] refers to which carbon in the molecule gave rise to the signal measured.

Compound	Abbreviation	Chemical shift
DHAP (Dihydroxyacetone phosphate)	DHAP-C2	214.6
Lactate	LAC-C1	185.3
Glutamate	GLU-C5	184.2
3PG (3-Phosphoglycerate)	3PG-C1	181.5
U178 (an uninditified amino acid)	U178	180.6
Alanine	ALA-C1	178.8
Serine/Glycine	SER-GLY-C1	175.5
Pyruvate	PYR-C1	173.3
PEP (Phosphoenolpyruvate)	PEP-C2	152.9
G3P (Glyceraldehyde 3-phosphate)	G3P-C1	92.1

Many of the signals show a characteristic pattern of doublet peaks of the same size, with a distance between them of ~55 hertz - the characteristic splitting pattern for a ^{13}C atom bound to one other neighbouring ^{13}C. Or, in the case of signal with two neighbouring ^{13}C atoms, a triplet

splitting with two peaks with the same coupling distance to a middle peak of twice their size, as for instance can be seen with the PEP signal at 153.9 ppm and the DHAP signal at 214.6 ppm. Several signals were clearly identified as metabolic products from the tracer, using information on chemical shift values and splitting patterns and comparing these to known metabolites.[86] Ten different metabolites were found to have easily measurable signals in the spectrum.

Some compromises were made with these ten metabolite features: A doublet signal around 180.6 ppm, were identified as belonging to an amino-acid, but we could not identify which. The other identified amino acid signals(alanine, glutamate, serine and glycine) were clearly identifiable by their chemical shift and splitting pattern, but there are multiple amino acids with a doublet carbonyle signal at 180.6 ppm. As this signal was clearly measurable and could possibly contain valuable information, it was included as a feature with the name "U178". The signals from serine and glycine, overlapped to a degree where they could not be seperated into two signals, so the choice was made to include them together as a single feature. Both DHAP and its unphosphorylated form, were seen in some spectra, at 214.6 and 216.9 ppm respectively. As it was suspected that the extraction process and dDNP facilitated the changes between these two compounds, they were included as one signal. The signal at 181.5 was unambiguously identified as 3PG with a dedicated experiment, in a previous study.[16]

Additionally, the peak from bicarbonate was also found to be measurable in some spectra, but absent in others. As we had reason to suspect that this was a result from small variations in pH neutralization process during metabolite extraction, and not from biological differences, we chose not to include bicarbonate in the study. We also chose not to include signals from the glucose as a feature for the analysis. The large quantity of glucose, that was given to the cells, meant that there was plenty of signal to measure. The C1 signals from both α and β -glucose is isolated in the spectra, but they have a relatively short $T1$, and would thus be very sensitive the transfer time used in this study (12 ± 2 s).

As we wanted to test our statistical models on a dataset containing the least possible noise and redundancy in its features, we chose to include only one signal from each metabolite. In this way, the analysis would not be biased by multiple features informing on the same metabolite. Different ways of achieving this was considered: In the case of multiple signals the integral values could be summed up or averaged for instance. We settled on the method of choosing only one representative signal for each metabolite. In this way we could get information from the signal optimized for minimal spectral overlap and longest $T1$, giving the highest SNR. With this approach we hoped to minimize technical variation from the small differences in transfer time and shim quality between the samples. Table 4.1 shows an overview of the metabolites used for further data analysis, with the abbreviations used and their chemical shift. All signals included were from carbonyle ^{13}C atoms, which had a large peak from its middle carbon, with no bound protons or deuterium atoms, and G3P, which had an isolated peak with no spectral overlap, at 92.1 ppm. in the otherwise crowded middle region of the spectrum.

The spectra were processed in MNova.[87] A line broadening of 3 Hz was added, they were phased manually and Bernstein baseline correction was applied. The spectra were referenced to the added HP001 at 25.7 ppm. The data matrix was constructed with integrals of the chosen

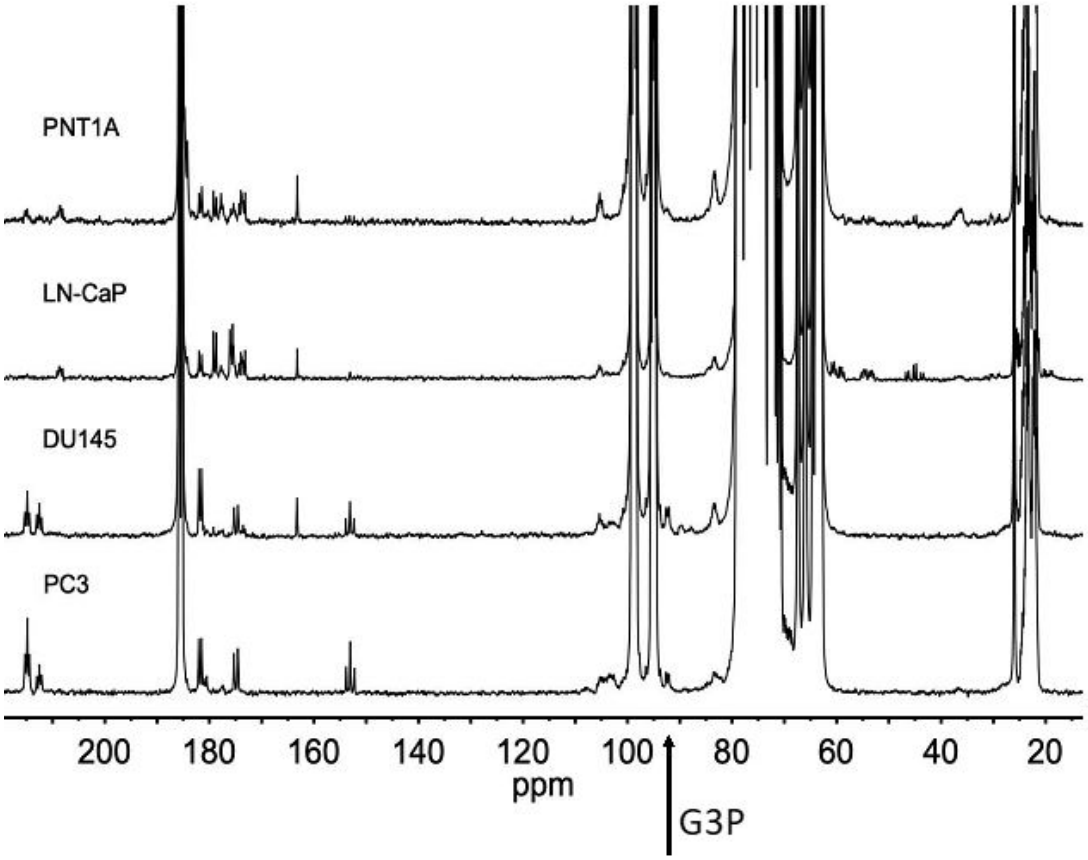

Figure 4.2: A representative spectrum for each of the four cell lines included in the study.

metabolites measured relative to the HP001 signal. As some of the data presented in this study was originally made for other, smaller projects, the cell count for the samples, were not kept consistent; some samples were made with 10 million cells and some with 20 million. To make all samples comparable, values for the samples containing only 10 million cells were doubled.

All further statistical analysis described bellow was carried out using Python[88] using functions included in the packages Scikit-learn[89] and Scipy[90].

4.2 SEPARATING THE CELL LINES

Our first question in the analysis of the data was whether the dDNP SIRM fingerprints captured sufficient information to separate each cell lines from the others. Figure 4.2 shows a representative spectrum for each of the four cell lines. From just looking at the figure, there appears to be clear visible differences between the cell lines: Some peaks present in some cell lines seems to be completely absent in the others, and other peaks vary in scale. It does not seem to be the case of some cell lines in general producing more metabolites across the board compared to the others. Rather for each cell line it seems to be that they produce more of some signals, and less of others, compared to the other cell lines. Of course, a plot of only representative samples, cannot tell us if these differences are persistent through all spectra.

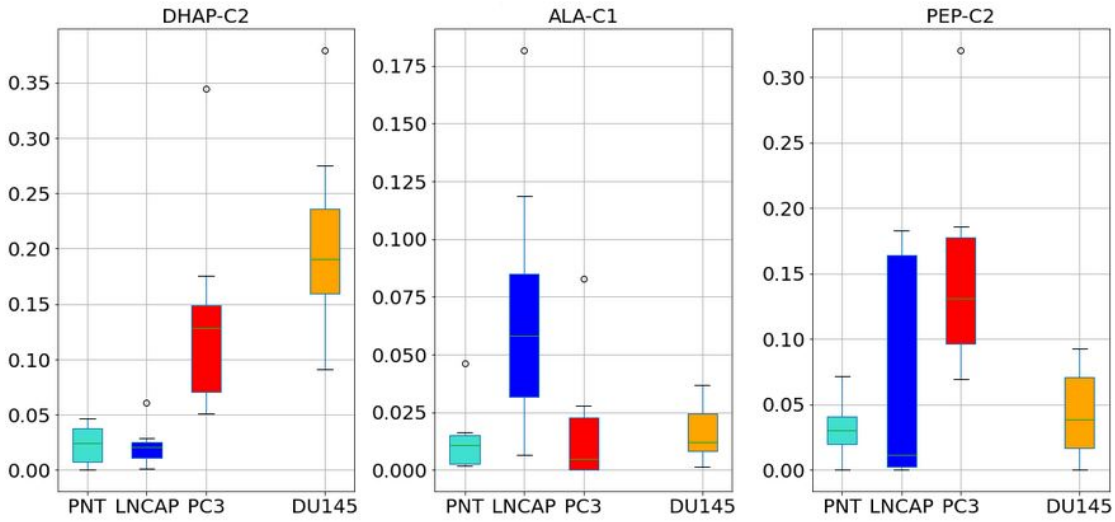

Figure 4.3: Box-plots of the three metabolites (DHAP, alanine and PEP) found to have significant differences in means, between the cell lines. Values are in arbitrary units.

To investigate if systematic differences in the mean values of the features could be found, a one-way ANOVA test, was carried out, with p-value thresholds Bonferroni corrected, to account for parallel testing. Of course, if it could be shown that one or more of the features fully separated the cell lines, setting up complex multivariate analysis could have been a wasteful affair. The ANOVA test found a significant difference in mean for DHAP, alanine and PEP (full test results were presented in the supplementary information to the paper, appendix A). Box-plots for these three metabolites are shown in figure 4.3. While there are clear, visible differences between the distributions of the data in the cell lines, the internal variance for the cell lines is so large, that none of the three plotted metabolites separates the cell lines by themselves. We therefore moved on to multivariate analysis and machine learning.

Based on the benefits and drawbacks of the different classification methods described in section 2.3, we chose to perform to the classification of the different cell lines with PC-DFA. As this was a multi-class problem, PC-DFA has the benefit of producing a clear illustration of the separation in the data and PC-DFA has been found to perform especially well in the case of a small feature set, like we had here.[56] As we were not particularly interested in investigating what features contributed to the separation between the four specific cell lines, the PC-DFA lack of robust feature ranking, was not a concern for us.

PC-DFA being a parametric function, relies on a Gaussian distribution in the data to perform optimally, we therefore chose to apply a Box-Cox transformation to the data first to transform it into a Gaussian shape.[91] The Box-Cox transformation can only be applied to positive values, and some values in the data matrix were slightly bellow zero (this could happen when a measured metabolite was not present in a detectable quantity for a sample, and a random fluctuation in the noise gave a lower value). Therefore, before transformation, every value in the data bellow zero was set to zero and a very small number(1^{-10}) was added to all values in the data-matrix. Then Box-Cox transformation was applied, and the data was mean centred and unit variance scaled.

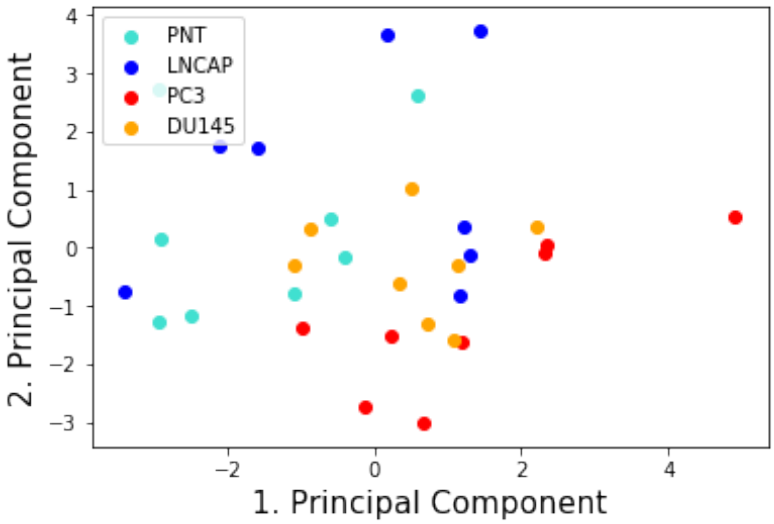

Figure 4.4: Plot of the first two principal components in the PCA analysis on the cell line data. 34.47% variance was captured in first component and 26.65% in the second.

The first step in applying PC-DFA, is the PCA. A plot of the two first principal components from the analysis is shown in figure 4.4. The two components plotted here captured most of the variance in the data; 61.12% in total. While there is some structure in the plot - the PNT and LN-CaP data points gravitate more towards the top-left corner of the plot, while PC3 and DU145 fall more in the middle and bottom of the plot - the unsupervised PCA is clearly not enough to separate cell lines from each other. The primary variance in the data was not only related to our biological question, if it was, data points from each cell line should have clustered together separately from each other in the plane made by these two principal components, as they contained most of the variance in the data. As the samples in each cell-line should be biologically identical to each other, the variance we see in the data is most likely introduced by technical factors.

Even though we included only one feature representing each of our ten measured metabolites, there was still covariance remaining in the data. This was to be expected: Some metabolites will naturally correlate with each other in levels of production. Therefore it made sense to run the LDA algorithm on the PCA transformed data, where each feature is orthogonal in relation to the others, to elliminate the bias that arises from correlated features. We chose to include enough PCA features to still account for a minimum of 95% of the variance of the original dataset. The first 7 variables gave a total of 95.68% of total variance and they were carried over to the second part of the analysis.

A plot of the two first discriminant functions of the PC-DFA is shown in figure 4.5. All data points except three (one PC3 and two LN-CaP) falls inside the coloured eclipses illustrating two standard deviations from each point cloud. There seems to be two groups in the data, one with PNT and LN-CaP data points and one with PC3 and DU145 which even this supervised algorithm can not separate. This is also illustrated in the confusion matrix, with the results of leave-one-out

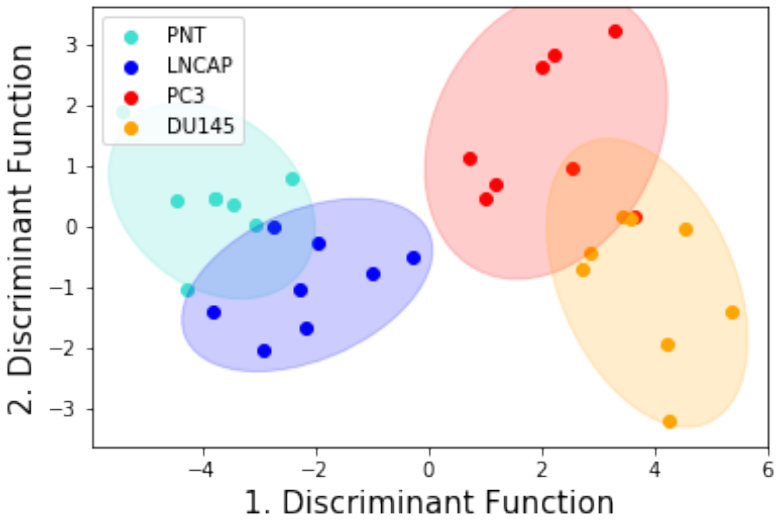

Figure 4.5: The first two discriminant functions of the PC-DFA classification, separating each cell line. Coloured ellipses show two standard deviations from each point cloud.

Table 4.2: Confusion matrix with leave-one-out cross validated, results from PC-DFA classification, seperating by cell line.

Actual \Predicted	DU145	LNCAP	PC3	PNT
DU145	7	0	1	0
LNCAP	0	5	0	3
PC3	1	0	7	0
PNT	0	2	0	6

cross validated classification of the samples, shown in table 4.2: The PC-DFA had a 78% successful classification rate, with 25 out of the 32 samples identified as their correct cell line of origin. But the errors are only between DU145 and PC3 (two misclassifications), and between PNT and LN-CaP (five misclassifications).

4.3 Classification between aggressive and indolent cancer cell lines

As the multi-class classification with PC-DFA showed evidence for two groups in the data, it made sense for us to move on to a binary classification. As we found that the PC3 and DU145 data points would group together separately from the group made by PNT and LN-CaP data points, we chose to view this as the distinction between samples representing aggressive prostate cancer versus indolent prostate cancer. The biological argument for splitting the data along this line, was that while the LN-CaP cell line is harvested from a metastatic tumour, it is an early metastasis and is still, like PNT, androgen dependent and show a low invasiveness.[92] This, combined with the PC-DFA results, made us move on to pursue a binary classification, exploring the seperation of aggresive prostate cancer cell line samples (PC3 and DU145) against indolent prostate cancer

cell line samples (PNT and LN-CaP).

Our priorities were to get a robust binary classification, as far as possible with the small sample size we had, together with feature ranking, making it possible for us to analyse which signals contribute positively to a separation of aggressivity. Based on the qualities of the methods laid out in section 2.3, we chose to use RF to do a feature ranking and then use SVM to build the classification using only the features chosen by RF. While RF gets out-performed by other algorithms in terms of producing high success-rate classification models, it is excellent for ranking variables. SVM, on the other hand, is a robust classifier, build specifically for binary problems, which has been shown to work well on datasets with a small number of features, and to benefit from feature extractions made with RF, especially in the case of a small training dataset.[68]

4.3.1 *Random Forest feature extraction*

To construct the feature ranking, the RF algorithm was set up to build classification forests with 500 trees, using gini impurity as splitting criteria, with no max tree depth and no minimums required for splitting when building the trees. As RF does not require scaling, no preprocessing was done to the data. As the trees made in the RF algorithm - like the name implies - are randomly constructed, it always uses only part of the data points and features in a given training set. There is therefore some variance in how the algorithm performs each time it is applied. An illustration of this concept is shown in figure 4.6, where the out-of-bag score (RF's internally validated classification success estimate) is plotted for the RF algorithm run with differing number of trees, from 20 to 1000. With a low number of trees the out-of-bag score fluctuates wildly between 91% (29 out of 32 samples) and 97% (31 out of 32 samples), sometimes dipping below this, but as the number of trees increases the score is most often 93% even though it still fluctuates. The decision of using 500 trees in the algorithm was made as a compromise between getting a stable classification rate in most RF runs and keeping running time reasonable.

When performing the feature ranking, the data was randomly split into two fractions: 70% of the data was used as a training set and 30% was used as a validation set. The split was stratified to keep an equal amount of aggressive and indolent cancer samples in each fraction. The RF algorithm was trained on the training data and prediction of class was made with the validation set, where the prediction accuracy was calculated as the ratio of correct classifications. Then the values of the first feature in the the validation set was randomly permuted, and a new classification of the validation set was calculated. The difference from the non-permuted accuracy was recorded. This circle was repeated for every feature, each time recording the difference in accuracy. Then the whole process was repeated from the split into training and validation tests. The algorithm of building the forest and permuting the training values, was done 1000 times in total, giving a stable average of the change in accuracy when using real data or randomly shuffled data for each feature. The difference in accuracy was then used as the measure for ranking the features: The larger the decrease between real and shuffled values, the more essential the feature is for making the classification.

The results of the RF feature ranking is shown in figure 4.7. We found that only four of the ten features contributed positively to the separation between the aggressive and indolent prostate

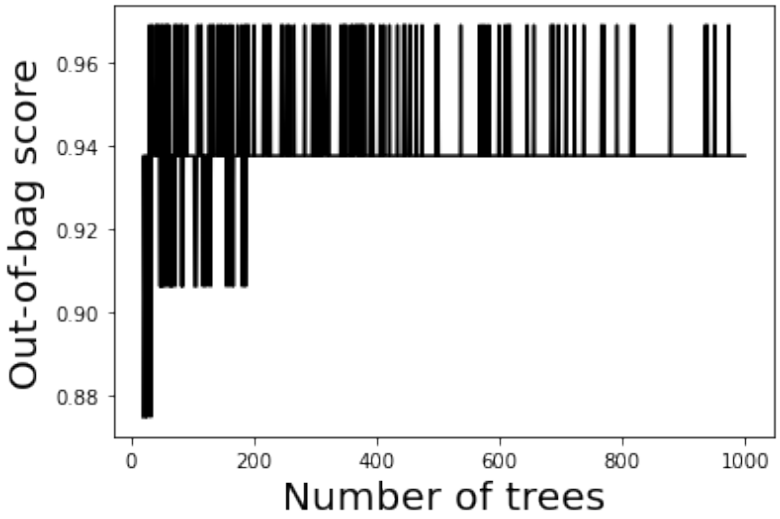

Figure 4.6: Out-of-bag classification success rate for RF with differing number of trees from 20 to 1000.

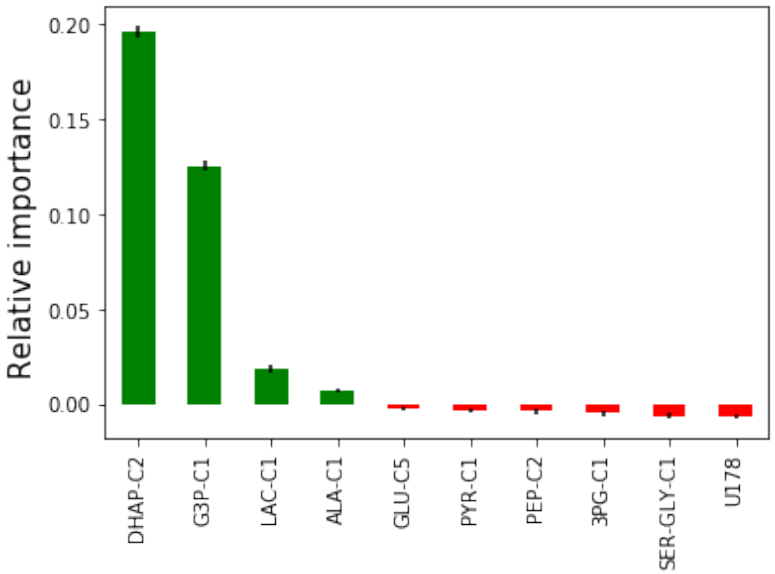

Figure 4.7: Results of feature importance ranking performed with RF. Black bars are standard error of the mean (SEM).

cancer samples. Two metabolic signals with a large importance; DHAP and G3P and two with a smaller, but still positive contribution; lactate and alanine.

4.3.2 *Classification with SVM*

With the feature ranking performed with RF, we were ready to make the final classification between the aggressive and indolent prostate cancer samples, with SVM. As we had a small dataset, we chose to not optimize the parameters of the SVM to the data. Instead the parameters

Table 4.3: SVM classification success rate for different subsets of the features in the data.

Features included	Success rate
All	93.75%
DHAP, G3P, LAC-C1, ALA-C1	96.88%
DHAP, G3P, LAC-C1	93.75%
DHAP, G3P, ALA-C1	93.75%
DHAP, LAC-C1, ALA-C1	93.75%
G3P, LAC-C1, ALA-C1	96.88%
DHAP, G3P	90.63%
DHAP, LAC-C1	90.63%
DHAP, ALA-C1	90.63%
G3P, LAC-C1	81.25%
G3P, ALA-C1	93.75%
ALA-C1, LAC-C1	81.25%
DHAP	90.63%
G3P	84.37%
LAC-C1	75.00%
ALA-C1	62.50%

were kept fixed, to not risk over-fitting them to the data. We used a linear kernel function and set the C parameter to 1, chosen as the range of our output variable (aggressive or indolent).[93] The data was mean subtracted and unit variance scaled, before SVM was applied and leave-one-out cross validation was used for obtaining accuracy results.

The classification was made with both the full feature set of the original data, and for all combinations possible of the four features, found important in the RF separation. The results are shown in table 4.3.

The results show that the use of RF for feature extraction, improved the performance of the SVM: When SVM was applied to the full dataset the accuracy was 93.8% (30 out of 32 samples), but when the data was reduced to only the four features that the RF analysis found, it had positive impact on the separation, and the accuracy rose to 96.9% (31 out of 32 samples). DHAP was the feature that by itself could support the best classification at 91%, and was the highest ranked feature by RF importance (which we could also suspect from the ANOVA and the box plot in figure 4.3). Curiously though, a classification equally as successful as the one made with all four RF approved metabolites, could also be made using only G3P, lactate and alanine. In both these cases only the same PC3 sample was misclassified.

4.4 DISCUSSION AND CONCLUSION

With a 78% accuracy, we found that the dDNP SIRM fingerprint spectra to some degree captured information to distinguish between all four cell lines, but that it with 97% accuracy could distinguish between samples from aggressive or indolent prostate cancer cell lines. We could also pinpoint the 3-4 metabolite signals that contributed to this successful classification, opening up the possibilities of identifying possible biomarkers for aggressivity.

With that being said, there are of course some severe caveats with a study designed like this, which should greatly limit how widely we interpret the results. Here we have statistically treated the samples as if they were independently sampled from a population (n = 32), when in actuality the situation is that we have four independent cell-lines with eight biological replicates each (n = 4).[94] In the worst case scenario, our findings reflect nothing relating to cancer biology, but only about an unrelated, biological trait that the two men supplying the original PNT and LN-CaP cells had in common with each other, but not with the PC3 and DU145 men.

Considerations on proper validation of the results should also be made. The proper procedure would of course be to run cross-validation (or even double cross-validation) and then do testing on an independent set of test samples, not used for training the models. Of course, with such a small dataset as we worked with here, this is just not possible. The results would be entirely dependent on which samples were used for training and which for testing, and of course the same problem from using biological replicates and not having true independence between samples would arise.[49] Concerns have been raised over the leave-one-out method of cross-validation, suggesting it to give less consistent results compared to higher k-fold cross-validation methods.[58] However, leave-one-out cross-validation has the benefit of taking the randomness element out of k-fold cross-validation, giving the benefit of stability to validation on small dataset, where this randomness could have a large effect.[95]

We chose in this study to do minimal optimization on both RF and SVM to prevent over-fitting. The choice to use the default parameters of the un-pruned trees has been argued as reasonable,[96] along with the default choice of number of boot-strapped features used to build each tree.[97] With SVM we are limiting the relationships between features and class, we could discover, by only considering a linear kernel: If, for instance, a metabolite was produced either in very high quantities or in very low quantities by aggressive cancer cells, but always in the same middle-level quantity by indolent cells, this biological relevant relationship, could be picked up by a non linear SVM-kernel. But, as we are already running the algorithm multiple times on the feature-subsets in the data, we did not want to introduce additional parameters, as long as we could not do any independent testing.

Our overall conclusion from this study is that the method of using RF+SVM on dDNP SIRM fingerprint data to classify types of prostate cancer, is a promising tool to develop further for biomarker discoveries in cancer metabolomics. The small, but easily readable feature set, is combined with machine learning methods suited, to provide clear information, not just on the class separation but also directly on exactly which metabolites support the separation. This, however still remains to be evaluated on more complex data.

ARTICLE 2: METABOLOMICS WITH dDNP SIRM FINGERPRINTS IN A COMPLEX BIOLOGICAL MODEL OF PROSTATE CANCER

5

The dDNP SIRM fingerprint method has the potential to be an useful tool for identification of the underlying metabolic features that can classify between prostate cancers of different aggressivities. The manuscript submitted for publication included in appendix B, presents the study done on prostate tissue samples from TRAMP mice. This chapter explores how to optimize the data handling for the RF+SVM analysis in this study, and how the results of the classification between prostate and tumour tissue, can best be interpreted.

With the dDNP SIRM fingerprint assay for extraction of metabolites, recording of NMR spectra and subsequent data analysis method of RF+SVM feature extraction and classification established from the previous study, we were ready to move on from the cell lines to a more complex system, for a better approximation of cancer growing in the human body. We chose in this study to work with samples taken from TRAMP (Transgenic Adenocarcinoma of Mouse Prostate) Mice.[98] Male mice with the TRAMP genotype spontaneously develop prostate cancer which grows metastatic over the animal's lifetime, making it a useful model for investigating the progression of aggressivity in prostate cancer. [99]

Our original plan with the study was to compare prostate samples from mice with well differentiated adenocarcinoma (WD) type prostate cancer with samples from mice with poorly differentiated adenocarcinoma (PD) type prostate cancer. To our surprise, however, of the 53 mice we sacrificed only 2 were discovered to be PD. The literature differs on how the PD grade cancer arises in the mice. Some have described it as two different sub-groups of mice where some mice develop the aggressive PD tumours early (from 13 weeks onwards, peaking at 21 weeks) and the more slow growing WD tumours only form in older mice.[100] Others have described it as WD cancer developing in every mouse from 12 weeks of age then progressing to PD by week 28,[101] or by week 39.[102]. As the ages of our mice at time of death ranged from 17 to 47 weeks, with the median being 29 weeks, we expected per any of these descriptions to find several more PD prostates than we did. We have no clear-cut explanation of the missing PD mice, but a contributing factor could be that the staff of the animal facility caring for the mice, were very contentious about examining the mice for tumours by palpitation. If a mouse was found to show signs of illness in this way, we would arrange to sacrifice it and all animals sharing its cage, in the days following, to prevent unnecessary suffering. Sometimes we would find tumours and some times we would not. If we had conducted more reliable screening on the mice besides palpitation, like ultrasound or MRI, we might have delayed the sacrifice of some of the mice, allowing them to develop PD prostate cancer.

Instead we focused the study on a binary separation between WD prostate tissue and the

tumour growths we found on prostates and seminal vesicles. As described in chapter 3 a total of 38 samples (19 each of prostate and tumour) were processed with both 1D NOESY proton NMR and 1D ^{13}C dDNP NMR. In this way, the prostate samples could serve as the indolent cancer and the tumours as the aggressive, metastatic form. Without histology of each sample, a sure-fire assessment of the cancerous development in the tissue cannot be made, but as the prostate tissue of mature TRAMP mice has been described as benign areas with adenocarcinoma growths, this classification was deemed to be suitable.[103]

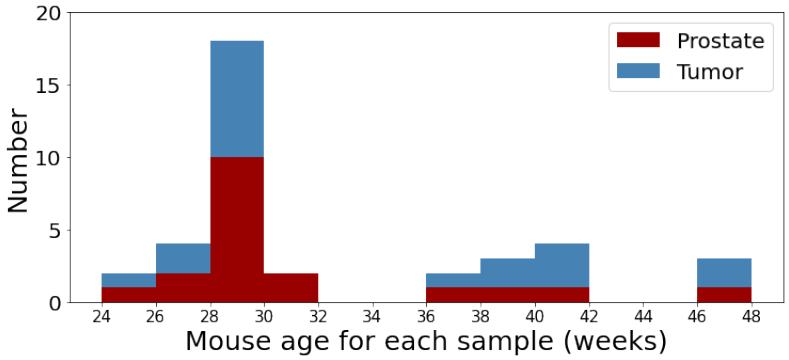

Figure 5.1: The age of the mouse at time of death, for each sample included in the study.

Figure 5.1 shows a histogram of the age of mouse at termination for each sample included in the study. Of the prostate samples, 15 were from mice 32 weeks or younger and 4 were from mice 36 weeks or older. For tumour samples this split was 10 to 9. This bias in the data of prostate samples tending to come from younger mice, were something we wanted to be conscious about, moving forward.

5.1 ANALYSIS OF DDNP DATA

The obtained dDNP spectra were processed in MNova, with an added line broadening of 0.3 Hz, manually phased and Whittaker smoother baseline correction was applied. The spectra were referenced to the added HP001 signal at 25.4 ppm, as this was found to match the lactate chemical shift to known values in chemical shift Human Metabolite Data Base.[86]

Figure 5.2 shows the dDNP SIRM fingerprint spectra for a sample from each of the two classes in the data. Like in the cell line study, the spectra are sparse, but due to the improvements in our NMR hardware, we see more metabolite signals outside of the long $T1$ carbonyle area. The largest signals in the spectra are those from the natural abundance ^{13}C in the deuterated glycerol, added to the samples to form the polarization matrix. This is seen as two, large multiplet peaks at 74 and 64.3 ppm. Of the signals pertaining to metabolite products, lactate is by far the largest, with all three signals clearly identifiable at 185.2, 71.2 and 22.8 ppm. These lactate signals tower over the rest of the metabolite signals.

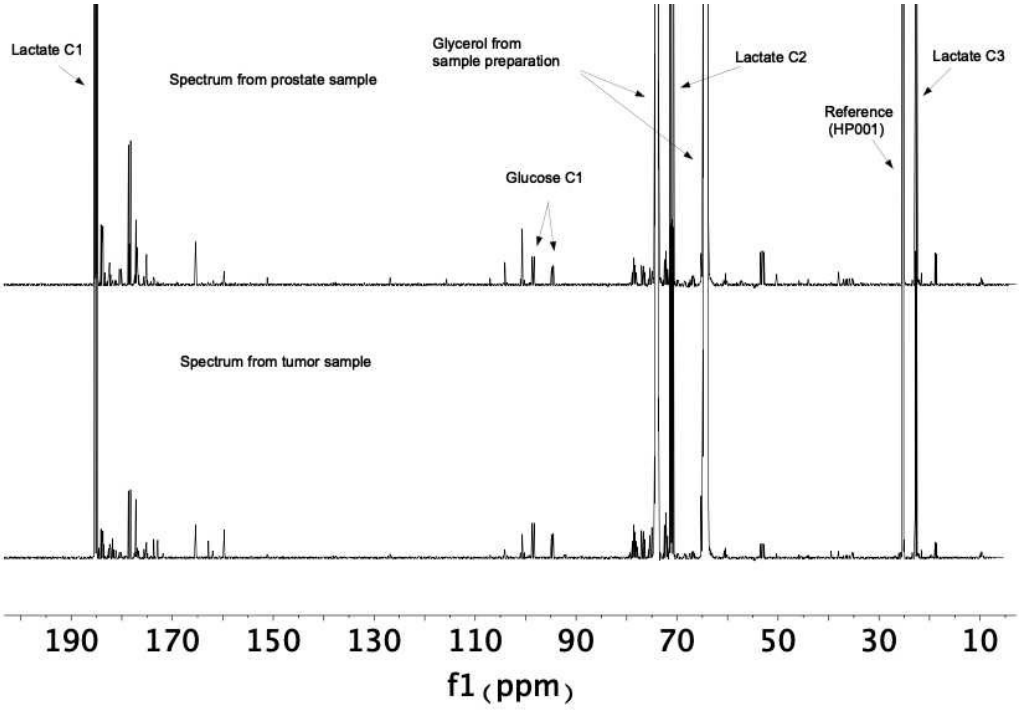

Figure 5.2: A representative dDNP fingerprint spectrum from a prostate sample (on top) and a tumour sample (on bottom).

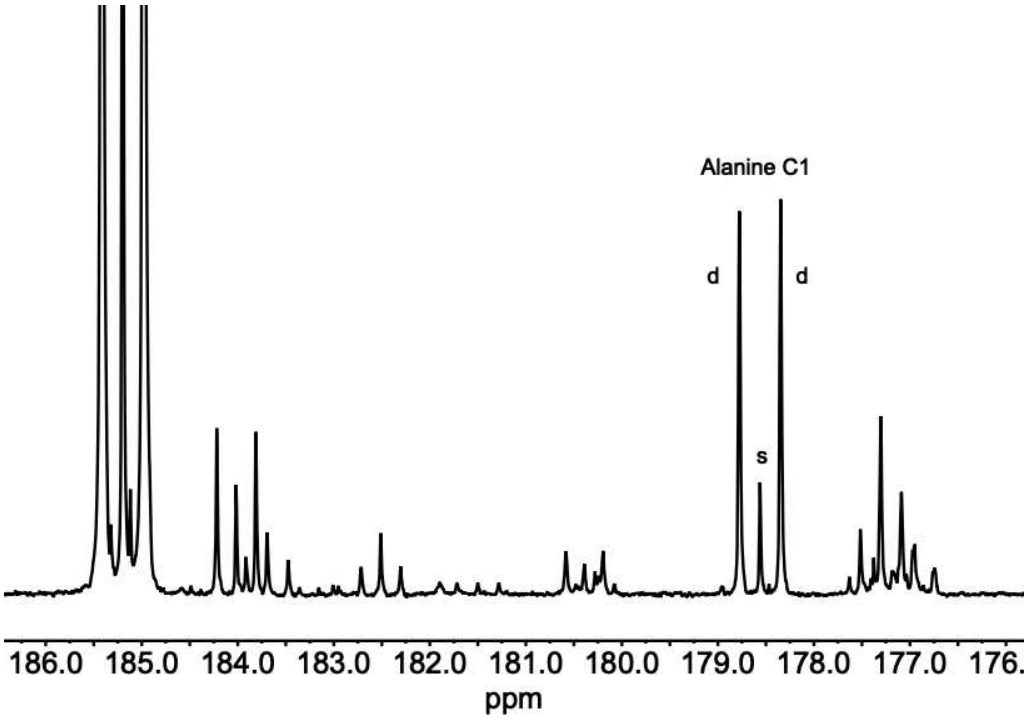

Figure 5.3: A zoom in on the carbonyl spectral region of the dDNP spectrum from a prostate and tumour sample.

In figure 5.3 the carbonyl area of the spectra is shown. Some of the signals, like the C1 of alanine placed at 178.6 ppm, shows a characteristic pattern of a doublet peak, surrounding smaller singlet, placed exactly in the middle of the doublet. This structure is consistent with two different isotopomers contributing to the signal; one where the ^{13}C neighbours another ^{13}C, causing the doublet splitting, and one where the ^{13}C neighbours a ^{12}C, causing no ^{13}C-^{13}C splitting, resulting in the singlet. Initially we assumed that the singlet signals were produced by the natural abundance ^{13}C from the metabolic pools present in the tissue before the introduction of the tracer. An analysis of the size of the signals ruled this simple explanation out: If the singlet was only a product of natural abundance ^{13}C, the actual quantity of the metabolic pool would be a hundred fold larger than what we observe, resulting in metabolic concentrations much larger than biologically possible. Therefore we concluded that the singlets observed were mainly products of the tracer having been combined with unlabelled metabolites present in the system, resulting in isotopomers of not fully labelled metabolites.[33]

5.1.1 *Classification of prostate vs. tumour using the full dDNP data set*

To explore the total information present in the dDNP fingerprints, we first chose to set up a data set including every metabolite peak from the spectra above the limit of detection (defined as having as SNR above 3.3). If five or more data points had a lower SNR for a feature, it was not included, as a feature. Signals from the glycerol and from the HP001 were excluded from the data, and integral values were measured relative to the HP001 signal. A total of 129 signals were included. All statistical analysis was done in Python.

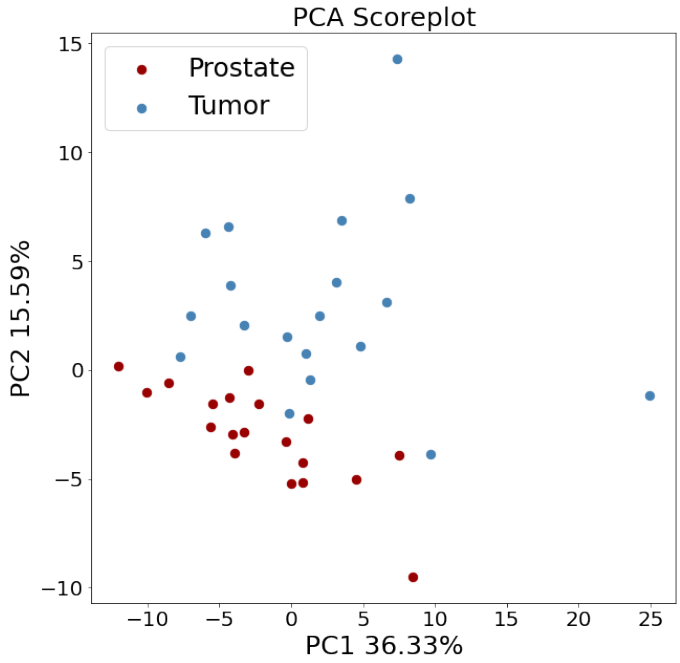

Figure 5.4: Score plot of the first two Principal components plotted against each other, from the PCA using all signals in the dDNP data set.

Figure 5.4, shows the results of a PCA done on this dataset, after mean subtraction and unit variance scaling. The plane made by the first two principal components accounts for a total of 51.92% of the variance in the data. There is a separation between the tumour and prostate data points to be seen in the plot, mostly on the second axis with the prostate data being confined to lower left of the plot and the tumours spreading out more to the top and the right. It seems that there is a greater variance in the tumour data, compared to the prostate, as the latter groups more together. The separation is not particularly strong; if the points were not labelled, it would not be clear that there are two groups in the data, and some tumour points are clearly closer to prostate points compared to other tumours.

RF feature ranking was performed by the same measures as described in chapter 4 except that the size of each forest was increased from 500 to 600 trees and the repetitions increased from 1.000 times to 10.0000 times. These increases were made to keep the SEM on the importance measures low, with the larger feature set compared to the first study. To avoid including a large number of features with an importance barely above zero, a significant importance cut-off was defined: A feature was deemed important if its measured importance minus its SEM were 5% or more of that for the feature with the highest importance found.

Figure 5.5, shows results of a feature ranking performed with RF. A total of 34 features were found to have a significant positive contribution to the separation between tumours and prostates. Out of these, the first six had a much higher measured importance, compared to the rest.

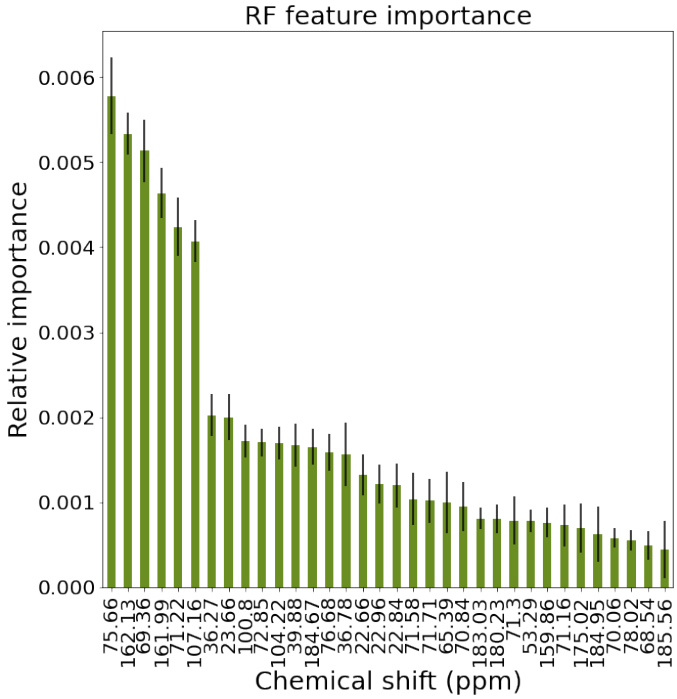

Figure 5.5: Analysis of the separation between prostate and tumour samples, using all signals in the data. The plot shows results of feature ranking performed with random forest, showing the 34 features found to be significant for the separation. Black bars are SEM.

SVM classification was set up with a linear kernel. The C-parameter was optimized for each

classification using leave-one-out cross-validation with $C = [2^{-5}, 2^{-4} \ldots 2^{5}]$ as possible options. Data was mean centred and unit-variance scaled before SVM was applied.

SVM on all 34 features found significant, gave a 97% (37 out of 38) correct classification between tumour and prostate samples, and using only the six highest ranked gave a 95% correct classification (36 out of 38 samples), with leave-one-out cross-validation. While this showed that the dDNP fingerprints have the ability to be used to classify between the tissue types, the results were not useful in terms of evaluating the metabolite production from the tracer: Of the six highest ranked features from RF, only two could be identified as labelled metabolites, one belonging to lactate and one belonging to glucose. The other four were singlet signals, three of which had a relatively low SNR (below 5).

5.1.2 *Classification of prostate vs. tumour using metabolite selected data*

In order to produce more interpretable results, in terms of how the prostate and tumour tissue metabolize the labelled glucose, a metabolite specific data sub-set was constructed, more like the one used in the cell line study. For each identified metabolite in the data one signal was included for each observed isotopomer, so for most metabolites both a ^{13}C-^{13}C douplet signal and a singlet signal were included as separate features. A total of 35 features were present in this metabolite data set.

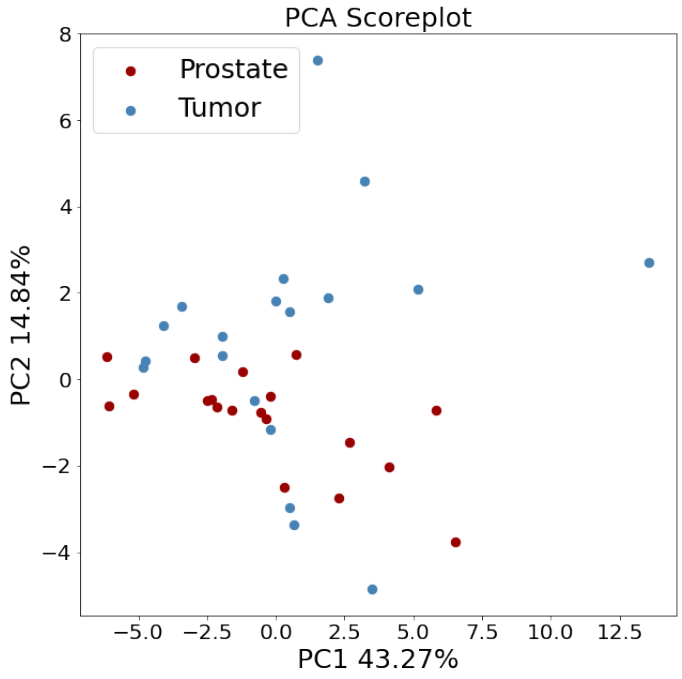

Figure 5.6: Score plot of the first two Principal components plotted against each other, from the PCA, using signals selected for specific metabolites.

The results of a PCA performed on the metabolite selected data set is shown in figure 5.6. The first two components plotted accounts for a total of 58.11% of the variance in the data. Compared to the PCA for the full data in figure 5.4, much of the separation between prostate and tumour

samples have disappeared. The prostate data points are still somewhat grouped together in the lower half of the plot, but the tumour data points are spread out through the plot. Clearly, some of the features removed from the data, had variance which contributed to separation the of the tissue types.

Exploring potential underlying features with PCA

A concern was that the difference in the age of the mice providing the samples and the difference in the size of the samples before the metabolite extraction, could be influencing the separation between the groups. Especially since the separation largely disappeared in the PCA plot for the metabolite selected data set (figure 5.6), we wanted to investigate if variance displayed in the plot was related to either sample weight or mouse age. If this was the case it could bias the classification, as the tumour samples were both more extreme in weights and the mice providing the tumour samples trended older.

In figure 5.7 the same PCA as in figure 5.6, is shown, but coloured to show the distribution of mouse age and calculated sample wet-weight for each data point, respectively. Circles are used to specify prostate data points and stars for tumours. Neither of the plots, seems to reveal any hidden structures in the data. If age or sample weight did explain most of the variance in the data, we would expect to see either a gradient through the plots, where the colors change from one end to the other, or clustering, where points of one color tend to be closer to one another. The closest thing to this that we see is that the two points with the highest weight, and thus the reddest colouring is located close together in the middle of the plot on the right, but as this describes only two of the data points and they are both tumours, this could be completely coincidental.

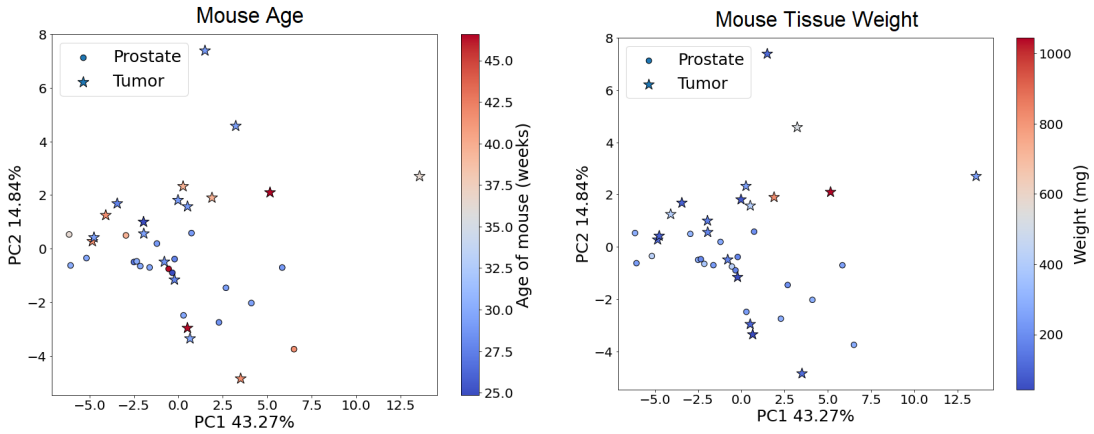

Figure 5.7: PCA analysis of the metabolite selected dDNP data. Tissue type is denoted by shape of points. On the left: Points are coloured after the age of the mouse that the sample was taken from. On the right: Points are coloured by the calculated weight of the tissue before metabolite extraction.

Of course, this surface exploration of how the factors of age and weight influence the variance in the data, does not mean that we can exclude that they influence the data and the results.

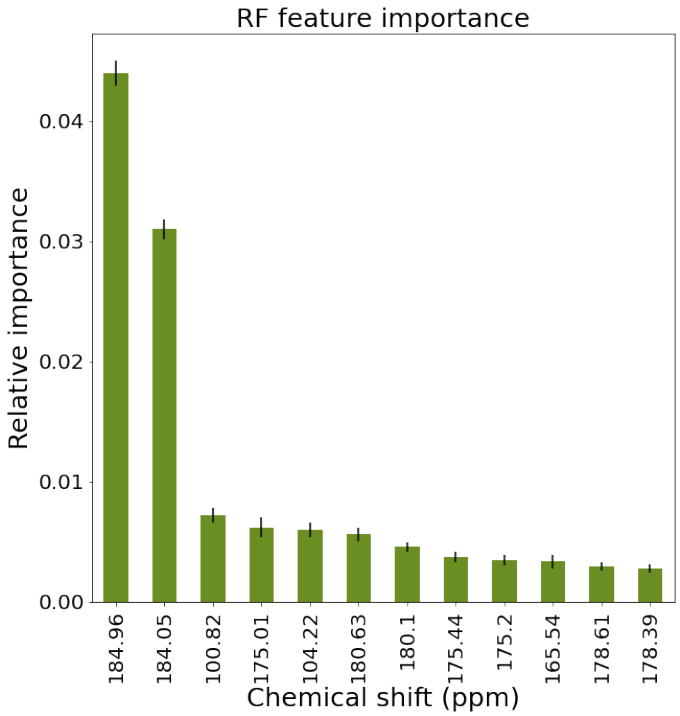

Figure 5.8: Analysis of the sepation between prostate and tumour samples, using signals selected for specific metabolites. Results of feature ranking performed with random forest, showing the 12 features found to be significant for the separation. Black bars are SEM.

However, since their influence seems to be less than that of our biological question of interest, we were satisfied in moving on with the analysis.

RF+SVM results on the metabolite selected data

Figure 5.8, shows the results of the RF feature ranking on the metabolite selected data. 12 features where found to have a significant measured importance, with two features scoring much higher than the rest; the signals at 184.96 and 184.05 ppm, assigned to the lactate carbonyl doublet and glutamate carbonyl singlet, respectively.

The features found significant with RF were iteratively used as input for the SVM classification algorithm. This meant that first a classification was made using only the highest ranking feature, thereafter one was made using both the first and the second and so on, with the final using all 12 features. The results of the classification with different number of features can be seen in table 5.1, along with the identity of the features. The best classification had a 95% success rate and was done by using all 12 significantly important features. This is of course a drop from the 97% success rate found when using the significantly important features from the full data set, but we have traded this for a result based only on 12 signals readily identifiable in terms of the glucose metabolism we sat out to investigate.

Table 5.1: Results from RF+SVM analysis on metabolite specific data. The 12 features found significant with RF, ranked by importance. SVM classification results reported are obtained when including the metabolite and every metabolite found to be more important.

Identity	Abbreviation	Chemical shift	SVM classification
Lactate - C1 Doublet	lac	184.96	81.6%
Glutamate - C5 singlet	glu	184.05	92.1%
Beta fructofuranose - singlet	b-ff	100.82	89.5%
Serine - C1 singlet	ser	175.01	92.1%
Alfa fructofuranose - singlet	a-ff	104.22	92.1%
Glutamine C5 - doublet	gln	180.63	92.1%
Aspartate C1 - singlet	asp	180.10	92.1%
Glycine C1 - singlet	gly,s	175.44	92.1%
Glycine C1 - doublet	gly,d	175.20	92.1%
Urea	urea	165.54	92.1%
Alanine C1 - singlet	ala,s	178.61	92.1%
Alanine C1 - doublet	ala,d	178.39	94.7%

5.1.3 *Redundancy in data for Random Forest feature ranking*

A point of interest for interpreting the results of the RF feature ranking, is how covariance in the features could influence the measured importance. As described in section 4.3.1, the importance is measured by how much worse the classification becomes, when the values of that single feature is randomized. A logical consequence of this is that a feature that separates the data well, but is highly correlated with other features in the data, would rank lower in importance compared to a feature with an equal ability to separate, but with no correlations. When the first feature gets randomized, the information it provided to the data will still be present in the correlated features.

To illustrate this effect, a test was run on dataset with artificially added redundant information. To limit the random forest run-time, a base data set using only the 12 features found important in the metabolite specific data set was used, and the number of repetitions of the RF algorithm was lowered to 1.000. The redundancy was introduced to the data in the simplest way possible; by including the same feature multiple times. We chose glutamate singlet (glu), as that feature had come out as a clear number second, in the original ranking, more important than every other feature except one.

Figure 5.9 shows the results of this redundancy experiment. In the plot on the top left, nothing has been altered in the data, and the importance of the glu feature (highlighted in purple) is the ranking, we were expecting. In the plot on the top right, one copy of glu has been added, and while the two glu's are still second and third ranked, each of their scores are lowered relative to the other features. In the plot on the bottom right, five copies have been added for a total of six glu features, and now the several other features out ranked them in importance. And finally, in the bottom right plot, ten glu copies have been added, and their importance is now barely above or generally below zero.

Of course, the situation of the same exact feature is present ten times over in data, is rather artificial, but these results show why this RF feature ranking method pairs well with the metabolite

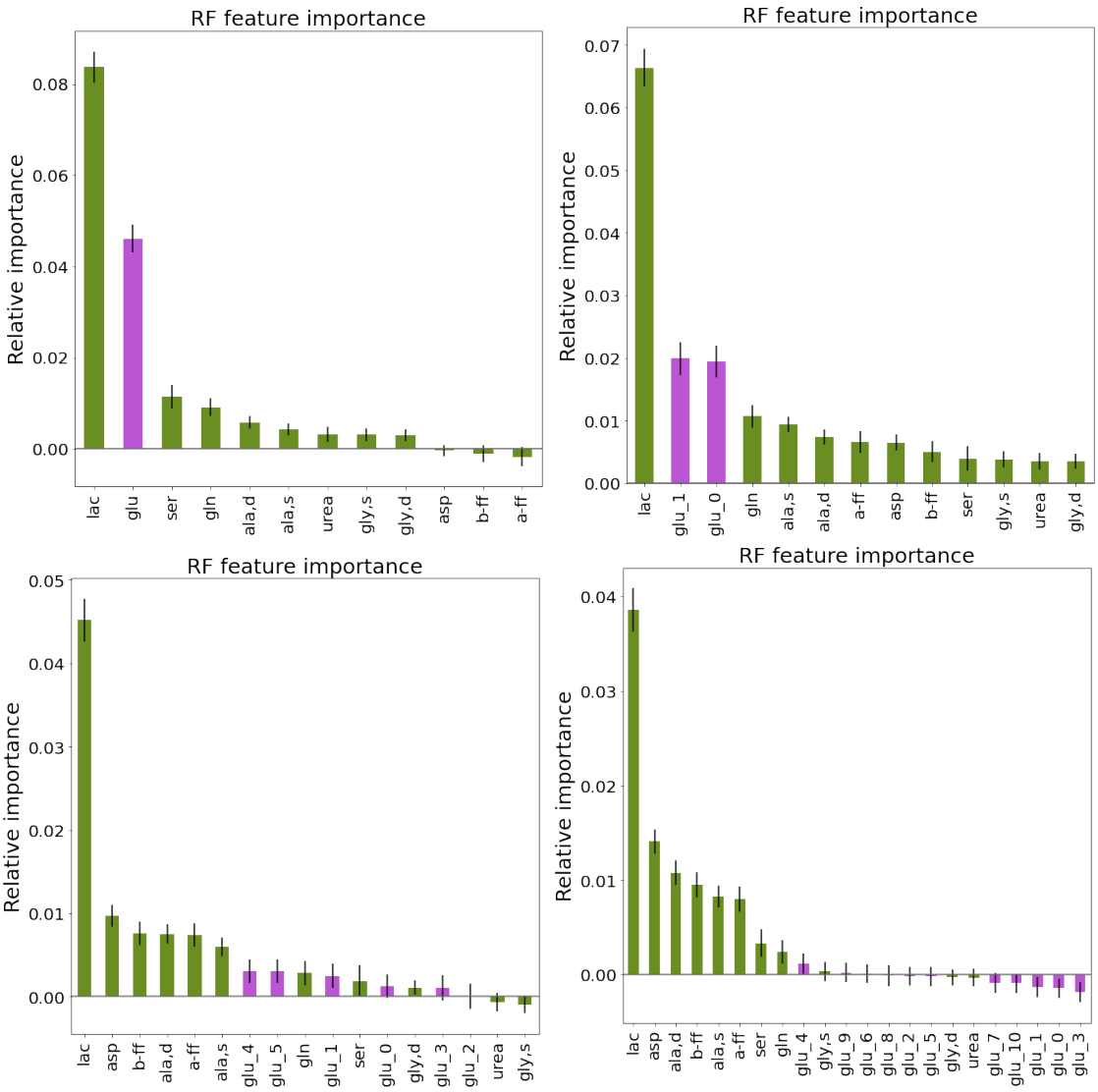

Figure 5.9: Random forest feature extraction with redundancy added to the data, measured importance for all features is plotted. Top left: No changes made to the data, glutamate importance highlighted in purple. Top right: Data with one copy of the glutamate feature added. Bottom left: Data with five copies of the glutamate feature added. Bottom right: Data with ten copies of the glutamate feature added.

selected data sets. If every peak in the spectra are used as separate features, and some metabolites, like lactate for instance, provides several peaks, which apart from the variation in noise, should correlate completely, then the importance of lactate would be lowered relatively to a metabolite providing fewer signals in the spectra. We also have to be mindful about different metabolites correlating with each other. In figure 5.9 it can be seen that the importance of urea and both glycine signals also starts to fall, with the addition of the glutamate duplicates. And curiously, aspartate and the two fructofuranose signals, which of course were found significant in the full, metabolite selected data set, were not found important when only the 12 top ranking features were included and no duplicates were added, but became important again as redundant information were added.

The important take away, is to remember that we are looking a relative importance between the features of a specific data set. How we construct our data is vital for whether we are able to measure the importance of specific metabolites.

5.2 NOESY DATA ANALYSIS - THE AUTO-READ SPECTRA

Along with the dDNP spectra, 1D proton NOESY spectra of the same samples were also obtained and analysed. Initial processing of the NOESY spectra was done in Bruker TopSpin (version 4.0.7), where a 0.3 Hz line broadening was applied and the phasing was adjusted. Then the spectra were transferred to MatLab[104] for further processing. The spectra were referenced to the TSP peak at 0 ppm and the area of interest was set from 0.05 to 10 ppm, with the suppressed water peak cut-out (4.59 to 5.04 ppm). To overcome small chemical shift differences between the spectra, spectral adjustment were done with ICOshift (version 3.0),[105] where the spectra were cut into smaller regions and the best possible alignment was made for each region. Finally, the spectral data was transferred to Python for further analysis.

There were some areas of the spectra sparse enough that the ^{13}C labelled metabolite signals could be identified, from chemical shift values and splitting patterns. The lactate and alanine signals shown in figure 5.10 on the left, have characteristic pattern of an uncoupled signal is surrounded by side-bands, caused by the H-^{13}C coupling. Other areas, however, like the one shown to the right in figure 5.10, were so crowded that separating and assigning each signal would be impossible. The inherent problem of the relative narrow chemical shift range in the proton spectrum, resulting in spectral crowding, was exacerbated for our data from the side-band splitting in the metabolite products of the ^{13}C labelled glucose tracer. We therefore opted to use automatic binning, to be able to use information from the entire spectrum, with minimum work of defining the features. The spectra were integrated into uniform bins of 0.2 ppm in length.

As it has been shown that random fluctuations in noise features can have a large impact on PCA on auto-binned NMR data,[106] we used a noise filter to remove most of the features with out any signal. We chose a noise feature in an area of the spectra where the noise level was high; the bin from 5.27-5.29 ppm. The noise filter was sat as the highest value in this representative noise bin. Any features where no value were higher than this filter, was discarded from the data set. A total of 176 noise features were removed this way, leaving 298 features in the data. Data

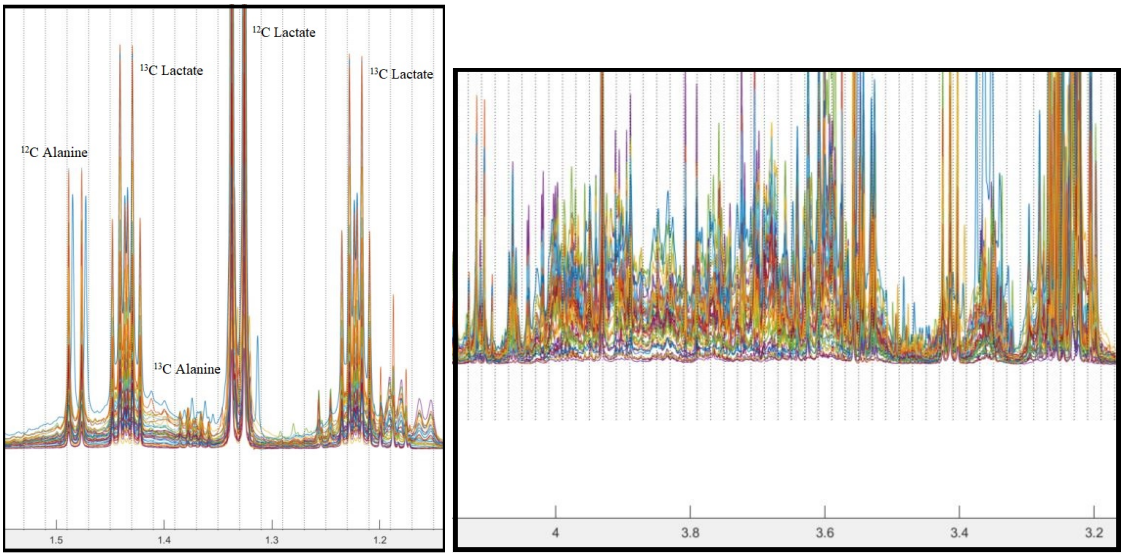

Figure 5.10: Examples from the Noesy spectra. Vertical lines show the locations of the bins. On the left: Relatively sparse spectral region, where the ^{13}Ccoupled satellites can easily be recognised. On the right: Very crowded spectral region, where metabolite assignment is impossible.

was normalized to the TSP signal and to the tissue weight of the sample.

Even with the noise filter, we could not be sure to remove every feature without signal from the data - at least not without also removing at lot of the smallest peaks along with them, if we had increased the filter value. To avoid scaling up the remaining noise, we chose not to apply unit variance scaling to the data before the PCA, instead the data was mean centered and Pareto scaled. With pareto scaling the data is divided by the square root of the the standard deviation, instead of the full standard deviations, giving the benefit of not scaling small fluctuations in noise up to a level with the largest variation in the signals. The drawback of this solution is that the data will be biased towards the larger signals.[107]

The results of the PCA can be seen in figure5.11. The plane of the two first components makes up 70.68% of the variance in the data. There seems to be a better separation between tumour and prostate samples in NOESY data, compared to the dDNP data sets. While the tumour data points are still somewhat more spread out, apart from the outliers, they are collected in the left side of the plot. Two prostate data points are closer to the tumours than to the other prostates, but otherwise the prostates are clustered together. Rather surprising; two tumour data points are completely separated from the rest at the right side of the plot, on the other side of the prostate samples. These two tumour data points did not particularly cluster with the prostates in the dDNP data (they are the two left most tumour data points in figure 5.4 and figure 5.8), but they were the two errors in the SVM classification using the six most important features in the full dDNP dataset, and one of them was an error in best classification with the metabolite selected data too. Nothing from the appearance of the tissue when it was taken from the mice, indicated that these samples were likely to be misclassified, but of course, dissection of mice prostates is delicate work, and as no histology was performed to cement the tissue grading, it is entirely

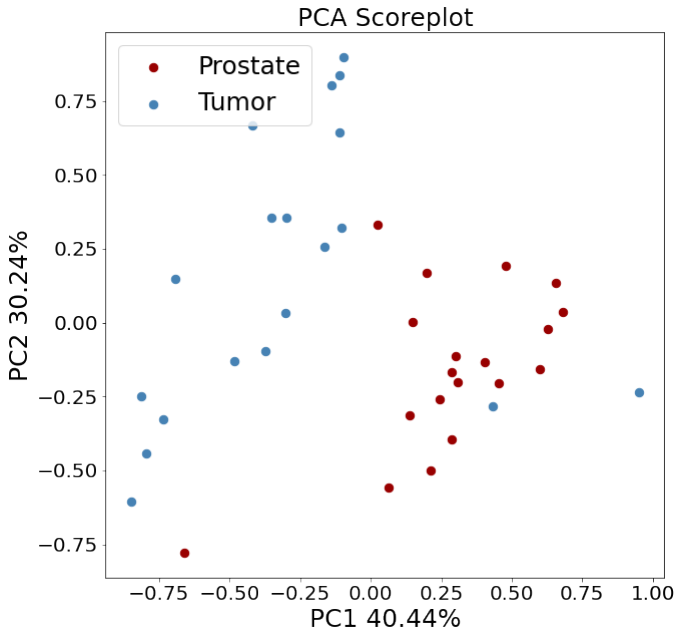

Figure 5.11: Score plot of the first two Principal components plotted against each other, from the PCA, made with the auto-read and Pareto scaled NOESY data.

within the realm of possibilities that some samples could have been misclassified.

In figure 5.12, the results from the RF feature ranking of the NOESY data is shown. A total of 20 features were found to have significant importance, with the top ranking feature having a much higher measured importance compared to the rest.

Like the dDNP data, the important features found, were mean centred and unit variance scaled, before iteratively being used as input for the SVM classification. Only the top three important features (bins starting at 7.13, 6.81 and 7.11 ppm) were found to be needed to support a 100% correct, leave-one-out cross-validated classification between prostate and tumour samples. There is reason to be highly sceptical of these results. A view of the spectra, zoomed in on the three features perfectly separating the two classes, is shown in figure 5.13. The defining characteristics of the classification, seems to be some very broad peaks, possible from a contamination with larger molecules. Especially since the PCA plot identified the two clear outliers and the separation is based on as flimsy a ground as these three features, it seems clear that the RF+SVM algorithm has over-fitted in this case. With only 38 samples and more than 300 input features, some of them still dominated by noise, there is too much room to create a successful classification where none should exist. If the RF+SVM algorithm should work with auto-read data, either many more samples should be collected or a much more stringent cross-validation protocol should be put in place.

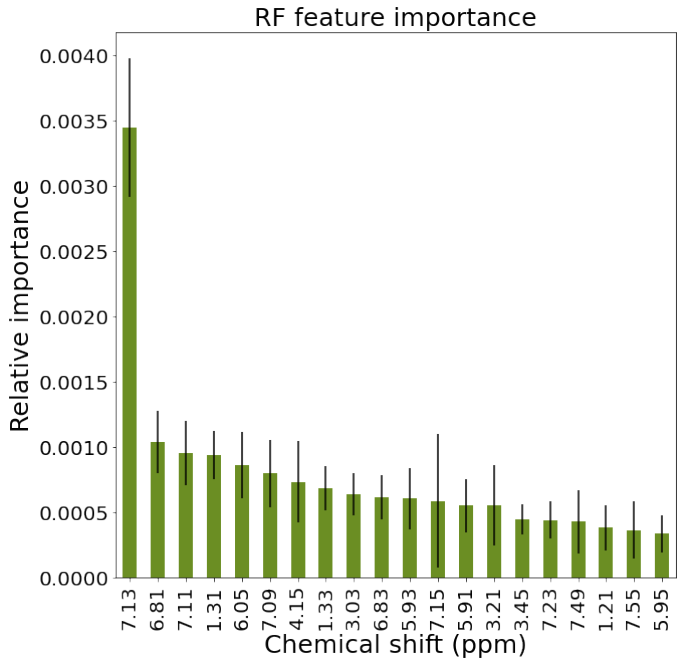

Figure 5.12: Analysis of the separation between prostate and tumour samples, using NOESY data. The figure shows the results of feature ranking performed with random forest, showing the 20 features found to be significant for the separation. Black bars are SEM.

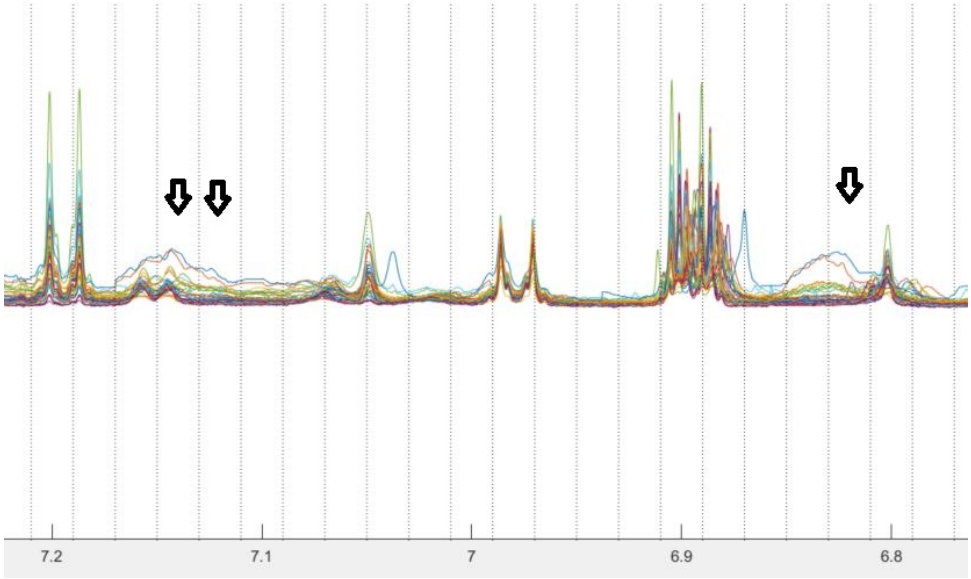

Figure 5.13: The NOESY spectra, zoomed to show the three features (marked with arrows) supporting the 100% correct classification obtained.

Table 5.2: Leave-one-out cross-validated results of testing the RF+SVM method on randomized data. The range of results of the five test is noted, with the average in parenthesis.

	Full dDNP data	**Metabolite selected data**
Significant important features	7-19 (11.6)	2-7 (5.2)
Highest success rate	65.8-76.3 (72.1) %	55.2-68.4 (59.5) %
Features needed for highest success rate	2-12 (6.6)	1-6 (2.6)
Success rate without feature selection	39.5 - 52.6 (46.8) %	50 - 60.5 (57.4) %
PLS-DA success rate	44.7 - 63.2 (51.6) %	47.4 - 60.5 (53.7) %

5.3 RESULTS ON SHUFFLED CLASSES

With the discouraging results on the NOESY data set, concerns were raised on whether the results obtained on the dDNP data actually reflected a biological separation of the tumour and prostate samples, or they too were over-fitted to the data; a 95% classification success rate is not impressive if an equal rate could have been made on pure noise. To verify this, we decided to test out the algorithm on data where no consistent classification should be made.

The experiment was made by shuffling the labels in the out-put variable i.e. whether a sample was "prostate" or "tumour". Other methods of generating a nonsense classification were also considered; the values of each feature could have been shuffled between the data points or entirely new datasets made up of randomly generated values could have been made. However, by keeping the input data intact and only shuffling the labels, we get to test the algorithm on realistic metabolomics data, just without a real, biological separation to be found. If factors like correlation between features or the distribution of values in certain features, contribute to make the algorithm over-fit, we are keeping them in the data, by testing this way. In addition to the RF+SVM method, classifications were also made using SVM on data with out feature reduction and with PLS-DA.

Table 5.2 shows the results of the shuffled label experiment. There seemed to be a degree of over-fitting happening with the full dDNP data set; the mean classification success rate of 72.1% is way higher than the 46.8% for the SVM without RF feature reduction and the 51.6% for the PLS-DA. Of course, the highest rate of 76.3% is still a good way from the 97% we saw with the real classification, so a true separation between the tumour and prostate samples were found, though it might not be as solid as we would have liked. The reduced sizes of the metabolite selected data set, seems to have alleviated the problem, the mean success rate found here, was only 59.5%, comparable to the 57.4% and 53.7% for the SVM with no reduction and the PLS-DA respectively.

Compared with the real classification, where 34 features were found significant for the full dDNP data and 12 for the metabolite selected, the numbers found in the labelled shuffled tests were much lower. These wete between 7 and 19 for the full data and between 2 and 7 for the metabolite selected. In the case where only a small number of features in the data were found to support the separation, this could indicate an artificial separation.

5.4 DISCUSSION AND CONCLUSION

Our investigation of the classification between tumour and prostate tissue from the TRAMP mice, confirms that the dDNP SIRM fingerprints do contain the information needed to separate between degrees of aggressivity in prostate cancer, not just in the simple cell line case, as we saw in the previous study, but also when working with extracts from complex tissue samples.

The RF+SVM method of feature ranking and classification, were found to be ideally suited to the sparse dDNP spectra, as this algorithm combination makes it possible to select the specific signals that contains the information produced from our labelled tracer. This is obtained by keeping the redundancy in the data low, and thus giving a better importance measure for some metabolites, and by keeping the number of features low compared to the number of samples in the study, and in that way limiting the possibility of overfitting.

The challenge of finding metabolite features important for the classification between tissue types, was embarked upon, without a clear definition of what "important" really should entail. As we have shown, the importance measured for one feature, with the RF algorithm used here, is conditional to the importance of other features in the data set - a so called partial importance, in contrast to marginal importance were each feature is taken as single predictor in it self. There is no settled consensus on which of these perspectives is the "correct" - different situations can benefit for different ways of measuring importance.[108] No matter what, it is of course important to be concious of how to interpret the results. Different methods of ranking features in importance using a permutation based scheme with RF have been shown to perform well, ours is relatively simple, and improvements could be made.[109–111]

The tendency to over-fit on the larger datasets, could stem from an inherent problem with the RF+SVM algorithm in its current form. While Leave-One-Out cross-validation is applied to the SVM classification, this part of the analysis builds on top of the feature ranking, which all samples (including the one used to validate) were used to form. It was not feasible to build the RF feature ranking into a cross-validation loop along with the SVM, as the RF algorithm already took multiple hours to run, with its internal validation. Another solution could be to use larger datasets, with sample size big enough that it could be possible to split it into two parts; one for feature ranking with RF and the other for classification with SVM. If a feature was both found significant by RF on the first data sub-set and improved classification with SVM on the second, we could be much more confident that it was not just selected due to random noise fluctuations. With further improvements on the automation of the dDNP process, larger data sets will be easier to produce in the future.

CONCLUSION AND FURTHER PERSPECTIVE

6

Through the studies in this thesis, we have established dDNP SIRM fingerprinting as a method for metabolomics. We have combined the benefits of high SNR and high spectral resolution of the dDNP NMR fingerprint, with the ability to monitor metabolic production from SIRM. The outcome is a method for easy identification and quantification of metabolites relevant for cancer biology. We have also provided the first application for this method developed in a complete study using prostate cancer tissue from animals.

Specifically, we found that the obtained dDNP SIRM spectra did contain sufficient information for biological classification between prostate cancer samples of different degrees of aggressivity. In the cell line study signals from four different metabolites were found to support a 96.9% successful classification, and in the mouse tissue study, twelve features supported a 94.7% success classification with the RF+SVM algorithm.

The combination of RF for feature selection and SVM for classification was found to work well with the obtained data, when each feature was selected to represent a unique metabolite. This approach yielded results directly interpretable with respect to the metabolism of the applied tracer. On the larger, less curated datasets RF+SVM were found to over-fit, and be of less value results in terms of feature selection.

Improvements made to the hardware between the two studies, in particular installation of a cryoprobe and development of a transfer line between the dDNP and NMR magnets, proved vital to obtaining signals of all but the most dominating metabolites in the mouse tissue study. With this increase in sensitivity and decrease in transfer time, even the short $T1$ carbons from the protonated glucose tracer were measurable.

Further improvements to the dDNP SIRM fingerprint assay can be made by implementing available technological developements:

1. An increase in SNR up to an approximate factor of two can be obtained by polarizing the extracted metabolite samples at higher field strength and lower core temperature compared to the Hypersense (3.3 T and 1.4 K).[112]

2. Repeatability and accuracy could be improved for field sensitive metabolite signals by construction of a magnet shielded transfer line. This would minimize differential polarization loss of metabolite signals from the sample passing through low magnetic field areas.[81]

3. A shorter delay between sample dissolution and acquisition could be achieved with Hellmanex treatment of the NMR tube. Such treatment has been shown to prevent microbubles in the sample.[15]

Ideas for a completely different dissolution process has been published. Specifically, a method for transferring a hyperpolarized sample as a solid from the polarizer to the NMR magnet at a rapid speed, before dissolution in the NMR magnet has been demonstrated.[113]. Such

developments where the transfer time is much faster than the approx. 1s transfer in our method could be interesting. It is however important to note that the high spectral resolution and high repeatability in the dDNP SIRM fingerprint method should not be compromised on the expense of sample transfer speed.

A challenge with using the combination of RF+SVM for feature selection and classification was the size of the datasets, which prevented proper training, validation and testing of the algorithms. There were simply not enough data points to make the needed data splits for such evaluation, since dDNP SIRM fingerprinting is not yet a high throughput method. Production of large scale dDNP datasets are limited by a current 1.5 hour polarization time. Also, even with the automated transfer line, dDNP is a hands-on procedure: A scientist has to be present to handle the sample insertion, the initiation of the transfer and preparation for the next sample. Data acquisition cannot happen automatically over-night. Although improvements to the polarization medium could cut down polarization time, allowing for a higher sample throughput,[114] hardware improvements are needed to improve sample turnover times. Design of multi-sample polarizers such as the clinical polarizer, SpinLab, has been published.[115] Even more interesting is the new ideas about storing frozen hyperpolarized samples in low field and cryogenic temperatures outside the polarizer for dissolution.[116] Such method could separate the DNP process from dissolution and NMR acquisition. Samples could be polarized and extracted for storage and sample accumulation. The stored hyperpolarized samples could be melted and connected with fast NMR sample handling.

The first application work with the dDNP SIRM fingerprint method using prostate cancer tissue from mice to extract metabolic biomarkers pointed out the possible importance of assessing several metabolites using a combination of ^{13}C tracers. Of particular note, fructose could be of interest for further studies, as fructose metabolism has been found to be altered in an array of cancers, including prostate cancer.[117] Further work should be performed to evaluate whether combinations of the metabolites could have relevance as a biomarker for prostate cancer using real-time dDNP NMR.

Metabolic pathway analysis could be performed with the data obtained in the mouse tissue study. Since different isotopomers were measured to have been produced as products of the glucose tracer, this could be an avenue to evaluate the dDNP SIRM fingerprint as a method for flux analysis.

BIBLIOGRAPHY

[1] Jan H Ardenkjær-Larsen, Björn Fridlund, Andreas Gram, Georg Hansson, Lennart Hansson, Mathilde H Lerche, Rolf Servin, Mikkel Thaning, and Klaes Golman. Increase in signal-to-noise ratio of> 10,000 times in liquid-state nmr. *Proceedings of the National Academy of Sciences*, 100(18):10158–10163, 2003.

[2] Ferdia A Gallagher, Mikko I Kettunen, Sam E Day, De-En Hu, Jan Henrik Ardenkjær-Larsen, Pernille R Jensen, Magnus Karlsson, Klaes Golman, Mathilde H Lerche, Kevin M Brindle, et al. Magnetic resonance imaging of ph in vivo using hyperpolarized 13 c-labelled bicarbonate. *Nature*, 453(7197):940–943, 2008.

[3] T Harris, H Degani, and L Frydman. Hyperpolarized 13c nmr studies of glucose metabolism in living breast cancer cell cultures. *NMR in Biomedicine*, 26(12):1831–1843, 2013.

[4] Alessia Lodi, Sarah M Woods, and Sabrina M Ronen. Treatment with the mek inhibitor u0126 induces decreased hyperpolarized pyruvate to lactate conversion in breast, but not prostate, cancer cells. *NMR in biomedicine*, 26(3):299–306, 2013.

[5] Sarah J Nelson, John Kurhanewicz, Daniel B Vigneron, Peder EZ Larson, Andrea L Harzstark, Marcus Ferrone, Mark Van Criekinge, Jose W Chang, Robert Bok, Ilwoo Park, et al. Metabolic imaging of patients with prostate cancer using hyperpolarized [1-13c] pyruvate. *Science translational medicine*, 5(198):198ra108–198ra108, 2013.

[6] John Kurhanewicz, Daniel B Vigneron, Jan Henrik Ardenkjaer-Larsen, James A Bankson, Kevin Brindle, Charles H Cunningham, Ferdia A Gallagher, Kayvan R Keshari, Andreas Kjaer, Christoffer Laustsen, et al. Hyperpolarized 13c mri: path to clinical translation in oncology. *Neoplasia*, 21(1):1–16, 2019.

[7] Niki Zacharias, Jaehyuk Lee, Sumankalai Ramachandran, Sriram Shanmugavelandy, James McHenry, Prasanta Dutta, Steven Millward, Seth Gammon, Eleni Efstathiou, Patricia Troncoso, et al. Androgen receptor signaling in castration-resistant prostate cancer alters hyperpolarized pyruvate to lactate conversion and lactate levels in vivo. *Molecular imaging and biology*, 21(1):86–94, 2019.

[8] Mark J Albers, Robert Bok, Albert P Chen, Charles H Cunningham, Matt L Zierhut, Vickie Yi Zhang, Susan J Kohler, James Tropp, Ralph E Hurd, Yi-Fen Yen, et al. Hyperpolarized 13c lactate, pyruvate, and alanine: noninvasive biomarkers for prostate cancer detection and grading. *Cancer research*, 68(20):8607–8615, 2008.

[9] Peder EZ Larson, Hsin-Yu Chen, Jeremy W Gordon, Natalie Korn, John Maidens, Murat Arcak, Shuyu Tang, Mark Criekinge, Lucas Carvajal, Daniele Mammoli, et al. Investigation

of analysis methods for hyperpolarized 13c-pyruvate metabolic mri in prostate cancer patients. *NMR in Biomedicine*, 31(11):e3997, 2018.

[10] Stacy Loeb, Marc A Bjurlin, Joseph Nicholson, Teuvo L Tammela, David F Penson, H Ballentine Carter, Peter Carroll, and Ruth Etzioni. Overdiagnosis and overtreatment of prostate cancer. *European urology*, 65(6):1046–1055, 2014.

[11] Henrik Gutte, Adam Espe Hansen, Helle Hjorth Johannesen, Andreas Ettrup Clemmensen, Jan Henrik Ardenkjær-Larsen, Carsten Haagen Nielsen, and Andreas Kjær. The use of dynamic nuclear polarization 13c-pyruvate mrs in cancer. *American journal of nuclear medicine and molecular imaging*, 5(5):548, 2015.

[12] Magnus Karlsson, Pernille R Jensen, Jens Ø Duus, Sebastian Meier, and Mathilde H Lerche. Development of dissolution dnp-mr substrates for metabolic research. *Applied Magnetic Resonance*, 43(1):223–236, 2012.

[13] Jean-Nicolas Dumez, Jonas Milani, Basile Vuichoud, Aurélien Bornet, Julie Lalande-Martin, Illa Tea, Maxime Yon, Mickaël Maucourt, Catherine Deborde, Annick Moing, et al. Hyperpolarized nmr of plant and cancer cell extracts at natural abundance. *Analyst*, 140(17):5860–5863, 2015.

[14] Aurélien Bornet, Mickaël Maucourt, Catherine Deborde, Daniel Jacob, Jonas Milani, Basile Vuichoud, Xiao Ji, Jean-Nicolas Dumez, Annick Moing, Geoffrey Bodenhausen, et al. Highly repeatable dissolution dynamic nuclear polarization for heteronuclear nmr metabolomics. *Analytical chemistry*, 88(12):6179–6183, 2016.

[15] Arnab Dey, Benoît Charrier, Estelle Martineau, Catherine Deborde, Elodie Gandriau, Annick Moing, Daniel Jacob, Dmitry Eshchenko, Marc Schnell, Roberto Melzi, et al. Hyperpolarized nmr metabolomics at natural 13c abundance. *Analytical chemistry*, 92(22):14867–14871, 2020.

[16] Mathilde H Lerche, Demet Yigit, Anne B Frahm, Jan Henrik Ardenkjær-Larsen, Ronja M Malinowski, and Pernille R Jensen. Stable isotope-resolved analysis with quantitative dissolution dynamic nuclear polarization. *Analytical chemistry*, 90(1):674–678, 2018.

[17] Jeremy K Nicholson and John C Lindon. Metabonomics. *Nature*, 455(7216):1054–1056, 2008.

[18] Anthony C Dona, Michael Kyriakides, Flora Scott, Elizabeth A Shephard, Dorsa Varshavi, Kirill Veselkov, and Jeremy R Everett. A guide to the identification of metabolites in nmr-based metabonomics/metabolomics experiments. *Computational and structural biotechnology journal*, 14:135–153, 2016.

[19] Gary J Patti, Oscar Yanes, and Gary Siuzdak. Metabolomics: the apogee of the omics trilogy. *Nature reviews Molecular cell biology*, 13(4):263–269, 2012.

[20] Warwick B Dunn, David I Broadhurst, Helen J Atherton, Royston Goodacre, and Julian L Griffin. Systems level studies of mammalian metabolomes: the roles of mass spectrometry and nuclear magnetic resonance spectroscopy. *Chemical society reviews*, 40(1):387–426, 2011.

[21] Kerem Bingol. Recent advances in targeted and untargeted metabolomics by nmr and ms/nmr methods. *High-throughput*, 7(2):9, 2018.

[22] Xiaojing Liu and Jason W Locasale. Metabolomics: a primer. *Trends in biochemical sciences*, 42(4):274–284, 2017.

[23] Abdul-Hamid Emwas, Raja Roy, Ryan T McKay, Leonardo Tenori, Edoardo Saccenti, GA Gowda, Daniel Raftery, Fatimah Alahmari, Lukasz Jaremko, Mariusz Jaremko, et al. Nmr spectroscopy for metabolomics research. *Metabolites*, 9(7):123, 2019.

[24] Eli Riekeberg and Robert Powers. New frontiers in metabolomics: from measurement to insight. *F1000Research*, 6, 2017.

[25] Thomas L James. Fundamentals of nmr. *Online Textbook: Department of Pharmaceutical Chemistry, University of California, San Francisco*, pages 1–31, 1998.

[26] David I Ellis, Warwick B Dunn, Julian L Griffin, J William Allwood, and Royston Goodacre. Metabolic fingerprinting as a diagnostic tool. *Pharmacogenomics*, 8(9):1243–1266, 2007.

[27] Ryan T Mckay. How the 1d-noesy suppresses solvent signal in metabonomics nmr spectroscopy: an examination of the pulse sequence components and evolution. *Concepts in Magnetic Resonance Part A*, 38(5):197–220, 2011.

[28] Chaevien S Clendinen, Brittany Lee-McMullen, Caroline M Williams, Gregory S Stupp, Krista Vandenborne, Daniel A Hahn, Glenn A Walter, and Arthur S Edison. 13c nmr metabolomics: Applications at natural abundance. *Analytical chemistry*, 86(18):9242–9250, 2014.

[29] Magesh Muthu and Anders Nordström. Current status and future prospects of clinically exploiting cancer-specific metabolism—why is tumor metabolism not more extensively translated into clinical targets and biomarkers? *International journal of molecular sciences*, 20(6):1385, 2019.

[30] Cholsoon Jang, Li Chen, and Joshua D Rabinowitz. Metabolomics and isotope tracing. *Cell*, 173(4):822–837, 2018.

[31] Teresa W-M Fan, Pawel K Lorkiewicz, Katherine Sellers, Hunter NB Moseley, Richard M Higashi, and Andrew N Lane. Stable isotope-resolved metabolomics and applications for drug development. *Pharmacology & therapeutics*, 133(3):366–391, 2012.

[32] Joerg M Buescher, Maciek R Antoniewicz, Laszlo G Boros, Shawn C Burgess, Henri Brunengraber, Clary B Clish, Ralph J DeBerardinis, Olivier Feron, Christian Frezza, Bart Ghesquiere, et al. A roadmap for interpreting 13c metabolite labeling patterns from cells. *Current opinion in biotechnology*, 34:189–201, 2015.

[33] F Mark H Jeffrey, Arun Rajagopal, Craig R Malloy, and A Dear Sherry. C-nmr: a simple yet comprehensive method for analysis of intermediary metabolism. *Trends in biochemical sciences*, 16:5–10, 1991.

[34] Ronald C Bruntz, Andrew N Lane, Richard M Higashi, and Teresa W-M Fan. Exploring cancer metabolism using stable isotope-resolved metabolomics (sirm). *Journal of Biological Chemistry*, 292(28):11601–11609, 2017.

[35] Otto Warburg. On the origin of cancer cells. *Science*, 123(3191):309–314, 1956.

[36] Camille Lehuédé, Fanny Dupuy, Rebecca Rabinovitch, Russell G Jones, and Peter M Siegel. Metabolic plasticity as a determinant of tumor growth and metastasis. *Cancer research*, 76(18):5201–5208, 2016.

[37] Eric Eidelman, Jeffrey Twum-Ampofo, Jamal Ansari, and Mohummad Minhaj Siddiqui. The metabolic phenotype of prostate cancer. *Frontiers in oncology*, 7:131, 2017.

[38] Jiangsha Zhao, Jieran Li, Teresa WM Fan, and Steven X Hou. Glycolytic reprogramming through pck2 regulates tumor initiation of prostate cancer cells. *Oncotarget*, 8(48):83602, 2017.

[39] Zhengzheng Pan and Daniel Raftery. Comparing and combining nmr spectroscopy and mass spectrometry in metabolomics. *Analytical and bioanalytical chemistry*, 387(2):525–527, 2007.

[40] Ludwig Boltzmann. Ableitung des stefanschen gesetzes, 1) betreffend die abhängigkeit der wärmestrahlung von der temperatur aus der elektromagnetischen lichttheorie. pages 152–156, 1978.

[41] Timothy DW Claridge. *High-resolution NMR techniques in organic chemistry*, volume 27. Elsevier, 2016.

[42] Jan Henrik Ardenkjaer-Larsen, Haukur Jóhannesson, J Stefan Petersson, and Jan Wolber. Hyperpolarized molecules in solution. In *In vivo NMR Imaging*, pages 205–226. Springer, 2011.

[43] Sami Jannin, Jean-Nicolas Dumez, Patrick Giraudeau, and Dennis Kurzbach. Application and methodology of dissolution dynamic nuclear polarization in physical, chemical and biological contexts. *Journal of Magnetic Resonance*, 305:41–50, 2019.

[44] Albert W Overhauser. Polarization of nuclei in metals. *Physical Review*, 92(2):411, 1953.

[45] VA Atsarkin. Dynamic nuclear polarization: Yesterday, today, and tomorrow. In *Journal of Physics: Conference Series*, volume 324, page 012003. IOP Publishing, 2011.

[46] Mathilde H Lerche, Magnus Karlsson, Jan H Ardenkjær-Larsen, and Pernille R Jensen. Targeted metabolomics with quantitative dissolution dynamic nuclear polarization. In *NMR-Based Metabolomics*, pages 385–393. Springer, 2019.

[47] Lloyd Lumata, Matthew E Merritt, Craig R Malloy, A Dean Sherry, and Zoltan Kovacs. Impact of gd3+ on dnp of [1-13c] pyruvate doped with trityl ox063, bdpa, or 4-oxo-tempo. *The journal of physical chemistry A*, 116(21):5129–5138, 2012.

[48] Aurélien Bornet and Sami Jannin. Optimizing dissolution dynamic nuclear polarization. *Journal of Magnetic Resonance*, 264:13–21, 2016.

[49] David I Broadhurst and Douglas B Kell. Statistical strategies for avoiding false discoveries in metabolomics and related experiments. *Metabolomics*, 2(4):171–196, 2006.

[50] Ewa Szymańska, Edoardo Saccenti, Age K Smilde, and Johan A Westerhuis. Double-check: validation of diagnostic statistics for pls-da models in metabolomics studies. *Metabolomics*, 8(1):3–16, 2012.

[51] Svante Wold, Michael Sjöström, and Lennart Eriksson. Pls-regression: a basic tool of chemometrics. volume 58, pages 109–130. Elsevier, 2001.

[52] Piotr S Gromski, Howbeer Muhamadali, David I Ellis, Yun Xu, Elon Correa, Michael L Turner, and Royston Goodacre. A tutorial review: Metabolomics and partial least squares-discriminant analysis–a marriage of convenience or a shotgun wedding. *Analytica chimica acta*, 879:10–23, 2015.

[53] Richard G Brereton and Gavin R Lloyd. Partial least squares discriminant analysis: taking the magic away. *Journal of Chemometrics*, 28(4):213–225, 2014.

[54] Carina M Rubingh, Sabina Bijlsma, Eduard PPA Derks, Ivana Bobeldijk, Elwin R Verheij, Sunil Kochhar, and Age K Smilde. Assessing the performance of statistical validation tools for megavariate metabolomics data. *Metabolomics*, 2(2):53–61, 2006.

[55] Johan A Westerhuis, Huub CJ Hoefsloot, Suzanne Smit, Daniel J Vis, Age K Smilde, Ewoud JJ van Velzen, John PM van Duijnhoven, and Ferdi A van Dorsten. Assessment of plsda cross validation. *Metabolomics*, 4(1):81–89, 2008.

[56] Piotr S Gromski, Yun Xu, Elon Correa, David I Ellis, Michael L Turner, and Royston Goodacre. A comparative investigation of modern feature selection and classification approaches for the analysis of mass spectrometry data. *Analytica chimica acta*, 829:1–8, 2014.

[57] Sankar Mahadevan, Sirish L Shah, Thomas J Marrie, and Carolyn M Slupsky. Analysis of metabolomic data using support vector machines. *Analytical chemistry*, 80(19):7562–7570, 2008.

[58] Bradley Worley and Robert Powers. Multivariate analysis in metabolomics. *Current Metabolomics*, 1(1):92–107, 2013.

[59] BF Manly. Multivariate statistical methods: a primer. 1986.

[60] Royston Goodacre, Eadaoin M Timmins, Rebecca Burton, Naheed Kaderbhai, Andrew M Woodward, Douglas B Kell, and Paul J Rooney. Rapid identification of urinary tract infection bacteria using hyperspectral whole-organism fingerprinting and artificial neural networks. *Microbiology*, 144(5):1157–1170, 1998.

[61] Harold Hotelling. Analysis of a complex of statistical variables into principal components. *Journal of educational psychology*, 24(6):417, 1933.

[62] William S Noble. What is a support vector machine? *Nature biotechnology*, 24(12):1565–1567, 2006.

[63] David Meyer, Friedrich Leisch, and Kurt Hornik. The support vector machine under test. *Neurocomputing*, 55(1-2):169–186, 2003.

[64] Patrick J Trainor, Andrew P DeFilippis, and Shesh N Rai. Evaluation of classifier performance for multiclass phenotype discrimination in untargeted metabolomics. *Metabolites*, 7(2):30, 2017.

[65] Bjoern H Menze, B Michael Kelm, Ralf Masuch, Uwe Himmelreich, Peter Bachert, Wolfgang Petrich, and Fred A Hamprecht. A comparison of random forest and its gini importance with standard chemometric methods for the feature selection and classification of spectral data. *BMC bioinformatics*, 10(1):1–16, 2009.

[66] D Richard Cutler, Thomas C Edwards Jr, Karen H Beard, Adele Cutler, Kyle T Hess, Jacob Gibson, and Joshua J Lawler. Random forests for classification in ecology. *Ecology*, 88(11):2783–2792, 2007.

[67] Leo Breiman. Random forests. *Machine learning*, 45(1):5–32, 2001.

[68] Mahesh Pal and Giles M Foody. Feature selection for classification of hyperspectral data by svm. *IEEE Transactions on Geoscience and Remote Sensing*, 48(5):2297–2307, 2010.

[69] Teppei Ebina, Hiroyuki Toh, and Yutaka Kuroda. Drop: an svm domain linker predictor trained with optimal features selected by random forest. *Bioinformatics*, 27(4):487–494, 2011.

[70] Xiaohui Lin, Quancai Wang, Peiyuan Yin, Liang Tang, Yexiong Tan, Hong Li, Kang Yan, and Guowang Xu. A method for handling metabonomics data from liquid chromatography/mass

spectrometry: combinational use of support vector machine recursive feature elimination, genetic algorithm and random forest for feature selection. *Metabolomics*, 7(4):549–558, 2011.

[71] Young Truong, Xiaodong Lin, and Chris Beecher. Learning a complex metabolomic dataset using random forests and support vector machines. In *Proceedings of the tenth ACM SIGKDD international conference on Knowledge discovery and data mining*, pages 835–840, 2004.

[72] Maciek R Antoniewicz. A guide to 13 c metabolic flux analysis for the cancer biologist. *Experimental & molecular medicine*, 50(4):1–13, 2018.

[73] Andrew N Lane, Jun Yan, and Teresa WM Fan. 13c tracer studies of metabolism in mouse tumor xenografts. *Bio-protocol*, 5(22), 2015.

[74] Sheng-Ping Wang, Dan Zhou, Zuliang Yao, Santhosh Satapati, Ying Chen, Natalie A Daurio, Aleksandr Petrov, Xiaolan Shen, Daniel Metzger, Wu Yin, et al. Quantifying rates of glucose production in vivo following an intraperitoneal tracer bolus. *American Journal of Physiology-Endocrinology and Metabolism*, 311(6):E911–E921, 2016.

[75] Olaf Beckonert, Hector C Keun, Timothy MD Ebbels, Jacob Bundy, Elaine Holmes, John C Lindon, and Jeremy K Nicholson. Metabolic profiling, metabolomic and metabonomic procedures for nmr spectroscopy of urine, plasma, serum and tissue extracts. *Nature protocols*, 2(11):2692–2703, 2007.

[76] Manuel Liebeke, Jie Hao, Timothy MD Ebbels, and Jacob G Bundy. Combining spectral ordering with peak fitting for one-dimensional nmr quantitative metabolomics. *Analytical chemistry*, 85(9):4605–4612, 2013.

[77] Andrea Capozzi, Saket Patel, W Thomas Wenckebach, Magnus Karlsson, Mathilde H Lerche, and Jan Henrik Ardenkjær-Larsen. Gadolinium effect at high-magnetic-field dnp: 70% 13c polarization of [u-13c] glucose using trityl. *The journal of physical chemistry letters*, 10(12):3420–3425, 2019.

[78] Estelle Martineau, Illa Tea, Gregory Loaëc, Patrick Giraudeau, and Serge Akoka. Strategy for choosing extraction procedures for nmr-based metabolomic analysis of mammalian cells. *Analytical and bioanalytical chemistry*, 401(7):2133–2142, 2011.

[79] Valentina Di Gialleonardo, Sui Seng Tee, Hannah N Aldeborgh, Vesselin Z Miloushev, Lidia S Cunha, George D Sukenick, and Kayvan R Keshari. High-throughput indirect quantitation of 13c enriched metabolites using 1h nmr. *Analytical chemistry*, 88(22):11147–11153, 2016.

[80] Sean Bowen and Christian Hilty. Rapid sample injection for hyperpolarized nmr spectroscopy. *Physical Chemistry Chemical Physics*, 12(22):5766–5770, 2010.

[81] Jonas Milani, Basile Vuichoud, Aurélien Bornet, Pascal Miéville, Roger Mottier, Sami Jannin, and Geoffrey Bodenhausen. A magnetic tunnel to shelter hyperpolarized fluids. *Review of Scientific Instruments*, 86(2):024101, 2015.

[82] Miroslava Čuperlović-Culf, David A Barnett, Adrian S Culf, and Ian Chute. Cell culture metabolomics: applications and future directions. *Drug discovery today*, 15(15-16):610–621, 2010.

[83] Kenneth R Stone, Don D Mickey, Heidi Wunderli, George H Mickey, and David F Paulson. Isolation of a human prostate carcinoma cell line (du 145). *International journal of cancer*, 21(3):274–281, 1978.

[84] ME Kaighn, K Shankar Narayan, Yasushi Ohnuki, John F Lechner, and LW Jones. Establishment and characterization of a human prostatic carcinoma cell line (pc-3). *Investigative urology*, 17(1):16–23, 1979.

[85] O Cussenot, PH Berthon, R Berger, I Mowszowicz, A Faille, F Hojman, P Teillac, A Le Duc, and F Calvo. Immortalization of human adult normal prostatic epithelial cells by liposomes containing large t-sv40 gene. *The Journal of urology*, 146(3):881–886, 1991.

[86] David S Wishart, Yannick Djoumbou Feunang, Ana Marcu, An Chi Guo, Kevin Liang, Rosa Vázquez-Fresno, Tanvir Sajed, Daniel Johnson, Carin Li, Naama Karu, et al. Hmdb 4.0: the human metabolome database for 2018. *Nucleic acids research*, 46(D1):D608–D617, 2018.

[87] MestreLab Research. Mnova version 11.0. https://mestrelab.com/software/mnova/, 2016.

[88] Guido Van Rossum and Fred L. Drake. *Python 3 Reference Manual*. CreateSpace, Scotts Valley, CA, 2009.

[89] F. Pedregosa, G. Varoquaux, A. Gramfort, V. Michel, B. Thirion, O. Grisel, M. Blondel, P. Prettenhofer, R. Weiss, V. Dubourg, J. Vanderplas, A. Passos, D. Cournapeau, M. Brucher, M. Perrot, and E. Duchesnay. Scikit-learn: Machine learning in Python. *Journal of Machine Learning Research*, 12:2825–2830, 2011.

[90] Pauli Virtanen, Ralf Gommers, Travis E. Oliphant, Matt Haberland, Tyler Reddy, David Cournapeau, Evgeni Burovski, Pearu Peterson, Warren Weckesser, Jonathan Bright, Stéfan J. van der Walt, Matthew Brett, Joshua Wilson, K. Jarrod Millman, Nikolay Mayorov, Andrew R. J. Nelson, Eric Jones, Robert Kern, Eric Larson, C J Carey, İlhan Polat, Yu Feng, Eric W. Moore, Jake VanderPlas, Denis Laxalde, Josef Perktold, Robert Cimrman, Ian Henriksen, E. A. Quintero, Charles R. Harris, Anne M. Archibald, Antônio H. Ribeiro, Fabian Pedregosa, Paul van Mulbregt, and SciPy 1.0 Contributors. SciPy 1.0: Fundamental Algorithms for Scientific Computing in Python. *Nature Methods*, 17:261–272, 2020.

[91] Jason Osborne. Improving your data transformations: Applying the box-cox transformation. *Practical Assessment, Research, and Evaluation*, 15(1):12, 2010.

[92] David Cunningham and Zongbing You. In vitro and in vivo model systems used in prostate cancer research. *Journal of biological methods*, 2(1), 2015.

[93] Vladimir Cherkassky and Yunqian Ma. Practical selection of svm parameters and noise estimation for svm regression. *Neural networks*, 17(1):113–126, 2004.

[94] Kristen Naegle, Nancy R Gough, and Michael B Yaffe. Criteria for biological reproducibility: what does" n" mean? *Science signaling*, 8(371):fs7, 2015.

[95] Tzu-Tsung Wong. Performance evaluation of classification algorithms by k-fold and leave-one-out cross validation. *Pattern Recognition*, 48(9):2839–2846, 2015.

[96] Ramón Díaz-Uriarte and Sara Alvarez De Andres. Gene selection and classification of microarray data using random forest. *BMC bioinformatics*, 7(1):1–13, 2006.

[97] Andy Liaw, Matthew Wiener, et al. Classification and regression by randomforest. *R news*, 2(3):18–22, 2002.

[98] JR Gingrich and NM Greenberg. A transgenic mouse prostate cancer model. *Toxicologic pathology*, 24(4):502–504, 1996.

[99] JR Gingrich, RJ Barrios, BA Foster, and NM Greenberg. Pathologic progression of autochthonous prostate cancer in the tramp model. *Prostate cancer and prostatic diseases*, 2(2):70–75, 1999.

[100] Anna Degrassi, Micaela Russo, Eugenio Scanziani, Anna Giusti, Roberta Ceruti, Gemma Texido, and Enrico Pesenti. Magnetic resonance imaging and histopathological characterization of prostate tumors in tramp mice as model for pre-clinical trials. *The Prostate*, 67(4):396–404, 2007.

[101] Andressa Ardiani, Benedetto Farsaci, Connie J Rogers, Andy Protter, Zhimin Guo, Thomas H King, David Apelian, and James W Hodge. Combination therapy with a second-generation androgen receptor antagonist and a metastasis vaccine improves survival in a spontaneous prostate cancer model. *Clinical Cancer Research*, 19(22):6205–6218, 2013.

[102] Chun X Hsu, Brian D Ross, Clarence E Chrisp, Solomon Z Derrow, Linda G Charles, KENNETH J PIENTA, Norman M Greenberg, ZHI Zeng, and Martin G Sanda. Longitudinal cohort analysis of lethal prostate cancer progression in transgenic mice. *The Journal of urology*, 160(4):1500–1505, 1998.

[103] Deborah K Hill, Andreas Heindl, Konstantinos Zormpas-Petridis, David J Collins, Leslie R Euceda, Daniel N Rodrigues, Siver A Moestue, Yann Jamin, Dow-Mu Koh, Yinyin Yuan, et al. Non-invasive prostate cancer characterization with diffusion-weighted mri: insight from in silico studies of a transgenic mouse model. *Frontiers in oncology*, 7:290, 2017.

[104] MATLAB. *version 9.6.0 (R2019a)*. The MathWorks Inc., Natick, Massachusetts, 2019.

[105] Francesco Savorani, Giorgio Tomasi, and Søren Balling Engelsen. icoshift: A versatile tool for the rapid alignment of 1d nmr spectra. *Journal of magnetic resonance*, 202(2):190–202, 2010.

[106] Steven Halouska and Robert Powers. Negative impact of noise on the principal component analysis of nmr data. *Journal of Magnetic Resonance*, 178(1):88–95, 2006.

[107] Robert A van den Berg, Huub CJ Hoefsloot, Johan A Westerhuis, Age K Smilde, and Mariët J van der Werf. Centering, scaling, and transformations: improving the biological information content of metabolomics data. *BMC genomics*, 7(1):1–15, 2006.

[108] Dries Debeer and Carolin Strobl. Conditional permutation importance revisited. *BMC bioinformatics*, 21(1):1–30, 2020.

[109] André Altmann, Laura Toloşi, Oliver Sander, and Thomas Lengauer. Permutation importance: a corrected feature importance measure. *Bioinformatics*, 26(10):1340–1347, 2010.

[110] Nantian Huang, Guobo Lu, and Dianguo Xu. A permutation importance-based feature selection method for short-term electricity load forecasting using random forest. *Energies*, 9(10):767, 2016.

[111] Carolin Strobl, Anne-Laure Boulesteix, Achim Zeileis, and Torsten Hothorn. Bias in random forest variable importance measures: Illustrations, sources and a solution. *BMC bioinformatics*, 8(1):1–21, 2007.

[112] Michał Fiedorowicz, Michał Wieteska, Katarzyna Rylewicz, Bartosz Kossowski, Ewa Piątkowska-Janko, Anna M Czarnecka, Beata Toczyłowska, and Piotr Bogorodzki. Hyperpolarized 13c tracers: Technical advancements and perspectives for clinical applications. *Biocybernetics and Biomedical Engineering*, 2021.

[113] Karel Kouřil, Hana Kouřilová, Samuel Bartram, Malcolm H Levitt, and Benno Meier. Scalable dissolution-dynamic nuclear polarization with rapid transfer of a polarized solid. *Nature communications*, 10(1):1–6, 2019.

[114] Luiz Fernando Pinto, Ildefonso Marín-Montesinos, Vega Lloveras, José Luis Muñoz-Gómez, Miquel Pons, Jaume Veciana, and José Vidal-Gancedo. Nmr signal enhancement of> 50000 times in fast dissolution dynamic nuclear polarization. *Chemical Communications*, 53(26):3757–3760, 2017.

[115] Jan H Ardenkjaer-Larsen, Andrew M Leach, Neil Clarke, John Urbahn, Denise Anderson, and Timothy W Skloss. Dynamic nuclear polarization polarizer for sterile use intent. *NMR in biomedicine*, 24(8):927–932, 2011.

[116] Xiao Ji, Aurélien Bornet, Basile Vuichoud, Jonas Milani, David Gajan, Aaron J Rossini, Lyndon Emsley, Geoffrey Bodenhausen, and Sami Jannin. Transportable hyperpolarized metabolites. *Nature communications*, 8(1):1–7, 2017.

[117] Nils Krause and Andre Wegner. Fructose metabolism in cancer. *Cells*, 9(12):2635, 2020.

Appendices

PAPER 1

A

TITLE

Stable isotope resolved metabolomics classification of prostate cancer cells using hyperpolarized NMR data

AUTHORS

Frahm, A.B.; Jensen, P.R.; Ardenkjær-Larsen, J.H.; Yigit, D.; Lerche, M.H.

STATUS

Published in *Journal of Magnetic Resonance*, 2020.

Journal of Magnetic Resonance 316 (2020) 106750

Contents lists available at ScienceDirect

Journal of Magnetic Resonance

journal homepage: www.elsevier.com/locate/jmr

Stable isotope resolved metabolomics classification of prostate cancer cells using hyperpolarized NMR data

Anne Birk Frahm, Pernille Rose Jensen, Jan Henrik Ardenkjær-Larsen, Demet Yigit, Mathilde Hauge Lerche *

Center for Hyperpolarization in Magnetic Resonance, Department of Health Technology, Ørsteds plads 349, 2800 Kongens Lyngby, Denmark

ARTICLE INFO

Article history:
Received 27 March 2020
Revised 3 May 2020
Accepted 7 May 2020
Available online 20 May 2020

Keywords:
Dissolution dynamic nuclear polarization
Stable isotope resolved metabolomics
Random forest
Support vector machine
Nuclear magnetic resonance

ABSTRACT

Metabolic fingerprinting is a strong tool for characterization of biological phenotypes. Classification with machine learning is a critical component in the discrimination of molecular determinants. Cellular activity can be traced using stable isotope labelling of metabolites from which information on cellular pathways may be obtained. Nuclear magnetic resonance (NMR) spectroscopy is, due to its ability to trace labelling in specific atom positions, a method of choice for such metabolic activity measurements. In this study, we used hyperpolarization in the form of dissolution Dynamic Nuclear Polarization (dDNP) NMR to measure signal enhanced isotope labelled metabolites reporting on pathway activity from four different prostate cancer cell lines. The spectra have a high signal-to-noise, with less than 30 signals reporting on 10 metabolic reactions. This allows easy extraction and straightforward interpretation of spectral data. Four metabolite signals selected using a Random Forest algorithm allowed a classification with Support Vector Machines between aggressive and indolent cancer cells with 96.9% accuracy, - corresponding to 31 out of 32 samples. This demonstrates that the information contained in the few features measured with dDNP NMR, is sufficient and robust for performing binary classification based on the metabolic activity of cultured prostate cancer cells.

1. Introduction

Metabolomics, the profiling and study of the small molecular products of a system, is a powerful tool for gaining insight into the biochemical state of an organism [1]. The snapshot of metabolites at a certain time point - the so-called metabolic fingerprint - can be correlated to the phenotype of the organism and can therefore be used for diagnostic purposes [2]. Metabolic fingerprints were, for instance, used as a basis for classifying the aggressiveness of cancers [3]. Machine Learning (ML) algorithms are especially useful for the classification of metabolic fingerprints as belonging to distinct biologies [4,5]. Such algorithms can be applied to make a feature based separation as well as to identify which measured features are important for a successful classification [5,6].

Nuclear Magnetic Resonance (NMR) and Mass Spectroscopy (MS) are the two most popular analytical techniques for generating metabolic fingerprints. NMR is reproducible and quantitative within a large dynamic range without need for authentic standards and it provides specificity on an atomic level. It is however relative to MS insensitive [7]. Metabolic fingerprints obtained with NMR are most often acquired as a single sampling of metabolites belonging to the investigated biological system. Biofluids or extracts from cells or tissue are directly processed and metabolite levels are quantified and compared. Such analysis provides a snapshot into a given biological system. Alternatively, biological function may be measured by profiling the metabolic activity in a network of biochemical transformations. In this case metabolic transformations may be traced by stable isotopes, e.g. ^{13}C [8]. Such method has been called stable isotope resolved metabolomics (SIRM) [9,10]. Metabolite levels and pathway activities represents complementary information about the biological system and both are needed for metabolic understanding [11].

Due to its high sensitivity ^{1}H NMR is widely used in metabolomics. These NMR experiments are however challenging to use for bio-marker identification due to extensive signal overlap that hampers both metabolite identification and quantification. Issues that are even more pertinent when traced metabolites are used for analysis of pathway activity due to further signal overlap from coupling satellites. In such studies NMR methods that take advantage of the larger chemical shift ranges of low-gamma nuclear spins are advantageous. These experiments, however, come with the penalty of longer acquisition times with sample stability as a complication.

A sensitivity boost to NMR may be obtained by applying dissolution Dynamic Nuclear Polarization (dDNP), where the polar-

* Corresponding author.
E-mail address: mhauler@dtu.dk (M.H. Lerche).

https://doi.org/10.1016/j.jmr.2020.106750
1090-7807/

ization of the nuclei is enhanced *ex situ* before the NMR spectra are recorded [12]. Using dDNP, the NMR signal can be enhanced several orders of magnitude compared to room temperature equilibrium. We have recently developed a method combining dDNP with isotope labelled metabolomics NMR. Specifically, we showed that metabolic activity can be measured reproducibly and quantitatively using [U-$^{13}C_6$, d_7]D-glucose as a tracer for glycolytic activity in cancer cells from dDNP signal enhanced 1D-^{13}C NMR spectra of transformation products [13]. dDNP enhanced ^{13}C NMR data has been shown to meet the repeatability demands of metabolomics, which further supports the methods potential as a complementary analytical tool [14]. The dDNP 1D-^{13}C NMR spectra are sparse and metabolite signals are readily identified and quantified.

Machine learning (ML) is by now an integrated tool in metabolomics where it is used e.g. for prediction of cancer progression from discriminations based on metabolite levels [15]. ML is, however, not commonly used on isotope labelled metabolite data reporting on metabolic transformations. Generally, NMR data from studies involving tracing of isotope labelled metabolites are sparse compared to those involving measurement of metabolite levels, which should be taken into account when choosing an appropriate ML algorithm: If an input data matrix (consisting of signal integrals in a number of samples) contains more NMR signals than samples this renders a proper validation of the separation and feature selection important for classification [5]. ML algorithms which are commonly used in such situations often perform worse in terms of prediction accuracy than other classifiers when challenged with lower number of variables [16].

The present study is the first study to evaluate whether dDNP ^{13}C NMR may be used to provide fingerprints of metabolic activity useful for classification of cancer cell phenotypes. The study goal was three-fold: To investigate whether it was possible to make a robust multi-class classification based on few NMR signals and capture differences between four prostate cell lines. Secondly, to evaluate if the use of metabolic activity measurements such as those obtained with dDNP ^{13}C NMR can be used to separate aggressive cancer cell lines from indolent cancer cells in a binary classification. And thirdly through a feature analysis to examine the importance ranking of NMR signals for identified metabolites in the binary separation.

2. Results

dDNP ^{13}C NMR spectra were obtained from four different prostate cancer cell lines: Two highly invasive, androgen independent cell types: PC3 (metastatic, derived from bone marrow) and DU145 (metastatic derived from brain), and two low invasive, androgen dependent cell types: LNCaP (early metastasis derived from lymph node), and PNT1A (PNT, immortalized cells from healthy prostate). A total of 32 samples (8 from each cell type), were made by the method described in Lerche et al. [13]. In brief, cell samples were incubated with [U-$^{13}C_6$, d_7]D-glucose for 30 min, before metabolism was quenched and metabolites were extracted with perchloric acid. The samples were lyophilized, and the metabolic mixture was prepared for dDNP in a mixture of water, glycerol and trityl radical with addition of a reference compound (HP001, 1,1-bis (hydroxymethyl) cyclopropane) for referencing and quantification. All samples were hyperpolarized with DNP for 1.5 h, dissolved in phosphate buffer (pH 7.4) and directly transferred to a 9.4 T NMR magnet for recording of 1D ^{13}C NMR spectra (see suppl. Inform. for detailed methods). The carbon NMR signals were straightforwardly identified as belonging to specific atoms in energy/glycolytic metabolites by consulting available databases [17]. This was done using distinct chemical shifts of carbonyl carbons and by comparing ^{13}C–^{13}C coupling constant pattern with simulations using the NMR analysis tool MNova [18], since all metabolite signals are derived from uniformly ^{13}C-labelled glucose, Fig. 1. In comparison to conventional SIRM NMR using 1D ^{1}H NMR with ^{13}C-couplings for analysis the dDNP 1D ^{13}C NMR spectra has less overlap, SI Fig. S2. Whereas ten metabolites were directly identified and quantified in the dDNP 1D ^{13}C NMR spectra only two of these, alanine and lactate, could be unambiguously identified and quantified from the 1D ^{1}H NMR spectra.

The spectral features used for further analysis are listed in Table 1. Signals representative of identified metabolites was included in the ML analysis as quantified peak areas relative to the internal standard. One carbon signal representative of each identified metabolite was included in the analysis; in general long T_1 carbons (e.g. carbonyl atoms) and carbon signals with less overlap in the spectra were prioritized as representatives, as an example of the latter PEP-C2, which lies completely isolated in the spectra was included rather than PEP-C1.

On average, there were visible differences in the metabolite production between cell lines. An analysis of variance (ANOVA) test on the distribution of all measured integrals over 8 samples for every cell type showed that there was a significant difference between the four cell lines in the measured integrals of DHAP-C2, ALA-C1 and PEP-C2. Although the data precision was generally low the ANOVA test suggests that these metabolites may carry discrimination value in a classification between the four prostate cancer cell types. Also, pairwise statistics were performed between each cell line, for every metabolite with a T-test. This test showed significant difference for the metabolite DHAP-C2 between the aggressive cell type DU145 and the indolent PNT and LNCaP, respectively (Bonferroni corrected significance, $P < 5\%$), SI, Table S2.

Our first point of inquiry was whether a classification, using an appropriate ML algorithm, could be made to identify each sample to the cell line it came from. Contrary to conventional NMR, dDNP NMR spectra, using ^{13}C labelled glucose as tracer contain fewer spectral features. Bearing this in mind, it was important to carefully choose the classification tools in order not to overfit when the number of samples was similar to the number of features. Partial Least Squares-Discriminant Analysis (PLS-DA) is widely used for classification with NMR in metabolomics [4,19], but have been shown to under-perform and over-fit, compared to other methods, especially in situations with a low number of features [16,20–22]. To perform this multiclass classification on the dDNP ^{13}C NMR data we chose instead Principal Component-Discrimination Function Analysis (PC-DFA). PC-DFA has been applied in a wide variety of metabolomics studies and have been shown to perform robustly with a small number of features [5,16,20]. Since PC-DFA is a parametric function and thus performs optimally on normal distributed data, a box-cox transformation [23] was applied to the data-matrix. In the first step of the PC-DFA, the Principal Component Analysis (PCA), 7 principal components were needed to account for 95.68% of the variance in the original data. These components were applied in the second step of the algorithm where a supervised Linear Discriminant Analysis (LDA) was used to construct a set of discriminant functions, which optimizes the distance between the cell lines and minimizes the distance between samples of the same cell line. Leave-One-Out cross validation were applied to the LDA. The results of the PC-DFA analysis are shown in Fig. 2. The unsupervised principal component analysis represented in Fig. 2A by the first two PC of the linear transformation of the scaled data is clearly not sufficient to separate the metabolic fingerprints by cell line. There is a tendency for the PNT and LNCaP samples to collect in the upper left of the plot, the DU145 samples to be near the middle and PC3 to generally be to the lower right. With supervision this improved and all data points (8 samples for each of the 4 cell lines) confined within two standard deviation point clouds of the respective cell lines, except two from the PNT

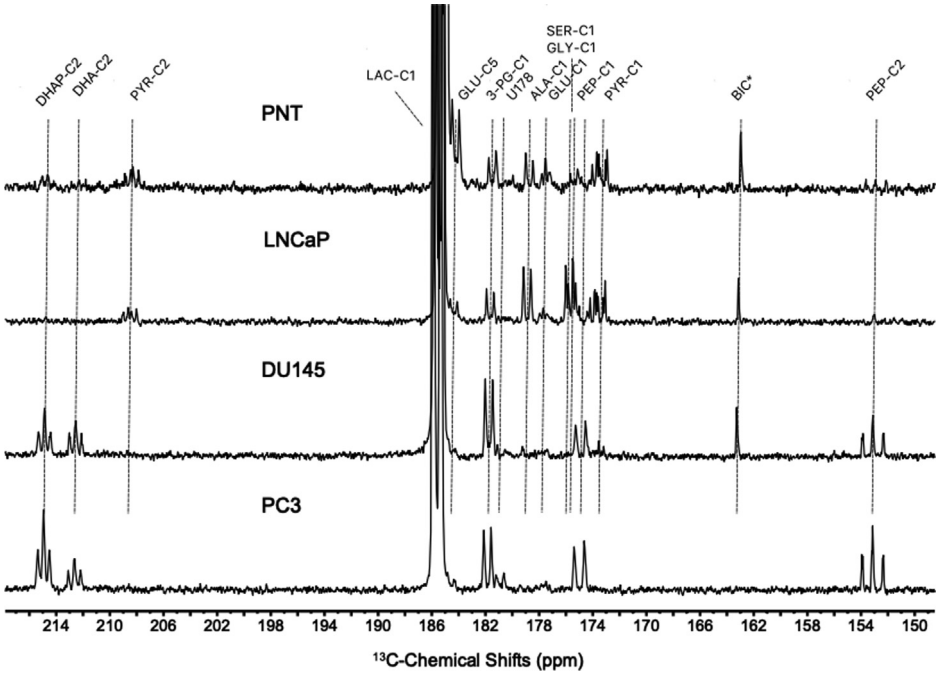

Fig. 1. Carbonyl region of dDNP ^{13}C NMR metabolic fingerprint. One representative spectrum of metabolite extracts from each of the four prostate cell types (PNT, LNCaP, DU145 and PC3) are shown. Full spectra are shown in SI Fig. S1. Identification of the signals as belonging to specific carbon atoms are indicated above the top spectrum, see Table 1 for name identification. * indicates that bicarbonate (BIC) was not reliable as a labelled metabolite in the analysis due to the applied extraction method and thus not included in the analysis.

Table 1
List of spectral features for which integrals were used as input in the ML algorithm. Chemical shifts were referenced to an added internal standard compound HP001 at 25.7 ppm. The abbreviations reflect the carbon position. Due to overlap the signals from amino acids, serine and glycine were integrated together.

Chemical shift (ppm)	Assigned compound	Abbreviation
214.6	Dihydroxyacetone phosphate	DHAP-C2
185.3	Lactate	LAC-C1
184.2	Glutamate	GLU-C5
181.5	3-Phosphoglycerate	3PG-C1
180.6	Unidentified amino-acid	U178
178.8	Alanine	ALA-C1
175.5	Serine and Glycine	SER-GLY-C1
173.3	Pyruvate	PYR-C1
152.9	Phosphoenolpyruvate	PEP-C2
92.1	Glyceraldehyde 3-phosphate	G3P-C1

cell line and one from the PC3 cell line, Fig. 2B. The success rate measured as accuracy (the sum of true positives and true negatives divided with the total number of observations) was for this model with leave-one-out cross validation the success rate of prediction from this model was 78.125% (25 out 32 samples). The encountered prediction errors were between cell lines characterized by being aggressive (PC3 and DU145) or between those characterized as indolent (PNT and LNCaP) respectively, Table 2.

These results prompted our second point of enquiry using the dDNP ^{13}C NMR data to discriminate cell lines by their aggressiveness. The PC-DFA algorithm was merely instructed to separate individual cell lines and not to separate for cell line aggressiveness, so the fact that the prediction errors were made only between cell lines of similar aggressiveness suggested that a binary classification of the data may be more robust. An accurate discrimination between aggressive and indolent cancer at the time of diagnosis is a pressing clinical need in managing prostate cancer [24]. Taken together this encouraged us to make a binary classification with the aim to separate between the highly invasive (DU145 and PC3, grouped as aggressive) and low invasive (PNT and LNCaP, grouped as indolent) cell lines. The LNCaP cell line is an early metastasis and as such not per se seen as a non-aggressive cell line. It is however androgen dependent and show a low invasiveness [25]. Since samples from this cell line separated with PNT in the multiclass separation it was therefore sorted together with PNT samples as an indolent cell line. A binary separation allows the use of Support Vector Machines (SVM) as a classifier. SVM has been shown to be particularly robust towards overfitting, compared with other classification methods commonly used in metabolomics [5]. This algorithm is non-parametric and thus enable data analysis without the need for transformations other than mean centering and scaling [5,22]. With the SVM algorithm a plane is found in the feature-space to maximize the separation between samples belonging to the two classes. Prior to the data analysis with SVM it is useful to make a dimensionality reduction, this has been shown to be particularly beneficial for small training datasets [26]. The dimensionality reduction was performed by the Random Forest (RF) algorithm. This algorithm provides at the same time a means to perform feature ranking. RF uses multiple decision trees, each made from a subset of features and samples, using the remaining samples for internal validation. The feature importance is measured directly by judging the importance of each individual feature in building the trees to separate the classes. By comparing the different forests to data with shuffled classes, a feature ranking is obtained which is unbiased to the covariance of the features.

The feature ranking made from classifications of the dDNP ^{13}C NMR data with RF (see SI for details on method) is shown in Fig. 3.

From this feature ranking it can be seen that only signals representing DHAP, G3P, lactate and alanine contribute positively to the classification of aggressive vs. indolent prostate cancer samples. Data from the remaining metabolites are either unnecessary or creating noise in this algorithm. It is important to note here, that the feature selection of RF is not perfect, especially when variables differ in scale [27], such as the lactate signal did in this study. However, the ranking is useful when as here it is used for constructing feature sets for classification with the SVM algorithm. Following

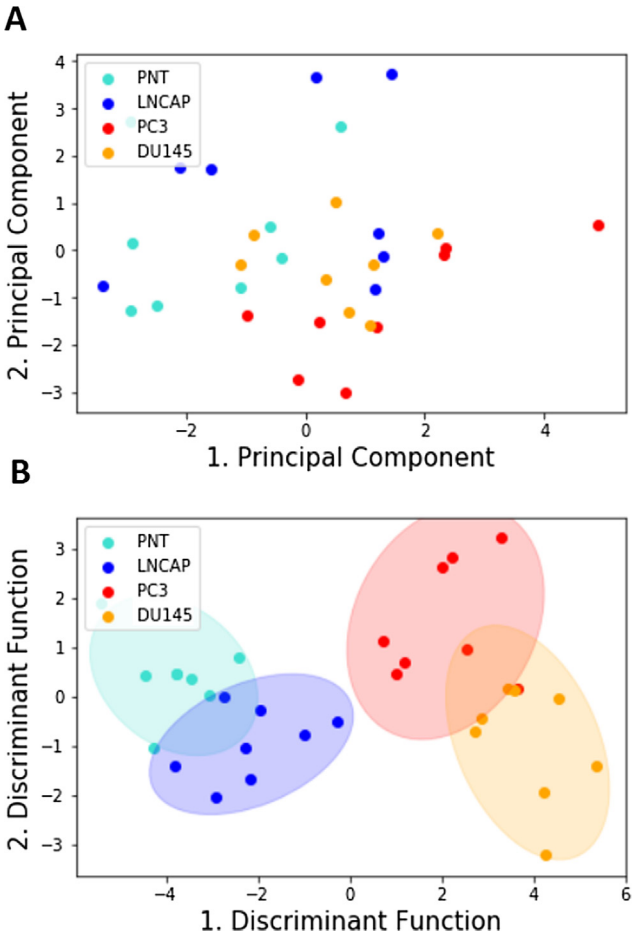

Fig. 2. A) Illustration of PCA on box-cox transformed data. First PC contains 34.47% of the variance in the data and second PC 26.65%. A total of 7 components were needed to explain more than 95% of all data variance. B) Plot of the two first PC-DFA functions, illustrating the results of separation between cell lines. The data has been Box-Cox transformed and normalized, before PC-DFA was performed, with 7 features used from PCA capturing 95.68% variance of the original data. Colored eclipses represent 2 standard deviations of point clouds. PC3 (red) and DU145 (orange) are aggressive prostate cancer cell lines and PNT (cyan) and LNCaP (blue) are characterized as indolent. (For interpretation of the references to colour in this figure legend, the reader is referred to the web version of this article.)

Table 2
Error matrix for PC-DFA classification, with Leave-One-Out cross validated predictions.

Predicted:	PNT	LNCaP	PC3	DU145
Actual:				
PNT	6	2	0	0
LNCaP	3	5	0	0
PC3	0	0	7	1
DU145	0	0	1	7

this feature ranking using the RF algorithm an SVM classification was performed, based on the features with high importance selected from the feature importance analysis.

Prediction successes from SVM are shown in Table 3. With leave-one-out cross validation a classification using all features, accurately predicted the aggressiveness of 93.75% (30 out 32) samples. When including only the four features found to have positive impact on the RF predictive power, DHAP, G3P, lactate and alanine, the highest observed success rate, 96.88% (31 out of 32) samples, was achieved. This high prediction success rate was kept eliminating DHAP but keeping G3P, Lactate and alanine. Any other combination of three features resulted in a success-rate level identical to the test with all features included. If only one feature was included the best prediction was found using DHAP (90.63% success rate) whereas alanine alone performed the worst with a 62.5% success rate. A similarly low prediction success of 75% was obtained when lactate was used as the only feature.

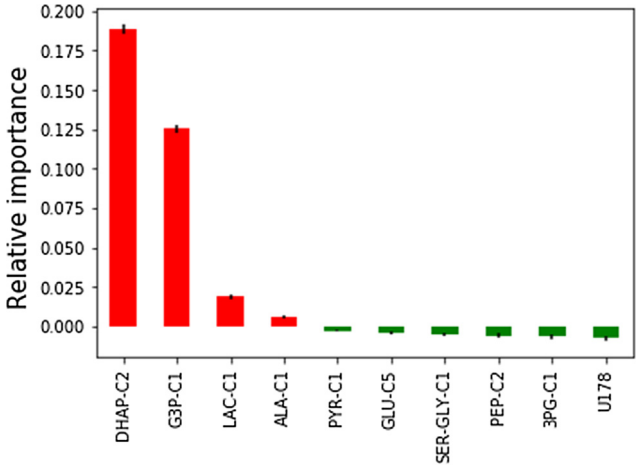

Fig. 3. Feature importance measured as the change in predictive power of Random Forest (RF) classification when compared to randomized values in testing data sets. A positive score (in red) means the classification became worse when the testing values were shuffled. Black bars are the standard error. (For interpretation of the references to colour in this figure legend, the reader is referred to the web version of this article.)

Table 3
Leave-One-Out cross validating (n = 32) results of classification with SVM for different sets of metabolite integrals. The tested sets of metabolite integrals were chosen on the basis of a RF feature ranking.

Features included	Success rate
all	93.75%
DHAP, G3P, LAC-C1, ALA-C1	96.88%
DHAP, G3P, LAC-C1	93.75%
DHAP, G3P, ALA-C1	93.75%
DHAP, LAC-C1, ALA-C1	93.75%
G3P, LAC-C1, ALA-C1	96.88%
DHAP, G3P	90.63%
DHAP, LAC-C1	90.63%
DHAP, ALA-C1	90.63%
G3P, LAC-C1	81.25%
G3P, ALA-C1	93.75%
ALA-C1, LAC-C1	81.25%
DHAP	90.63%
G3P	84.37%
LAC-C1	75.00%
ALA-C1	62.50%

The SVM analysis showed that information on as few as three or four metabolites, G3P, lactate and alanine or these metabolites plus DHAP were needed for highest observed prediction value among the tested data sets. It could be expected that lactate would be a decisive metabolite based on the numerous studies suggesting diagnostic value of this metabolite for detection of prostate cancer malignancy both in animal studies [28,29] and in clinical studies [30]. However, the SVM analysis was significantly worse including only lactate in the analysis suggesting that accumulation of DHAP and G3P and lower alanine production adds crucial diagnostic information about the metabolic strategy of aggressive prostate cancer cells. Accumulation of the trioses, DHAP and G3P may provide evidence for a flexible glycolytic strategy of highly proliferating prostate cancer cells. This notion is supported by recent reports

on strict regulation of ATP production by the presence of a less active isoform of pyruvate kinase (PKM2) to keep an increased glycolytic activity in highly proliferating cells [31]. Also accumulation of DHAP suggest a shift in glucose catabolism to glycerol, which fit well with the ability of late stage prostate cancer cells to be producers of de novo lipids independent on androgen regulation [32].

Although it is early days for the dDNP ^{13}C NMR metabolomics method it is promising as a complementary method to conventional SIRM NMR. The dDNP ^{13}C NMR spectra allowed easy identification and quantification of the trioses important for the metabolomic classification. These metabolites would not have been identified in a conventional SIRM 1D ^{1}H NMR spectrum due to spectral overlap, (SI, Fig. S2). NMR methods that take advantage of the larger chemical shift ranges of low-gamma nuclear spins could solve some of these issues with spectral overlap. An experiment such as high resolution ^{1}H–^{13}C-HSQC where ^{13}C–^{13}C-coupling information is available could prove to be an alternative valuable method [8]. These experiments crave however long acquisition times and thus puts demand on sample stability. While promising ultra-fast NMR acquisition methods with detection on ^{1}H are developing for metabolomics [33], schemes for correspondingly fast ^{1}H–^{13}C-HSQC are still in their early stage [34]. For the dDNP ^{13}C NMR metabolomics method to make its way into broader application in the field of metabolomics it will in the future be important to make a dedicated comparative study to conventional metabolomics tools such as 1D ^{1}H NMR and 2D ^{1}H–^{13}C-HSQC to understand the comparative benefits and challenges of each method.

This study showed that carefully chosen ML methods robust against overfitting and tailored the classification problem allowed both a semi successful multi-class separation and a highly successful binary discrimination of prostate cancer cell types. In particularly it was shown that metabolic fingerprints obtained with dDNP ^{13}C NMR provided sufficient information to successfully classify 31 of 32 prostate cancer cell line samples as belonging to the aggressive or indolent cell type. Subsets of only three or four of the measured features (assigned to (DHAP), G3P, lactate and alanine) were sufficient to support this classification. A caveat to note with the design of this study, is however, that the assumption of independence between each sample is not met, since they are taken from the same four cell lines, and not e.g. individual animals. The method should therefore be further evaluated in a study involving relevant tissue samples. On such basis this method is expected to meet requests in the field of metabolic imaging [35] and provide identity of metabolic activities important for selection of agent(s) central to specific diseases.

Declaration of Competing Interest

The authors declare that they have no known competing financial interests or personal relationships that could have appeared to influence the work reported in this paper.

Acknowledgements

The authors gratefully acknowledge funding by the Danish National Research Foundation (Grant DNRF124) and the work of Emma Lundsgaard and Amalia Matei in the initial part of the statistical analysis for selection of relevant tools. The NMR center at DTU is acknowledged for the ^{1}H 1D Spectra acquired on their 800 MHz Avance II NMR spectrometer.

Appendix A. Supplementary data

Supplementary data to this article can be found online at https://doi.org/10.1016/j.jmr.2020.106750.

References

[1] A. Rosato, L. Tenori, M. Cascante, P.R.-D.-A. Carulla, V.A.P. Martins dos Santos, E. Saccenti, Metabolomics 14 (37) (2018) 2–20.
[2] G.J. Patti, O. Yanes, G. Siuzdak, Nat. Rev. Mol. Cell Biol. 13 (2012) 263–269.
[3] D.I. Ellis, W.B. Dunn, J.L. Griffin, J.W. Allwood, R. Goodacre, Pharmacogenomics 8 (9) (2007) 1243–1266.
[4] G. Blekherman, R. Laubenbacher, D.F. Cortes, P. Mendes, F.M. Torti, S. Akman, S. V. Torti, V. Shulaev, Metabolomics 7 (2011) 329–343.
[5] P.S. Gromski, H. Muhamadali, D.I. Ellis, Y. Xu, E. Correa, M.L. Turner, R. Goodacre, Anal. Chim. Acta 879 (2015) 10–23.
[6] B.H. Menze, B.M. Kelm, R. Masuch, U. Himmelreich, P. Bachert, W. Petrich, F.A. Hamprecht, BMC Bioinform. 10 (2009) 213.
[7] Z. Pan, D. Raftery, Anal. Bioanal. Chem. 387 (2007) 525–527.
[8] R. Saborano, Z. Eraslan, J. Roberts, F.L. Khanim, P.F. Lalor, M.A.C. Reed, U.L. Günther, Sci. Rep. 9 (2019) 2520.
[9] A.M. Lane, T.W.-M. Fan, Arch. Biochem. Biophys. 628 (2017) 123–131.
[10] A.M. Lane, T.W.-M. Fan, M. Bousamra, R.M. Higashi, J. Yan, D.M. Miller, Omics J. Integrative Biol. 15 (3) (2011) 173–182.
[11] C. Jang, L. Chen, J.D. Rabinowitz, Cell 173 (2018) 822–837.
[12] J.H. Ardenkjær-Larsen, B. Fridlund, A. Gram, G. Hansson, L. Hansson, M.H. Lerche, R. Servin, M. Thaning, K. Golman, Proc. Natl. Acad. Sci. 100 (2003) 10158–10163.
[13] M.H. Lerche, D. Yigit, A.B. Frahm, J.H. Ardenkjær-Larsen, R.M. Malinowski, P.R. Jensen, Anal. Chem. 90 (2017) 674–678.
[14] A. Bornet, M. Maucourt, C. Deborde, D. Jacob, J. Milani, B. Vuichoud, X. Ji, J.-N. Dumez, A. Moing, G. Bodenhausen, S. Jannin, P. Giraudeau, Anal. Chem. 88 (12) (2016) 8179–8183.
[15] K. Kourou, T.P. Exarchos, K.P. Exarchos, M.V. Karamouzis, D.I. Fotiadis, Comput. Struct. Biotechnol. J. 13 (2015) 8–17.
[16] P.S. Gromski, Y. Xu, E. Correa, D.I. Ellis, M.L. Turner, R. Goodacre, Anal. Chim. Acta 829 (2014) 1–8.
[17] D.S. Wishart, Y.D. Feunang, A. Marcu, A.C. Guo, K. Liang, et al., Nucl. Acids Res. 46 (D1) (2018) D608–D617.
[18] MNova version 11.0; MestreLab Research.
[19] E. Szymańska, E. Saccenti, A.K. Smilde, J.A. Westerhuis, Metabolomics 8 (2012) 3–16.
[20] R.G. Brereton, G.R. Lloyd, J. Chemometrics 28 (2014) 213–225.
[21] C.M. Rubingh, S. Bijlsma, E.P. Derks, I. Bobeldijk, E.R. Verheij, S. Kochhar, A.K. Smilde, Metabolomics 2 (2006) 53–61.
[22] S. Mahadevan, S.L. Shah, T.J. Marrie, C.M. Slupsky, Anal. Chem. 80 (2008) 7562–7570.
[23] J.W. Osborne, Practical Assess. Res. Eval. 15 (2010) 1–9.
[24] H.G. Welch, W.C. Black, J. Natl. Cancer Inst. 102 (2010) 605–613.
[25] D. Cunningham, Z. You, J. Biol. Methods 2 (1) (2015) e17.
[26] M. Pal, G.M. Foody, IEEE Trans. Geosci. Remote Sensing 48 (2010) 2297–2307.
[27] C. Strobl, A.-L. Boulesteix, T. Kneib, T. Augustin, A. Zeileis, BMC Bioinform. 9 (2008) 307.
[28] R. Bok, J. Lee, R. Sriram, K. Keshari, S. Sukumar, S. Daneshmandi, D.E. Korenchan, R.R. Flavell, D.B. Vigneron, J. Kurhanewicz, et al., Cancers 11 (2019) 257.
[29] H.-Y. Chen, P.E. Larson, R.A. Bok, C. von Morze, R. Sriram, R.D. Santos, J.D. Santos, J.W. Gordon, N. Bahrami, M. Ferrone, et al., Cancer Res. 77 (2017) 3207–3216.
[30] S.J. Nelson, J. Kurhanewicz, D.B. Vigneron, P.E. Larson, A.L. Harzstark, M. Ferrone, M. Van Criekinge, J.W. Chang, R. Bok, I. Park, et al., Sci. Translat. Med. 5 (2013) 198ra108.
[31] T.L. Dayton, T. Jacks, M.G. Vander Heiden, EMBO Rep. 17 (2016) 1721–1730.
[32] E. Eidelman, J. Twum-Ampofo, J. Ansari, M.M. Siddiqui, Front. Oncol. 7 (2017) 131.
[33] A.L. Guennec, P. Giraudeau, S. Caldarelli, Anal. Chem. 86 (2014) 5946–5954.
[34] L. Rouger, S. Akoka, P. Giraudeau, JMR 283 (2017) 89–95.
[35] J. Kurhanewicz, D.B. Vigneron, J.H. Ardenkjaer-Larsen, J.A. Bankson, K. Brindle, C.H. Cunningham, F.A. Gallagher, K.R. Keshari, A. Kjaer, C. Laustsen, et al., Neoplasia 21 (2019) 1–16.

Supporting information

Stable Isotope Resolved Metabolomics Classification of Prostate Cancer Cells using Hyperpolarized NMR Data

Anne B. Frahm, Pernille Rose Jensen, Jan Henrik Ardenkjær-Larsen, Demet Yigit, and Mathilde Hauge Lerche.

Center for Hyperpolarization in Magnetic Resonance, Department of Health Technology, Ørsteds plads 349, 2800 Kongens Lyngby, Denmark.

Methods:

Sample preparation:

The experimental protocol was adapted from (Lerche et al., 2018).[1] All cell lines were purchased from ATCC: PC3, CRL-1435; DU145, HTB-81; LNCAP, CRL-1740; PNT1A, no longer available at ATCC but can be purchased from Sigma-Aldrich. All chemicals including ^{13}C-labelled compounds and cell medium were purchased from Sigma-Aldrich.

Human prostate cells of the types PC3 (grade IV prostatic adenocarcinoma derived from bone metastasis), DU145 (carcinoma derived from brain metastasis), LNCaP (carcinoma derived from lymph node metastasis) and PNT1A (normal, immortalized cell line) were grown to approximately 90% confluence in 175 cm^2 flasks, kept in an environment with 5% CO_2, at 37 °C in regular RPMI-1640 medium with FBS and antibiotics. The cells were harvested by trypsination, washed and resuspended in 40 mM phosphate buffer with pH 7.3. Cells were counted using an automatic cell counter and diluted to a concentration of either 20 or 40 million cells/mL, Table S.1.

Table. S.1. Number of cells per experiment for different cell types.

Number of cells/Cell line	PC3	DU145	LNCAP	PNT1A
20 mill cells/ml	5	3	3	4
40 mill cells/ml	3	5	5	4

500 µL of this cell suspension (10 or 20 mio. cells) in 2 mL Eppendorf tubes were placed in a shaking thermostat, kept at 37°C. 100 µL of [U-$^{13}C_6$, d_7]D-glucose (120 mM) was added and the cells were incubated for 30 minutes. Cell samples analyzed with conventional NMR was instead incubated with [U-$^{13}C_6$]D-glucose. Following the 30 min. incubation the metabolism was stopped and metabolites extracted by addition of perchloric acid (PCA): 400 µL of 2.2 M PCA solution, kept ice cold. The metabolism quenched samples were then kept on ice for at least 10 min, before soluble metabolites were extracted by centrifugation (10 min, 10,000 rpm, 4°C). The supernatant was pH neutralized with 3 M potassium hydroxide (KOH), kept on ice for at least 10 min for effective metabolite extraction and centrifuged. The neutralized supernatants were freeze-dried.

dDNP sample preparation:

The lyophilized samples were dissolved with 150 µL of polarization medium (70 mg trityl radical OX063, 1227 mg glycerol, 944 mg Milli-Q water, 28.8 mg Gadoteridol (100 µmol/g) and 5 µL of 1-^{13}C-HP001 (1.1-bis (hydroxymethyl) cyclopropane), 50 mM). The latter was added as an internal standard and used for referencing and quantification.

SIRM 1D-^{1}H NMR sample preparation:

A subset of samples was used to acquire conventional SIRM NMR before dDNP SIRM NMR. The lyophilized samples were dissolved in 250 ul 40 mM deuterated phosphate buffer with DSS as a standard (40 mM, 0.2 mM DSS, 100% D_2O, pH 7.5) and 300 µl D2O. The pH was subsequently adjusted to 7.5 using solutions of NaOD or D_2SO_4. Following analysis with conventional SIRM NMR, see below, the samples were lyophilized and re-prepared for dDNP, see above.

dDNP and NMR:

dDNP were performed in a HyperSense polarizer at 3.35 T and 1.4 K, with microwave irradiation at $f_{\mu w}$ = 94 GHz and $P_{\mu w}$ = 100 mW, for 90 min. Samples were then dissolved in 5 mL phosphate buffer (40 mM, pH 7.4) and transferred to a 5 mm NMR tube in the NMR spectrometer. Transfer time was approximately 12 s. ^{13}C 1D NMR spectra were measured with a 9.4T Varian Inova spectrometer at approx. 50°C, with a 90° pulse, Figure S1.

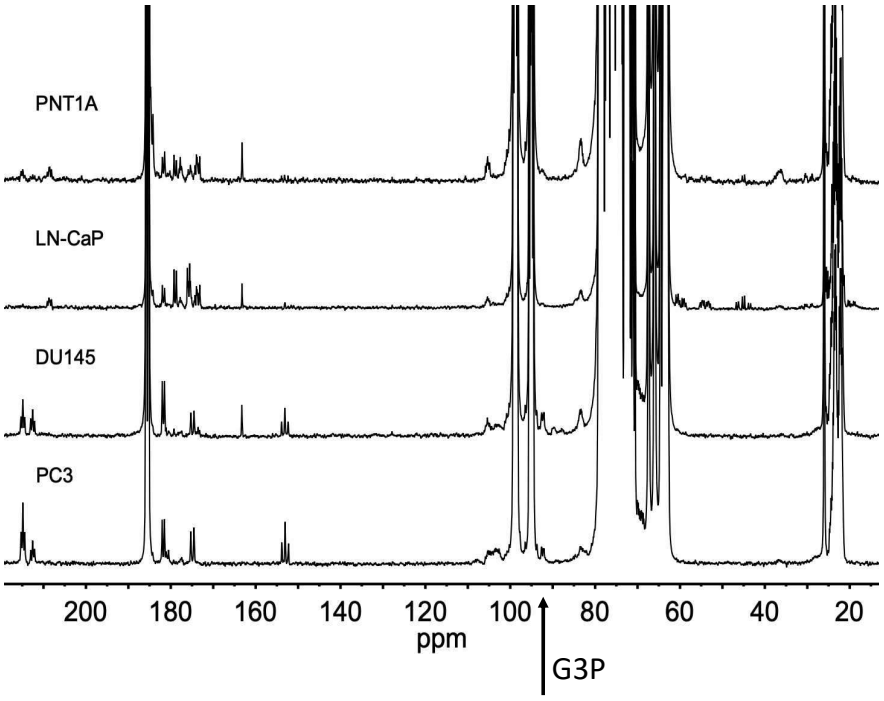

Figure S1. Representative hyperpolarized ^{13}C 1D NMR spectra of each of the four included cell types in the analysis. From top the non-invasive PNT1A and LN-CaP followed by the invasive cell types DU145 and PC3. The Signal from glyceraldehyde-3-phosphate (G3P) is pointed out with the arrow at 92.1 ppm.

For SIRM 1D ^{1}H spectra, a standard Bruker pulse sequence noesygpr1d for a 1D NOESY was used (TD 32768; interscan delay (d1) 4 s; acquisition time 1.7 s, number of scans 256). In total each spectrum took approx. 25 min. to acquire. All spectra were acquired at 298 K on an 800 MHz Avance III NMR spectrometer (Bruker, Switzerland) with a TCI z gradient CryoProbe.

Comparison between SIRM 1D dDNP ^{13}C-NMR and SIRM 1D ^{1}H-NMR

Samples prepared for conventional NMR were used to acquire SIRM 1D ^{1}H-NMR, Figure S2A and hereafter lyophilized and used to acquired SIRM 1D dDNP ^{13}C-NMR, Figure S2B. Currently the dDNP NMR spectra takes approx. 3 times longer to acquire than the SIRM 1D ^{1}H-NMR and the equipment used to perform the dDNP part of the experiments is less abundant than high field NMR spectrometers. Tracer tracking with direct 1D ^{13}C NMR such as that in the 1D dDNP ^{13}C-NMR is however for most metabolic reactions more straight forwardly analyzed and quantified than in 1D ^{1}H NMR spectrum.

A

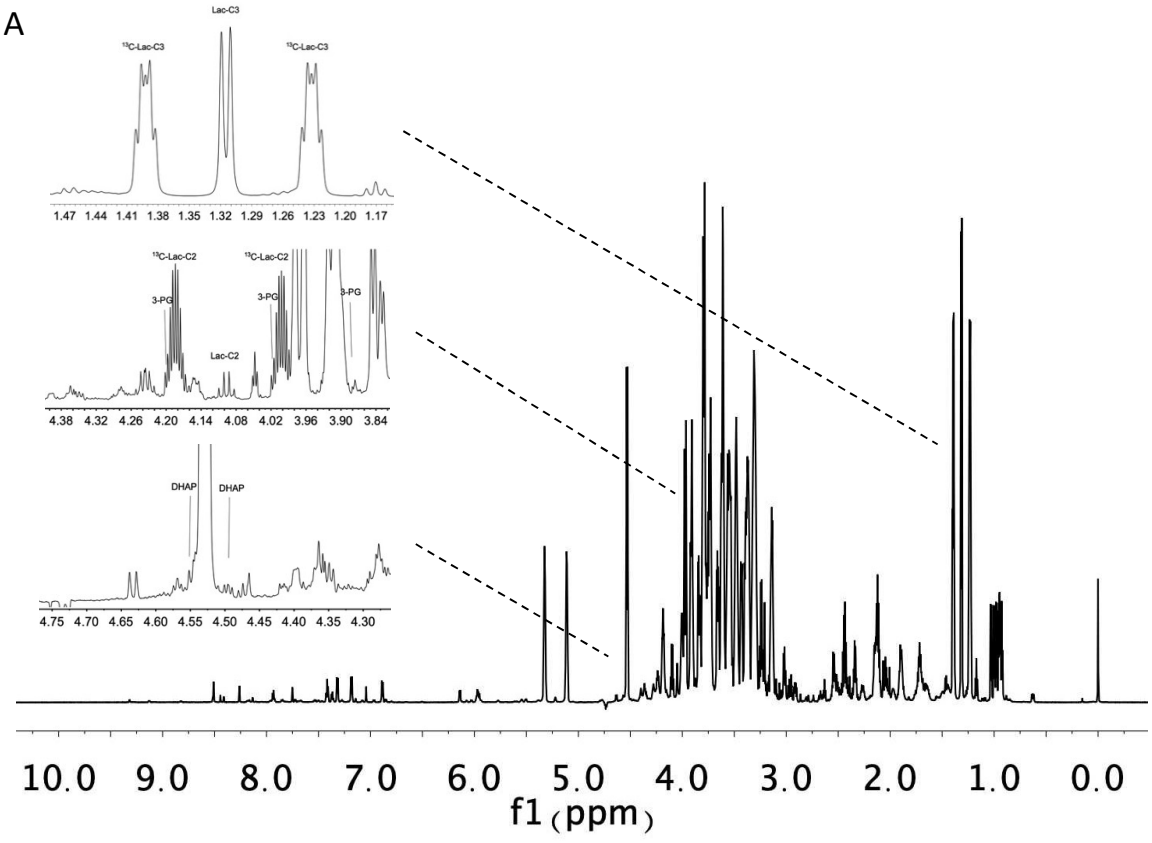

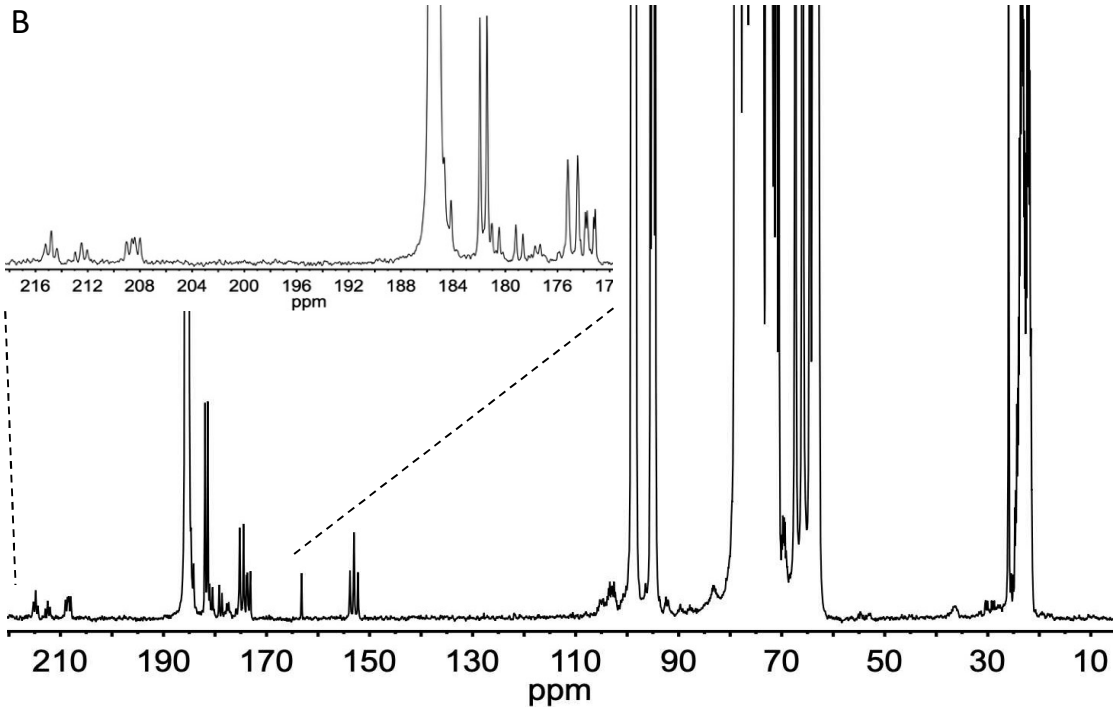

Figure S2. 1D NMR spectra of a representative extract from 10 mill cells of the prostate cancer type DU145. A) 1D ^{1}H-^{13}C-NMR spectrum referenced to DSS at 0 ppm. The excerpts show an area of the spectrum where ^{13}C-satelites are easily identified and quantified, top: lactate, as well as two areas of the spectrum where ^{13}C-satelites were expected to be found for signals belonging to 3-PG and DHAP, respectively but not identifiable and quantifiable due to spectral overlap. B) 1D dDNP ^{13}C-NMR spectrum referenced to HP001 at 25.7 ppm. The excerpt shows the carbonyl area in which 10 metabolites are readily identified and quantified based on their unique chemical shift and in some cases their coupling constant pattern.

Peak picking and preprocessing data:

The spectra were analyzed in Mnova, a line broadening of 3 Hz was added, they were manually phased, and a Bernstein baseline correction was applied. The spectra were referenced to HP001 at 25.7 ppm.

The ten signal integrals used for ML analysis were chosen as representative peaks belonging to identifiable products derived from the glycolysis, which did not overlap with other peaks in the spectra. Exceptions were U178 included as an unspecified amino acid and serine/glycine included together because they overlapped in the spectra. Signals were fitted using the peak fitting tool in MNova to guide the integral and where overlap existed half of the signal was integrated and multiplied with 2. For metabolites with multiple well-separated peaks, only one signal was included (selected as the longest T_1 signal in the molecule).

Integral values were measured relative (normalized) to the HP001 signal and collected in a data matrix. For the samples containing only 10 mio. cells, values were doubled.

Figure S3 provide a distribution of the measured integrals for the ten signals used in the statistical analysis with standard deviations over 8 samples for each cell type.

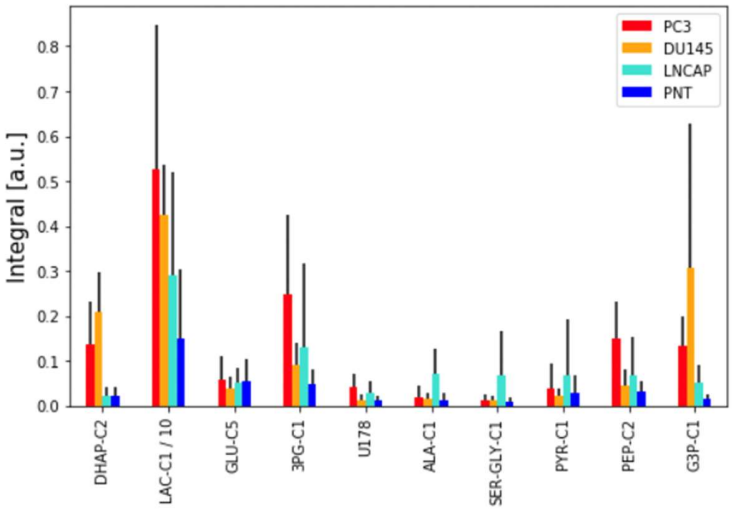

Figure S3 Average of integral values of peaks representative of the 10 identified metabolites, listed in Table 1. Cell lines are presented as PC3 (red), DU145 (orange) LN-CaP (light blue), and PNT1A (dark blue). Integrals were normalized to the internal standard. n = 8 for each cell line. Black bars are standard deviation. Lactate is scaled down by a factor of ten.

Univariate statistical analysis:

Table S2 ANOVA test results for differences between cell lines for each metabolite, with Bonferroni corrected significance levels.

	F value	P value	Bonferroni corrected significance
DHAP-C2	15.70	3.52E-06	Significant > 99%
LAC-C1	4.52	0.01047	Not significant
GLU-C5	0.2952	0.8285	Not significant
3PG-C1	3.371	0.03235	Not significant
U178	3.572	0.02639	Not significant
ALA-C1	5.336	0.004917	Significant > 95%
SER-GLY-C1	2.597	0.07214	Not significant
PYR-C1	0.6675	0.5791	Not significant
PEP-C2	5.652	0.003705	Significant > 95%
G3P-C1	4.874	0.00751	Not significant

Machine Learning:

PC-DFA analysis

All statistical analysis where done with Python(*Python Language Reference*, n.d.) using SciPy[2] and scikit-Learn.[3] The function for generating a standard deviation cloud in the PC-DFA plot is error_eclipse.py.[4]

As PC-DFA is a parametric function and thus performs optimally on normal distributed data, a box-cox transformation was applied prior to the application of the PC-DFA algorithm. In the box-cox transformation the λ parameter was optimized for the data, afterwards the data was scaled by subtraction of the mean and division of the standard deviation for each feature.

95% accumulated explained variance was chosen as the limit for how many PCA components to include in PC-DFA analysis.

RF analysis

Random Forest feature ranking was done with RFs of 500 trees (with gini as impurity measure, no maximum depth), applied to a set made of 70% of the data randomly picked but stratified so that ratio of aggressive to less aggressive was preserved. Then by shuffling the values in the remaining 30% of data points, a comparison was made between unshuffled and shuffled classification success. This process was repeated 1000 times over to get the importance ranking.

SVM analysis

SVM was applied to data scaled by subtracting the mean and dividing by the standard deviation for each feature. Linear, polynomial and radial basis function kernels were tested for SVM, but for all feature subsets linear performed as good or better than the others. The regularizations parameter (C) was set to 1.

Public available scripts and data

The data and Python scripts are available through this link:

https://github.com/Afrhm/SIRM-classification-2020

Literature:

[1] Lerche, M. H., Yigit, D., Frahm, A. B., Ardenkjær-Larsen, J. H., Malinowski, R. M., & Jensen, P. R. (2018). Stable Isotope-Resolved Analysis with Quantitative Dissolution Dynamic Nuclear Polarization. *Analytical Chemistry*, *90*(1), 674–678.

[2] Jones, E., Oliphant, T., Peterson, P., & others. (n.d.). *{SciPy}: Open source scientific tools for {Python}*. Retrieved from http://www.scipy.org/

[3] Pedregosa, F., Varoquaux, G., Gramfort, A., Michel, V., Thirion, B., Grisel, O., … Duchesnay, E. (2011). Scikit-learn: Machine Learning in {P}ython. *Journal of Machine Learning Research*, *12*, 2825–2830.

[4] Kington, J. D., & Tobin, H. J. (2013). Balanced Cross Sections, Shortening Estimates, and the Magnitude of Out-of-Sequence Thrusting in the Nankai Trough Accretionary Prism, Japan. *American Geophysical Union, Fall Meeting 2013, Abstract Id. T31F-2580*. Retrieved from http://adsabs.harvard.edu/abs/2013AGUFM.T31F2580K

PAPER 2

B

TITLE

Classification and biomarker identification of prostate tissue from TRAMP mice with hyperpolarized 13C-SIRA

AUTHORS

Frahm, A.B.; Hill, D.; Katsikis, S.; Andreassen, T.; Ardenkjær-Larsen, J.H.; Bathen, T.F.; Moestue, S.A.; Jensen, P.R.; Lerche, M.H.

STATUS

Submitted to *Talanta*, 2021.

Classification and biomarker identification of prostate tissue from TRAMP mice with hyperpolarized ^{13}C-SIRA

Anne B. Frahm[a], Deborah Hill[b], Sotirios Katsikis[a], Trygve Andreassen[b], Jan Henrik Ardenkjær-Larsen[a], Tone Frost Bathen[b], Siver Andreas Moestue[b,c], Pernille Rose Jensen[a], Mathilde Hauge Lerche[a,*]

a: Center for Hyperpolarization in Magnetic Resonance, Department of Health Technology, Ørsteds plads 349, 2800 Kongens Lyngby, Denmark.

b: Department of Circulation and Medical Imaging, Norwegian University of Science and Technology, Trondheim, Norway

c: Department of Pharmacy, Nord University, Bodø, Norway

*Corresponding author. E-mail: mhauler@dtu.dk

Supporting information is available.

Keywords: dissolution Dynamic Nuclear Polarization, prostate cancer, Support Vector Machines, Random Forest, Stable Isotope Resolved Analysis, isotopic fingerprinting

Abstract

Hyperpolarized ^{13}C isotope resolved spectroscopy boosts NMR signal intensity, which improves signal detection and allows metabolic fluxes to be analyzed. Such hyperpolarized flux data may offer new approaches to tissue classification and biomarker identification that could be translated *in vivo*.

Here we used hyperpolarized stable isotope resolved analysis (SIRA) to measure metabolite specific ^{13}C isotopic enrichments in the central carbon metabolism of mouse prostate. Prostate and tumor tissue samples were acquired from transgenic adenocarcinomas of the mouse prostate (TRAMP) mice. Before euthanasia, mice were injected with [U-^{13}C]glucose intraperitoneally (i.p.). Polar metabolite extracts were prepared, and hyperpolarized 1D-^{13}C-NMR spectra were obtained from normal prostate (n=19) and cancer tissue (n=19) samples. Binary classification and feature analysis was performed to make a separation model and to investigate differences between samples originating from normal and cancerous prostate tissue, respectively.

Hyperpolarized experiments were carried out according to a standardized protocol, which showed a high repeatability (CV=15%) and an average linewidth in the 1D-^{13}C NMR spectra of 2±0.5 Hz. The resolution of the hyperpolarized 1D-^{13}C spectra was high with little signal overlap in the carbonyl region and metabolite identification was easily accomplished. A discrimination with 95% success rate could be made between samples originating from TRAMP mice prostate and tumor tissue based on isotopomers from uniquely identified metabolites.

Hyperpolarized ^{13}C-SIRA allowed detailed metabolic information to be obtained from tissue specimens. The positional information of ^{13}C isotopic enrichments lead to easily interpreted features responsible for high predictive classification of tissue types. This analytical approach has matured, and the robust experimental protocols currently available allow systematic tracking of metabolite flux *ex vivo*.

Introduction

For studies of metabolic activity in intact biological systems, tracking of metabolites originating from isotopically enriched tracer molecules has been the method of choice for decades. Such isotopic profiling has been applied *in vivo* to interrogate dynamic activities of metabolic pathways [1-3] and to evaluate contributions of individual enzymatic reactions to production or consumption of specific metabolites [4,5]. Biological interpretations are supported by the isotopic patterns contributing to group discrimination [6]. In particular, isotopic profiling studies take advantage of unsupervised, multivariate statistical classification (such as principal component analyses) to discriminate strains or conditions based on ^{13}C-labeling data, without a priori knowledge of the metabolic system [7,8].

Metabolic activity can be quantitatively studied with nuclear magnetic resonance (NMR). By performing NMR in conjunction with ^{13}C-isotope enriched tracers, specific metabolic pathways can be investigated [9,10]. In recent years real-time analysis of metabolic flux in intact cells and whole organisms has become possible with magnetic resonance spectroscopy (MRS) developed in conjunction with hyperpolarization of ^{13}C enriched tracers. Such hyperpolarized ^{13}C metabolic MRS tracers enable non-invasive monitoring of tumor progression [11] and cancer treatment efficacy [12]. In particular, hyperpolarization of ^{13}C isotopic labelled pyruvate provides a sensitivity boost that allows its metabolic transformation to be followed *in vivo* in humans after an intravenous injection of this molecule [13,14]. In humans, this technology has currently only been clinically approved for a single substrate (^{13}C pyruvate), however, biomarker identification is likely to push for clinical approval of additional substrates [15].

Identification of biomarkers in biological samples is a major challenge that is addressed by metabolomics [16]. The vast majority of NMR metabolomics studies use ^{1}H for quantitative high throughput analysis. This is due to a high sensitivity of ^{1}H NMR owing to the large gyromagnetic ratio of ^{1}H, as well as its abundance in biological tissues. The detection limit of ^{1}H NMR is in the order of μM concentrations and furthermore it has shown high reproducibility and specificity [17]. In biomarker studies, however, the benefits of ^{1}H NMR are compromised by severe signal overlap due to a narrow chemical shift scale and couplings. The main challenge is to identify relevant and related signals amongst a background of complex biology that results in overlapped spectral patterns. Great efforts have been devoted to address this challenge, including the development of dedicated 1D and 2D NMR methods combined with databases, as well as statistical methods based on correlations or ratio analysis [18]. Also, recently, sensitivity enhancement with hyperpolarization techniques have allowed direct detection of nuclei such as ^{13}C and ^{15}N in metabolite extracts [19-22]. These methods exploit the much larger chemical shift dispersion of nuclei with low gyromagnetic ratios to resolve individual metabolite signals.

Combining isotopic labelling with hyperpolarized 1D-^{13}C NMR provides for a highly sensitive, specific, and quantitative method to identify biomarkers in biological systems [23,24]. This method

has been named hyperpolarized ^{13}C-stable isotope resolved analysis (^{13}C-SIRA). Comparable results between this *ex vivo* method and the *in vivo* real time flux applications using hyperpolarized ^{13}C-MRS implies that the discovery of important biomarkers *ex vivo* using ^{13}C-SIRA could also be regarded as important biomarkers *in vivo*.

Inspired by this possibility, we wanted to evaluate the ^{13}C-SIRA method for tissue classification and biomarker identification in a relevant model of human disease. With ongoing clinical trials and published studies of real time hyperpolarized ^{13}C metabolism in prostate cancer patients [25-26,13] we decided to make the *ex vivo* study in a model of prostate cancer. To this end we chose the transgenic adenocarcinoma of mouse prostate (TRAMP) model, which has gained widespread attention for its ability to mirror disease pathogenesis of the human prostate [27]. TRAMP mice spontaneously develop autochthonous prostate tumors following the onset of puberty [28]. The tumor progression is androgen-driven and developmentally regulated [29] which could challenge a discrimination between tumor and prostate tissue. In addition, the TRAMP model has been used in several real-time metabolic MRS studies [30,31].

In this study, we used the hyperpolarized ^{13}C-SIRA method on tissue extracts from TRAMP mice administered with isotopic labelled [U-^{13}C]glucose by intraperitoneal injection. This resulted in a highly repeatable, fast, easily interpretable, and generally applicable method for extraction of metabolic information from a complicated biological system. Having established the methodology, it was successfully applied to the challenging task of discriminating between normal and cancerous prostate tissue from TRAMP mice. Furthermore, since signals in the hyperpolarized 1D-^{13}C NMR spectrum could easily be identified as belonging to specific metabolites, the features that were responsible for tissue classification could be evaluated and related to reported *in vivo* findings.

Materials and Methods

Materials and ethics

[U-^{13}C]glucose (99%) and deuterium oxide (99.9%) was purchased from Sigma-Aldrich.
All other chemicals were the purest grade available from Sigma-Aldrich.

Prostate tissue was collected from TRAMP mice, which were genetically modified from C57BL/6 mice (Jackson Labs, USA) and bred on the same background in NTNU's comparative medicine core facility. The genotype of the mice was confirmed using PCR, and the animals were regularly monitored for general health status. Breeding, daily care, and experimental work were approved by the Norwegian National Animal Research Authority (FOTS ID 11843).

In vivo experiments

Male TRAMP mice selected for the experiments were 24 – 48 weeks old. The mice were anaesthetized using 1.5% to 2.5% isoflurane with a flowrate of 0.5 l/min; 5 to 1 air to oxygen mixture, before intraperitoneal administration of 10 mg/gram body weight [U-^{13}C]glucose in saline. The mice were kept anaesthetized for 30 minutes before sacrifice by cervical dislocation and dissection of the prostate tissue. It has previously been reported that prostate cancer in TRAMP mice can be classified into two groups: well-differentiated (WD) and poorly differentiated (PD) [32,33]. WD tumors are histologically similar to low-grade prostate adenocarcinomas in humans,

whereas PD tumors resemble carcinomas of neuroendocrine origin [34], which is rarely seen in the clinic. In this project, we chose to study WD tumors as their phenotype resembles the most prevalent human prostate cancer. Prostate lobes were dissected and defined as normal or WD based on a visual examination during dissection, where overall size, irregular shape and discoloration/hypervascularization were the criteria used to identify cancerous tissue. Cancers located in the seminal vesicles were also included in the experiment. Due to a minimum sample weight requirement of 50 mg wet weight for the hyperpolarized ^{13}C NMR analysis, normal prostate lobes were combined together to form a single sample, whereas WD samples were large enough to be separated individually.

Tissue metabolite extraction

Perchloric acid ($HClO_4$) extraction was carried out as described previously [35]. Briefly, $HClO_4$ (7% v/v) solution was added in a 1:4 w/v tissue:$HClO_4$ ratio to the frozen tissue that was homogenized using a mortar and pestle (while keeping the tissue-$HClO_4$ sample cold on ice). Soluble metabolites were extracted by centrifugation (10 min, 10000 rpm, 4 °C). Supernatant was pH neutralized with KOH, centrifuged, and supernatant was freeze-dried. Tissue metabolite extracts were stored at − 80 °C until prepared for nuclear magnetic resonance spectroscopy.

Conventional NMR on tissue metabolite extracts

Lyophilized tissue metabolite extracts for individual samples were dissolved in 250 µl 40 mM deuterated phosphate buffer and 300 µl D_2O. The pH was adjusted to 7.90±0.05 with NaOD or sulfuric acid in D_2O. The samples were transferred to 5mm NMR tubes.

^1H NMR spectra were recorded at 300 K on a Bruker Avance III 600 MHz (Bruker BioSpin GmbH, Rheinstetten, Germany) spectrometer, equipped with a 5 mm QCI CryoProbe. Samples were analyzed in automation using a SampleJet autosampler and IconNMR running under Topspin 3.5 pl6. One-dimensional nuclear Overhauser effect (NOE) spectra (pulse program “noesygppr1d”) were recorded with 64k data points, 20 ppm spectral width and 128 scans. For residual water suppression, low power (25 Hz) presaturation of the water resonance was applied during relaxation delay (4 s) and mixing time (10 ms). Spectra were Fourier transformed to 128k data points using 0.3 Hz line broadening.

Following conventional NMR the samples were transferred to eppendorf tubes and freeze dried before preparation for ^{13}C-hyperpolarization.

^{13}C-hyperpolarization with Dynamic Nuclear Polarization on tissue metabolite extracts

The lyophilized metabolite samples were dissolved in 50 mg of polarization medium (77 mg trityl radical OX063, 1533 mg glycerol-d_8, 1085 mg D_2O, 35 mg gadoteridol (100 µmol/g)), and 5 µl of HP001 (50 mM, 1.1-bis (hydroxymethyl)-[1-^{13}C]cyclopropane)) was added as an internal standard.

DNP was performed at 3.35 T and 1.4 K in a HyperSense polarizer with microwave irradiation at $f_{\mu W}$ = 94 GHz and $P_{\mu W}$ = 100 mW. Samples were polarized for 90 min.

Hyperpolarized 1D-^{13}C-NMR of tissue metabolite extracts

All hyperpolarized tissue metabolites samples (38) were washed out of the polarizer with 5 mL of deuterated phosphate buffer (50 mM, pH 7.4), the front of which dissolved the sample (approx. 1.5 ml). An amount (550 ± 10 µL) of the dissolved sample was automatically transferred from the polarizer to an 11.7 T Bruker NMR spectrometer equipped with a cryoprobe for recording of 1D ^{13}C-NMR spectra.

NMR parameters: ^{13}C 1D NMR spectra of hyperpolarized metabolite samples were acquired using an automated trigger signal after sample arrival to the spectrometer and 3 seconds preacquisition delay. The 1.088 s acquisition time was set at 1.088 s, at 300 K (27 °C) with a 90° pulse. Proton decoupling was applied during acquisition.

Sample transfer: A custom-made sample transfer device was designed to work as an add-on to the Hypersense polarizer based on published principles [36], see supp. info. Figure S5 for details. The following delay settings were used: Pre-acquisition delay of 3s and a stabilization delay of 305 ms. The travel time between the two sensors were experimentally determined (dependent on tube diameter, sample viscosity and transfer pressure) and was in this study observed to be approx. 800 ms. In total the sample transfer time including stabilization was thus approx. 4.1 s.

Sample preparation for precision measurements and metabolite identity verification

Metabolite samples (10) originating from prostate tissue, redundant and split from samples included in the main study, were dissolved into one batch in 5 ml water. This batch sample was then divided into 10 samples of 500 µl metabolite extract and freeze dried. Of these samples 8 were prepared and hyperpolarized as the samples included in the main study, see above. The remaining samples were used for conventional NMR (^{1}H-^{13}C-HSQC and ^{1}H-^{13}C-HMBC) to aid metabolite identification between overlapping carbonyl signals (between glutamine C1 and aspartate C4 and between glycine C1 and serine C1).

NMR data processing

All spectra were processed in Mnova [37].

Hyperpolarized 1D-^{13}C NMR: spectra were Fourier transformed to 128K points with a 64K points zero filling and 0.3 Hz line broadening, subsequently manually phased, and a Whittaker smoother baseline correction was applied. The spectra were referenced to HP001 at 25.4 ppm (corresponding to lactate C1 at 185.2 ppm).

Proton NMR: 1D NOESY spectra were processed with Bruker TopSpin version 4.0.7. The phase was manually corrected. No baseline correction was found to be needed. The spectra were referenced to the TSP peak at 0 ppm in MatLab [38]. An area of interest was set from 0.05 to 10 ppm with the area of the water peak removed (4.59 to 5.04 ppm). ICOshift (version 3.0) was used to align the spectra [39]. The spectra were autobinned with bin size of 0.02 ppm. Noise filtering was performed by choosing a representative bin with high level noise (5.27-5.29 ppm) and removing all bins with no values higher than the values in this noise bin, leaving 298 features in the dataset.

2D NMR: The NMR signals were identified as belonging to specific atoms in energy/glycolytic metabolites by consulting available databases [40]. This was done using distinct chemical shifts of carbonyl carbons and by comparing ^{13}C-^{13}C coupling constant pattern with simulations using the

NMR analysis tool box in MNova based on the knowledge that all ^{13}C-labelled metabolite signals are derived from uniformly [U-^{13}C]glucose. The assignment for especially glycine and glutamine for which the carbonyl chemical shift is close to serine and aspartate, respectively, were further verified with ^{1}H-^{13}C HSQC and ^{1}H-^{13}C HMBC spectra acquired on a sample from the repeatability study.

Data analysis

Data-matrices of hyperpolarized ^{13}C NMR spectra: Two datasets were created named "full spectrum" and "metabolite spectrum", respectively. Both datasets were made by manually integrating individual NMR signals in the 38 overlaid spectra and normalizing these integrals to sample weight and to the internal reference (HP001) for the individual spectra.

In the "full spectrum" dataset all NMR signals with an SNR above 3.3 were included, except for signals belonging to the polarization medium, deuterated-glycerol and internal standard (HP001) and impurities from these compounds, as identified from a hyperpolarized spectrum of these. In the "metabolite spectrum" dataset ideally only one unique carbon signal from each metabolite was included. Carbon signals with long T_1 (non-protonated carbons) were prioritized. Where several isotopomers of the carbon were identified, a carbon signal representing each isotopomer was included.

All multivariate statistical analysis was done with Python [41]. Available at http://www.python.org using algorithms from Scikit-Learn [42] and SciPy [43]. Retrieved from https://scikit-learn.org/ and http://www.scipy.org/.

Prior to Principal component analysis (PCA), the data was mean subtracted and scaled to unit variance.

Feature analysis with random forest algorithm (RF)

Random Forest feature ranking was performed with RFs of 600 trees (with gini as impurity measure, no maximum depth), applied to 70% of the randomly picked but stratified so that the ratio of prostate to tumor samples was preserved. Then by shuffling the values in the remaining 30% of data points, a comparison was made between unshuffled and shuffled classification success. This process was repeated 10.000 times over to obtain the importance ranking. No independent testing was done for the RF analysis, and all the data points were included.

Each features importance was calculated as the mean decrease in accuracy when it was shuffled, with the standard error on the mean (SEM) subtracted. A feature was deemed as significantly important if its measured importance was at least 5% of the importance of the highest ranked feature.

Classification with support vector machine algorithm (SVM)

Features found significantly important were mean subtracted and scaled to unit variance before being used as input for a linear SVM analysis. The SVM soft margin parameter (C) was optimized in a grid search, ranging $C = [2^{-5}, 2^{-4} \ldots 2^{5}]$. Leave-one-out cross validation was applied.

Results and discussion

Isotopic labelling and dissection of prostate tissue from TRAMP mice

Experimental design

A pilot study was performed to evaluate critical parameters in the study design including tracer choice, administration route, incubation time and the possibility to perform thermal NMR and hyperpolarized 1D-^{13}C NMR analysis on the same samples. The data from this pilot study is presented in supp. info and Figures S1-S3.

To probe the central carbon energy metabolism, [U-^{13}C]glucose was chosen as a tracer. The short carbon T_1s of protonated glucose (0.6-1.2 s, 11.2 T, 37 ºC) have previously led to the use of fully deuterated carbon labelled glucose when applied in hyperpolarization studies [44]. The pilot study, however, showed that an automatic transfer of extracted hyperpolarized [U-^{13}C]glucose allowed quantification with high precision despite short carbon T_1s. The protonated carbon labelled tracer made it possible to collect thermal NMR spectra on the extracted tissue metabolite samples before acquiring hyperpolarized 1D-^{13}C NMR spectra. The pilot study also allowed optimizing the amount of metabolic labelling. We injected 300 mg/ml [U-^{13}C]glucose intraperitoneal (i.p.) into the abdominal cavity of sedated mice followed by a 30-minute waiting time before sacrifice. Mice remained under isoflurane anesthesia during the 30-minute waiting time and were euthanized by cervical dislocation prior to tissue collection. This protocol gave a robust isotopic labelling in prostate tissue of high concentration metabolites (lactate, alanine and glutamate). A similar timing profile for i.p. injections in mice has previously been reported [45] and was in accordance with labelling from intravenous injection (i.v.) protocols [46].

Tissue sample collection and characterization

TRAMP mice from a c57BL/6 background (n=23) with ages varying from 24 to 48 weeks were included in this study. In total, 38 samples were included: 19 from prostates and 19 from tumors. The tumors originated either from the prostate (8 samples) or from the seminal vesicles (11 samples). Tumor bearing mice were identified by palpation. Palpable tumors are reported to be present in 80% of 32 weeks old TRAMP mice, whereas only about 10% have palpable tumors at 22 weeks of age [48]. Similarly, in our study we had few mice with palpable tumors at early age (none before 22 weeks). The ages of the included mice fell into two groups: 22-32 weeks (15 prostate samples and 10 tumor samples) and 36-48 weeks (4 prostate and 9 tumors), Figure 1.A. The tissue sample sizes varied from the smallest tumors (40 mg wet weight) to the largest tumor (> 1g wet weight), Figure 1.B. In order to standardize tissue amounts, all samples above 240 mg were split to obtain at least 120 mg tissue per split sample. There was no apparent correlation between mouse age or tissue weight and tissue grouping, supp. info. Figure S4. Thus, all samples were treated as belonging to one cohort.

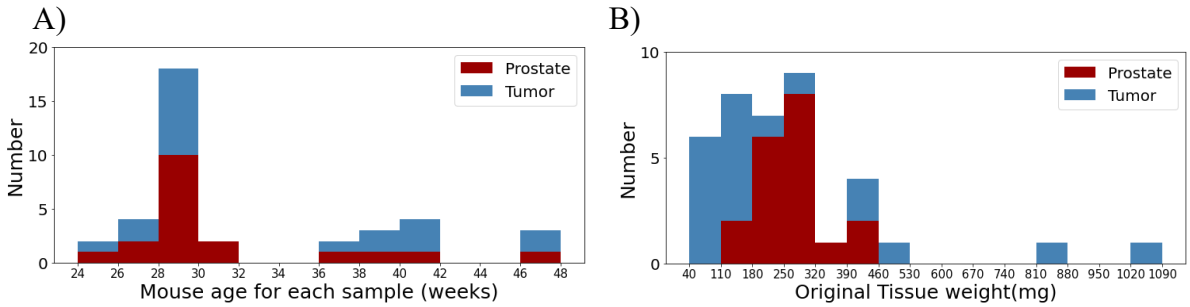

Figure 1. Stacked histogram showing age (A) and weight (B) of the mouse for each sample.

In this study, we chose to study WD tumors due to their more clinically prevalent phenotype. The two PD tumors that were found (in mice of 25 and 26 weeks of age, respectively) were accordingly excluded from the study. Generally, characterization of prostate cancer tissue in TRAMP mice is non-trivial due to the gradual progression from prostate to tumor tissue. We chose to combine tumors found in the prostate and in the seminal vesicles into one group - tumors - partly due to the number of available tumors and partly due to uncertainty in characterization of the tumor origin in two mice. Characteristics of the different types of tissue samples included in the study can be found in Table 1.

Table 1. Characteristics of grouped tissue samples. Variance is given as standard deviations.

Grouped tissue type	Number of samples	Average mouse age (weeks)	Average received [U-^{13}C]glucose dose (ml)	Average original excised tissue size (mg)	Average sample size for hyperpolarized 1D-^{13}C NMR (mg)
Prostate	19	31.4±5.5	1.14±0.10	271±74	149±26
Tumor from prostate	8	33.8±8.1	1.16±0.12	93±53	93±53
Tumor from seminal vesicle	11	34.3±6.7	1.14±0.09	179±134	119±37

Analytical performance of hyperpolarized ^{13}C-SIRA of tissue extracts

Building on a published protocol for dissolution Dynamic Nuclear Polarization (dDNP) NMR measurement of cell extracts [23], we developed a method for dDNP NMR measurement of tissue extracts. Critical parameters to be improved were identified including sample preparation and sample transfer time between dissolution of hyperpolarized sample and NMR detection. To address the latter, we built a sample transfer system based on published principles [36]. Details on the set-up can be found in supp. info. and Figure S5.

With this device, sample transfer time between the polarizer and the NMR detection magnet was significantly reduced to 1.10 ± 0.05 s compared to manual transfer (approx. 12s). Once inside the NMR magnet an additional 3s delay was added before data acquisition to stabilize the sample, resulting in a total transfer time of 4.1s. An added benefit of the automated transfer was a 3-fold concentrated sample, see supp. info. and Figure S6. The spectral quality of a hyperpolarized 1D-^{13}C NMR spectrum acquired on an extract from TRAMP prostate is shown in Figure 2.

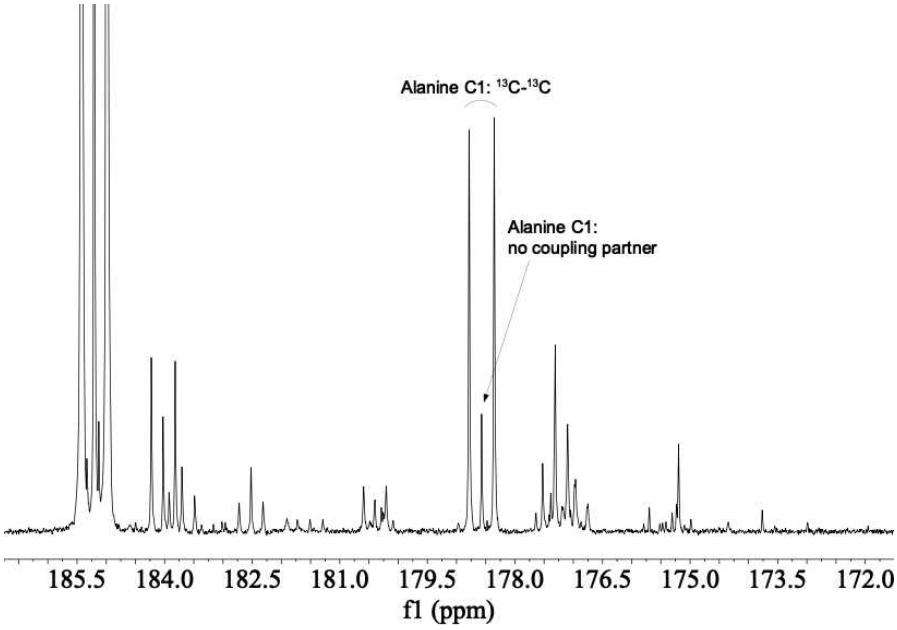

Figure 2. Carbonyl region of hyperpolarized 1D-^{13}C NMR spectrum of prostate extract from TRAMP mouse injected i.p. with [U-^{13}C]glucose 30 minutes prior to tissue harvest. A full spectrum is shown in supp. info. Figure S7. Characteristic isotopomer patterns, highlighted for Alanine C1 as an example, are generally measurable in the spectrum due to a narrow line shape and the large spread of carbon chemical shifts.

A transfer time of 1.1s over a distance of 4 meters is good compared to current published protocols for water dissolved samples [22,48]. Further reduction in the waiting time (currently 3s) may be achieved by coating the receiving NMR tube with Hellmanex® (Hellma analytics), which has shown to reduce microbubbles and improve signal line shape [22].

To assess the performance of the improved sample preparation and transfer we performed a repeatability study on the established tissue extract ^{13}C-SIRA assay. Redundant samples from the main study were pooled and made into identical samples of 135 mg wet tissue each (corresponding to 1 mg dry powder). Samples (8) were prepared for DNP and processed with the established assay. The average precision was CV=15% for all signals above Limit of Detection (LoD, defined as SNR 3.3). The linewidth of representative signals in the carbonyl region was 2±0.5 Hz. Such high repeatability is comparable to what was found in studies with hyperpolarized natural abundance ^{13}C-spectra of extracts from tomato fruit [20].

Classification of tumor and prostate tissue based on isotopic fingerprints

1D ^{13}C NMR spectra were acquired from 38 samples hyperpolarized with dDNP. From an initial visual inspection, the spectra originating from prostate and tumor tissue appear very similar (supp. info, Figure S8). Also, the mean and variance of the three highest metabolite signals did not clearly divide the two types of samples, prompting a more extensive data analysis, Figure 3.

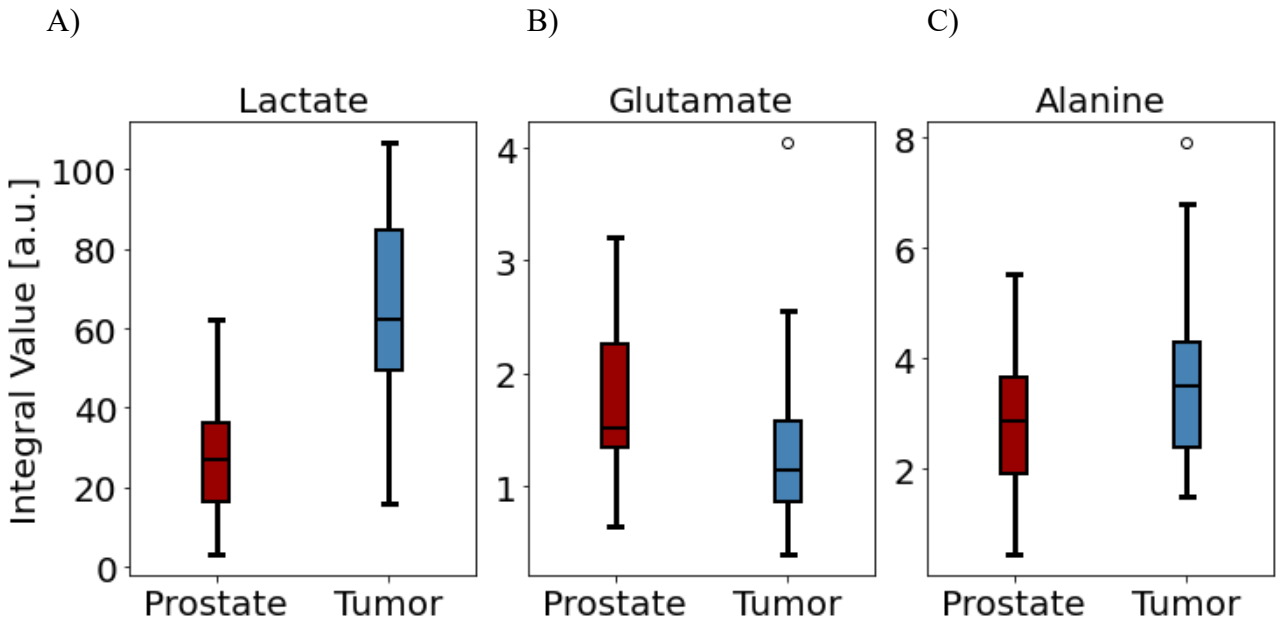

Figure 3. Box plots for high signal metabolites, A) lactate C1, B) glutamate C5 and C) alanine C1. Signal areas were measured as summed integrals over all isotopomers and referenced to the internal standard, HP001. Values are in arbitrary units and represents total integral over the C1 position for lactate and alanine and over C5 for glutamate. The metabolites were identified based on chemical shift and ^{13}C-^{13}C coupling constants.

Full spectrum analysis of hyperpolarized 1D-^{13}C NMR spectra

Initially, we wanted to understand whether the hyperpolarized 1D-^{13}C NMR spectra as a whole contained sufficient information to separate prostate and tumor samples into the groups they originated from. A dataset was constructed with the measured integral value of all signals above the LoD in the 38 spectra. Peaks that did not originate from the extracted tissue samples were excluded, i.e. the internal standard and signals from the glass former, deuterated glycerol. In total, this amounted to 129 signals, each normalized to the internal standard and the sample weight.

The normalized signal integrals were first subjected to a Principal Component Analysis (PCA). PCA is a commonly used multivariate data analysis technique in metabolomics [17], which transforms the multidimensional dataset into a two-dimensional dataset. To get an overview of the biological variance in the data and a visual on the separation between prostate and tumor samples, we made a plot of the first two PCA components, Figure 4.A. Point proximity indicates sample similarity. A separation could be seen along both the first-principal component (PC1, explained 36.3% of the variance) and along PC2 (explained 15.6% of the variance) between prostate and tumor samples. The much bigger spread seen within the tumor samples in the PCA analysis is to be expected since biological variability may be high based on the complexity of the TRAMP model, where progression from prostate to tumor metabolism is gradual [29].

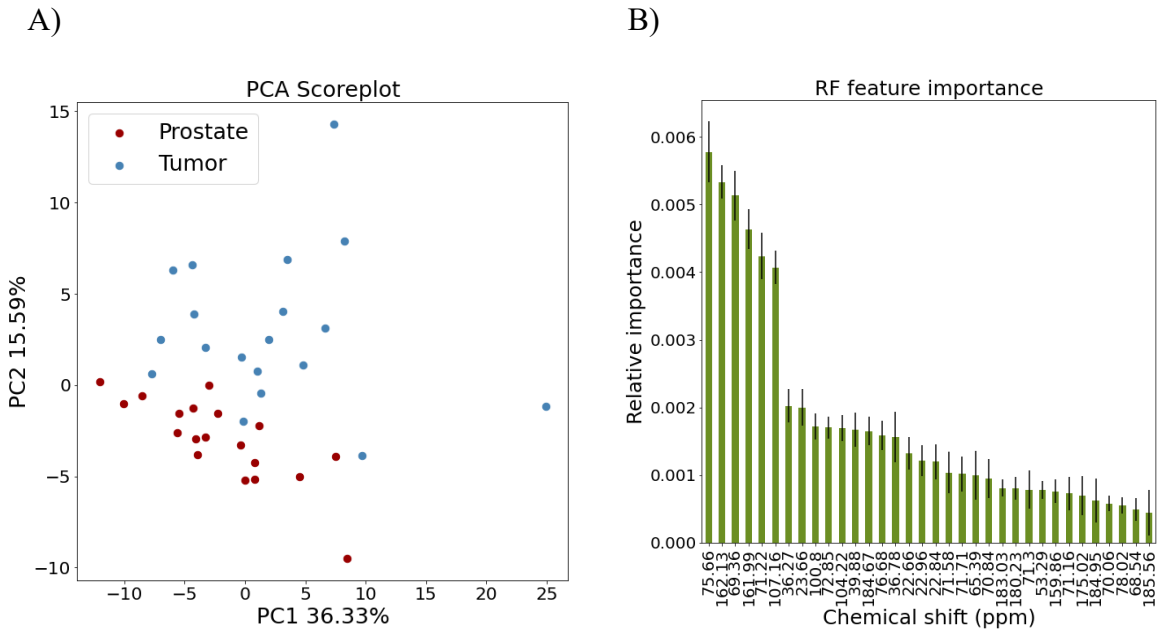

Figure 4. Full spectrum analysis of hyperpolarized 1D-^{13}C NMR spectra A) Score plot of PCA analysis. Each point represents a single sample, the coordinates of which are determined by the collective contributions of all sample corresponding signal integrals. Data was mean centered and unit variance scaled before PCA was applied. The PC1 x PC2 plan accounted for 51.9% of total variation among data points. B) Feature ranking performed with the Random Forest (RF) algorithm. 34 signals contributed positively to the discrimination between tumor and prostate tissue, 30 of these are shown). Six signals had a relatively higher importance than the rest.

To understand if it was possible to make a model that could separate prostate from tumour samples, a binary classification analysis was performed with Support Vector Machines (SVM) as a classifier based on all signals in the hyperpolarized 1D-^{13}C NMR spectra. In a previous study, this algorithm proved robust towards small datasets [24]. With the SVM algorithm, a plane was found in the feature-space to maximize the separation between samples belonging to the two classes, prostate or tumor. Prior to the data analysis with SVM we performed a dimensionality reduction by means of feature ranking using the Random Forest (RF) algorithm. Figure 4.B shows the result of the feature ranking of the 129 normalized integrals included in the dataset.

Several signals (n=34) contributed positively to the discrimination and resulted in a 97% success rate. Of these signals, six had a high relative importance. Performing the discrimination using only the 6 most important signals allowed a discrimination with 95% success rate between tumor and prostate tissue samples.

An inspection of the six signals that allowed a 95% successful discrimination showed that these signals carried little information about metabolites originating from isotopic labelled glucose: Three signals (including two carbamates, 162.1 and 162 ppm) had very low SNR (< 5) and were singlets. This indicated that they originated from non-isotopic labelled signals. One additional singlet was not identified (107.2 ppm, SNR<10). The last two signals were from a singlet originating from the lactate C2 isotopomer and from glucose C4α. Although highly valuable as a tool to discriminate between tissue samples with similar origin, this full spectrum analysis without prior knowledge did not provide clear information to be extracted about metabolites originating from the isotope labelled substrate.

Since the most commonly used data type for NMR metabolomics is ^{1}H NMR data, we chose to cross examine the supervised classification of the tissue samples based on full spectrum hyperpolarized 1D-^{13}C NMR with a similar analysis performed with ^{1}H NMR data collected on the same samples. A full account on the ^{1}H NMR spectral analysis can be found in supp. info and Figure S9. The signals in the ^{1}H NMR spectra were binned into 298 spectral areas (0.02 ppm/bin). In general, the errors in the RF analysis were high, however one bin that included a signal at 7.13 ppm was significantly more important than the rest and an SVM analysis with this feature alone allowed a 97% discrimination. Including additional two bins (signals at 6.81 and 7.11 ppm, respectively) allowed a perfect discrimination of 100%. These chemical shifts suggest that the metabolite behind includes a phenol group, where para-cresol or p-hydroxyacetic acid are likely candidates. Both of these metabolites are bacterially produced and constituents in urine. While these metabolites could separate the two sample groups included in this study, they are not likely to originate from the molecular ^{13}C-tracer.

Isotopic labelled metabolite information and interpretation

To investigate the value of molecular ^{13}C-tracer related metabolites for discrimination between prostate and tumor tissue, we created a metabolite selective dataset. The resolution of ^{13}C resonances is much higher than for ^{1}H due to the large chemical shift range of ^{13}C (250 ppm vs. 14 ppm) resulting in well separated metabolite signals. The isotopic labelling of metabolites originating from [U-^{13}C]glucose further allows biochemically related metabolites to be identified in a background of unlabelled metabolites, which can be two orders of magnitude lower in signal intensity. The uniform isotopic label, if transferred into the metabolite, also results in ^{13}C-^{13}C couplings that, along with the chemical shift of the ^{13}C signal, generally permit an unambiguous assignment of the signal as belonging to an isotopomer of a specific metabolite. Thus, a metabolite selected dataset could be created using this prior knowledge that allowed direct interpretation of isotopic labelled signals important for classification.

Metabolite based analysis of hyperpolarized ^{13}C-SIRA spectra

A dataset was constructed with integral values of identified metabolite signals from the carbonyl area of the spectra in the 38 included spectra. One carbon position was included per metabolite selected from the carbonyl region representing the longest T_1 carbons. For most metabolites both a doublet and a singlet isotopomer were present in the spectrum, Figure 2. Both isotopomer signals were included with the ^{13}C-^{13}C doublet represented in the dataset by one of its signals. In total this amounted to 35 signals, each normalized to the internal standard and the sample weight.

A plot of the first two PCA components, Figure 5.A, showed less variance between the prostate and tumor group compared to the full spectrum dataset (Figure 4.A.) even though the total explained variance was greater (58.1% vs. 51.9%). It could seem from this group separation that there were two fractions of tumor samples. We thus investigated if the PCA plot could indicate a separation between the tumor samples e.g. into tumors found in the prostate and tumors found in the seminal vesicles, supp. info. Figure S10. However, the study sample number did not support such separation.

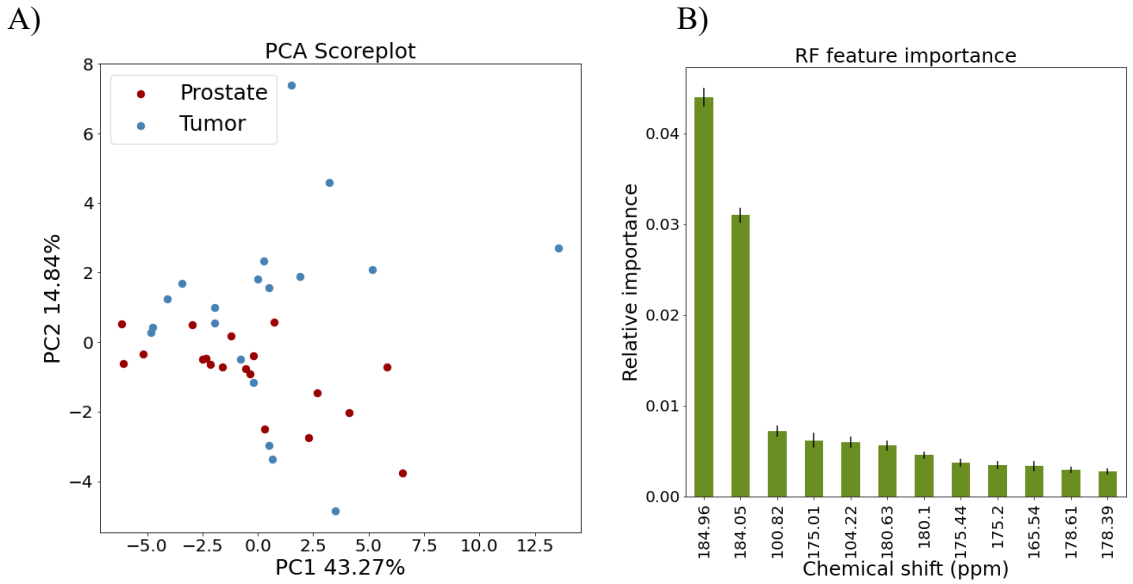

Figure 5. Metabolite analysis of hyperpolarized 1D-^{13}C NMR spectra A) Score plot of PCA analysis. Data was mean centered and unit variance scaled before PCA was applied. The PC1 x PC2 plan accounted for 58.1% of total variation among data points. B) Feature ranking performed with the Random Forest (RF) algorithm. 12 signals contributed positively to the discrimination between tumor and prostate tissue. Two signals had a relatively higher importance.

With the supervised model, 12 signals contributed positively to the discrimination. Two signals had a high relative importance as seen from the RF analysis, Figure 5.B. Using only these two features, a discrimination with 92.1 % success rate could be obtained, whereas including the 12 highest ranked signals allowed a discrimination with 95 % success rate between tumor and prostate tissue sample. This success rate did not increase further by including the remaining 6 signals that showed positive ranking from the RF analysis. The identity of the 12 signals, which allowed a 95 % successful discrimination is shown in Table 2.

Table 2. Identity of 12 features with highest rank in an RF analysis of the metabolite dataset. The score is given as the success rate obtained when including the metabolite and all previous metabolites, i.e. a 92.1 score is obtained when including both lactate C1 and glutamate C5.

Feature #	RF Ranking	Score (%)	Chemical shift	Identity
1	0.044±0.0010	81.6	184.96	lactate C1, doublet
2	0.031±0.0008	92.1	184.05	glutamate C5, singlet
3	0.007±0.0006	89.5	100.82	beta fructofuranose, singlet
4	0.006±0.0008	92.1	175.01	serine C1, doublet
5	0.006±0.0006	92.1	104.22	alfa fructofuranose, singlet
6	0.004±0.0006	92.1	180.63	glutamine C5, doublet
7	0.004±0.0004	92.1	180.10	aspartate C1, singlet
8	0.003±0.0004	92.1	175.44	glycine C1, singlet
9	0.003±0.0005	92.1	175.20	glycine C1, doublet
10	0.003±0.0003	92.1	165.54	urea
11	0.003±0.0004	92.1	178.61	alanine C1, singlet
12	0.002±0.0004	94.7	178.39	alanine C1, doublet

Whereas metabolites originating from the molecular ^{13}C-tracer is straightforwardly identified in the hyperpolarized 1D-^{13}C NMR spectra it is difficult to make use of such prior knowledge from

analysis of ^{1}H NMR spectra. Administration of [U-^{13}C]glucose significantly increase the signal overlap on the narrow ^{1}H chemical shift scale due to the carbon proton couplings, which at the same time are those that carry the valuable biochemical information. Usually only a few metabolites, such as high concentration metabolites in less crowded spectral regions, e.g. alanine methyl and lactate methyl groups and proton attached to C2 in lactate, can be unambiguously identified and quantified in a ^{1}H NMR spectra [50,24]. For this reason, we did not attempt to make a comparison to ^{1}H NMR performance using a dataset where only tracer specific metabolites had been selected.

Biomarker identification

In Table 2 it was seen that isotopomers from several metabolites could play a role in the discrimination of prostate and tumor tissue from TRAMP mice. We further investigated their individual and relative contribution to a separation using a PCA loading plot, Figure 6. The loading plot showed that fructo-furanoses mostly influences PC2. Lactate, aspartate and glutamate have almost equal weight on both components and the remaining metabolites mostly contributes to PC1. Not surprisingly, the two fructo-furanoses have identical impact. The signals from lactate and aspartate are closely and positively related but negatively correlated to the fructo-furanoses. The rest of the signals correlate positively in two groups. Serine and alanine signals in one group and glutamine, glutamate, glycine and urea in another group. A box-plot analysis of these 12 metabolite isotopomers, supp. info. Figure S11, showed lactate and serine to be increased in tumor tissue whereas the fructofuranoses, glutamate, glutamine and urea were lower in tumor tissue compared to prostate tissue.

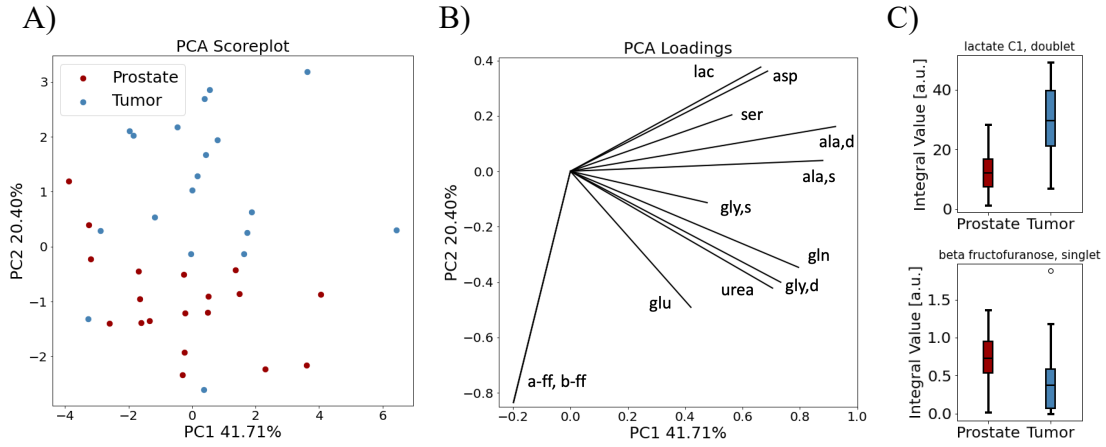

Figure 6. PCA plots using only the 12 RF selected highest ranked features. A. Score plot of PCA analysis. Each point represents a single sample, the coordinates of which are determined by the collective contributions of all sample corresponding signal integrals. Data was mean centered and unit variance scaled before PCA was applied. The PC1 x PC2 plan accounted for 62.11% of total variation among data points. B. Loading plot of PCA analysis. The Impact and correlation of the 12 features listed in Table 2 are shown. Interpretation: Projection of vectors to the respective axes infer their weight on the PCs. Close proximity of vectors, forming a small angle between them, suggest positive correlation between the features whereas vectors meeting at 90° suggests no correlation and vectors with larger angles infer negative correlation. Shorter length vectors suggest less importance (ser and gly,s). Here shown for the PC1 x PC2 plan, why interpretation could be influenced by including more dimensions. C. Box-plot for Lactate and beta fructofuranose. Values are in arbitrary units and represents integral over the specific isotopomer included in the analysis. Box-plot for the remaining 10 high ranking metabolites are shown in supp. info. Figure S11.

Lactate was expected to contribute to discrimination between prostate and tumor tissue from TRAMP mice. Several metabolic imaging studies of prostate and tumors in TRAMP mice have

shown how lactate signal increase with tumor progression [30,31]. Using lactate alone for the discrimination between prostate tissue and WD tumors gave however a success rate (81.6%) similar to what could be obtained by chance for the metabolite dataset (highest score from randomizing tumor and prostate samples was 79%). The success rate could be significantly increased to 92.1% by including at least one of the other 11 features discussed above.

The finding that fructose is negatively correlated with lactate in the discrimination of WD tumor tissue from normal prostate tissue is especially interesting to include in further biomarker investigations. Fructose metabolism is emerging as important in cancer biology, which can be explained by an increased intake of this nutrient in cancers [50]. Although most fructolysis takes place in the liver, both normal prostate cells and prostate cancer cells take up and metabolize fructose. GLUT5 is a specific transporter of fructose and it has been reported to be overexpressed both in normal human prostate and in prostate cancer [51]. The so-called polyol pathway consists of two reversible reactions; using sorbitol as an intermediate it allows conversion of fructose to glucose, or alternatively allows for an endogenous production of fructose from glucose. The latter makes it possible for cells to bypass glycolytic regulation and increase the glycolytic rate [52]. The polyol pathway has been reported as active both in normal prostate and prostate cancer [53]. Fructose is also connected to lipogenesis, which is another important requirement of proliferating cancer cells. The large fructose signal in TRAMP prostate tissue seen in our study could, due to a 30 min. circulation time of the molecular ^{13}C-tracer, result in production of ^{13}C labelled fructose in the liver rather than directly in the prostate. In that case the difference in fructose signal between the two tissue types would be due to uptake capability rather than production.

Hyperpolarized ^{13}C-fructose has already been developed as a real time metabolic imaging marker and tested in TRAMP mice for spectroscopic imaging of PD tumors [54]. With an improved understanding of fructolysis in different stages of the prostate cancer development it is likely that a biomarker could be developed with a combination of ^{13}C-pyruvate and ^{13}C-fructose. Such combined tracer would target lactate derived from pyruvate and fructose metabolism simultaneously and thus potentially improve the diagnostic accuracy of prostate cancer compared to focusing solely on ^{13}C-lactate derived from pyruvate.

Conclusion

In this study, we used the hyperpolarized ^{13}C-SIRA method to collect 1D-^{13}C NMR data on normal and cancerous prostate tissue extracts from TRAMP mice administered with isotopic labelled [U-^{13}C]glucose.

With a combination of a random forest algorithm applied to evaluate signal importance and support vector machines for classification it was possible to make a discrimination with 95% success rate between tumor and normal prostate tissue.

Signals in the hyperpolarized 1D-^{13}C NMR spectrum could easily be assigned to specific metabolites. The signals that were responsible for tissue classification could be evaluated and related to reported *in vivo* findings. In particular, the evaluation suggested that targeting pyruvate and fructose metabolism in combination could provide additional information compared to pyruvate alone for prostate cancer diagnosis.

Acknowledgements

The authors gratefully acknowledge funding by the Danish National Research Foundation (Grant DNRF124).

Hyperpolarized 1D-^{13}C NMR data in this study was acquired with equipment partially funded by the Novo Nordisk Foundation (NNF19OC0055825).

The tissue extraction procedures and ^{1}H -NMR experiments were performed at the MR Core Facility, Norwegian University of Science and Technology (NTNU). MR core facility is funded by the Faculty of Medicine and Health Sciences at NTNU and Central Norway Regional Health Authority

TRAMP mice breeding, housing, and genotyping was provided by the Comparative medicine Core Facility (CoMed), Norwegian University of Science and Technology (NTNU). CoMed is funded by the Faculty of Medicine at NTNU and Central Norway Regional Health Authority.

The NMR center at DTU is acknowledged for the high-resolution ^{1}H-^{13}C HSQC and HMBC Spectrum acquired on their 800 MHz Avance II NMR spectrometer.

Anne B. Frahm was supported by a travel and study grant from the Danish Cancer Society for a visiting stay at NTNU (Grant R235-A14222-19-S44).

Competing interests

The authors declare no competing interests

References

[1] T.W.M. Fan, A.N. Lane, R.M. Higashi, M. A. Farag, H. Gao, M. Bousamra, D. M. Miller, Altered regulation of metabolic pathways in human lung cancer discerned by ^{13}C stable isotope-resolved metabolomics (SIRM), Molecular Cancer 8 (2009) 41-60. DOI:10.1186/1476-4598-8-41

[2] E. A. Maher, I. Marin-Valencia, R. M. bachoo, T. Mashimo, J. Raisanen, K. J. Hatanpaa, A. Jindal, F. M. Jeffrey, C. Choi, C. Madden, D. Mathews, J. M. Pascual, B.E. Mickey, C. R. Malloy, R. J. DeBerardinis, Metabolism of [U-^{13}C]glucose in Human Brain Tumors In Vivo, NMR Biomed. 25, 11 (2012) 1234-1244. DOI: 10.1002/nbm.2794

[3] C. T. Hensley, B. Faubert, Q. Yuan, N. Lev-Cohain, E. Jin, J. Kim, L. Jiang, B. Ko, R. Skelton, L. Loudat, M. Wodzak, C. Klimko, E. McMillan, Y. Butt, M. Ni, D. Oliver, J. Torrealba, C. R. Malloy, K. Kernstine, R. E. Lenkinski, R. J. DeBerardinis, Metabolic Heterogeneity in Human Lung Tumors, Cell 164 (2016) 681-694. DOI: 10.1016/j.cell.2015.12.034

[4] A. L. Holleran, G. Fiskum, J. K. Kelleher, Quantitative analysis of acetoacetate AS-30D hepatoma cells with 13C and metabolism in 14C isotopic techniques, American J. Physiol-endocrinol and Metab., 272, 6 (1997) E945-951. DOI: 10.1152/ajpendo.1997.272.6.E945

[5] S. C. Burgess, T. T. He, Z. Yan, J. Lindner, A. D. Sherry, C. R. Malloy, J. D. Browning, M. A. Magnuson, Cytosolic Phosphoenolpyruvate Carboxykinase Does Not Solely Control the Rate of Hepatic Gluconeogenesis in the Intact Mouse Liver, Cell Metab., 5,4 (2007) 313-320. DOI:10.1016/j.cmet.2007.03.004

[6] S. Heux, C. Bergés, P. Millard, J-C. Portais, F. Létisse, Recent advances in high-throughput ^{13}C-fluxomics, Current Opinion in Biotech., 43 (2017) 104-109. 10.1016/j.copbio.2016.10.010

[7] N. Zamboni, U. Sauer, Model-independent fluxome profiling from ^{2}H and ^{13}C experiments for metabolic variant discrimination, Genome Biology, 5 (2004), R99. DOI: 10.1186/gb-2004-5-12-r99

[8] S. Heux, J. Poinot, S. Massou, S. Sokol, J-C. Portais, A novel platform for automated high-throughput fluxome profiling of metabolic variants, Metabolic Engineering, 25 (2014), 8-19. DOI:10.1016/j.ymben.2014.06.001

[9] A. N. Lane, J. Tan, Y. Wang, J. Yan, R. M. Higashi, T.W.M. Fan, Probing the metabolic phenotype of breast cancer cells by multiple tracer stable isotope resolved metabolomics, Metabolic Engineering, 43 (2017) 125-136. DOI: 10.1016/j.ymben.2017.01.010

[10] P. Giraudeau, NMR-based metabolomics and fluxomics: developments and future prospects, Analyst, 145 (2020) 2457. DOI: 10.1039/D0AN00142B

[11] P. J. Shin, Z. Zhu, R. Camarda, R. A. Bok, A. Y. Zhou, J. Kurhanewicz, A. Goga, D. B. Vigneron, Cancer recurrence monitoring using hyperpolarized [1-^{13}C]pyruvate metabolic imaging in murine breast cancer model, Magnetic Reson. Imaging, 43 (2017) 105-109. DOI:10.1016/j.mri.2017.07.014

[12] S.E. Day, M. I. Kettunen, F. A. Gallagher, E-E. Hu, M. Lerche, J. Wolber, K. Golman, J-H Ardenkjaer-Larsen, K. M. Brindle, Detecting tumor response to treatment using hyperpolarized ^{13}C magnetic resonance imaging and spectroscopy, Nature Medicine, 13,11 (2007). DOI: 10.1038/nm1650

[13] S. J. Nelson, J. Kurhanewicz, D. B. Vigneron, P.E.Z Larson, A. L. Harzstark, M. Ferrone, M. Van Criekinge, J. W. Chang, R. Bok, I. Park, G. Reed, L. Carvaljal, E.J. Small, P. Munster, V. K. Weinberg, J-H. Ardenkjaer-Larsen, A. p. Chen, R. E. Hurd, L-I. Odegardstuen, F.J. Robb, J. Tropp, J.A. Murray, Metabolic Imaging of Patients with Prostate Cancer Using Hyperpolarized [1-^{13}C]Pyruvate, Science Translation Medicine, 5, 198 (2013) 108. DOI: 10.1126/scitranslmed.3006070

[14] J. T. Grist, M. A. McLean, F. Riemer, R.F. Schulte, S.S. Deen, F. Zaccagna, R. Woitek, C.J. Daniels, J:D. Kaggie, T. Matys, I. Patterson, R. Slough, A.B. Gill, A. Chharbra, R. Eichenberger, M-C, Laurent, A. Comment, J.H. Gillard, A.J. Coles, D.J. Tyler, I. Wilkinson, B. Basu, D.J. Lomas, M.J. Graves, K. M. Brindle, F.A. Gallagher, Quantifying normal human brain metabolism using

hyperpolarized [1-^{13}C] pyruvate and magnetic resonance imaging, NeuroImage, 189 (2019) 171-179. DOI: 10.1016/j.neuroimage.2019.01.027

[15] J. Kurhanewicz, D. B. Vigneron, J-H. Ardenkjaer-Larsen, J. A. Bankson, K.M. Brindle, C.H. Cunningham, F.A. Gallagher, K. R. Keshari, A. Kjaer, C. Laustsen, D.A. Mankoff, M.E. Merritt, S.J. Nelson, J.M. Pauly, P.Lee, S. Ronen, D.J. Tyler, S.S. Rajan, D.M.Spielman, L. Wald, X. Zhang, C.r.Malloy, R. Rizi, Hyperpolarized ^{13}C MRI: Path to clinical translation in oncology, Neoplasia, 21,1 (2019) 1-16. DOI: https://doi.org/10.1016/j.neo.2018.09.006

[16] G.A. N. Gowda, D. Raftery, Biomarker Discovery and Translation in Metabolomics, Curr. Metabolomics, 1,3 (2013) 227-240. DOI: 10.2174/2213235X113019990005

[17] K. Bingol, R. Brüschweiler, Multidimensional Approaches to NMR-Based Metabolomics, Anal. Chem, 86 (2014) 47-57. DOI: 10.1021/ac403520j

[18] P. Giraudeau, Challenges and perspectives in quantitative NMR, Magn. Reson. Chem. 55 (2016) 61-69. DOI: 10.1002/mrc.4475

[19] J-N. Dumez, J. Milani, B. Vuichoud, A. Bornet, J. Lalande-Martin, I. Tea, M. Yon, M. Maucourt, C. Deborde, A. Moing, L. Frydman, G. Bodenhausen, S. Jannin, P. Giraudeau, Hyperpolarized NMR of plant and cancer cell extracts at natural abundance, Analyst, 140 (2015) 5860-5863. DOI: 10.1039/C5AN01203A

[20] A. Bornet, M Maucourt, -c. Deborde, D. Jacob, J. Milani, B. Vuichoud, X. Ji, J-N. Dumez, A. Moing, G. Bodenhausen, S. Jannin, P. Giraudeau, Highly Repeatable Dissolution Dynamic Nuclear Polarization for Heteronuclear NMR Metabolomics, Anal. Chem., 88 (2016) 6179-6183. DOI: 10.1021/acs.analchem.6b01094

[21] N. Hemkens, N. Eshuis, B.J.A. van Weerdenburg, M.C. Feiters, F.P.J.T. Rutjes, S. S. Wijmenga, M. Tessari, NMR-Based Chemosensing via p-H_2 Hyperpolarization: Application to Natural Extracts, Anal. Chem, 88 (2016) 3406-3412. DOI: 10.1021/acs.analchem.6b00184

[22] A. Dey, B. Charrier, E. Martineau, C. Deborde, E. Gandriau, A. Moing, D. Jacob, D. Eshchenko, M. Schnell, R. Malzi, D. Kurzbach, M. Ceillier, Q. Chappuis, S. F. Cousin, J. G. Kempf, S. Jannin, J-N. Dumez, P. Giraudeau, Hyperpolarized NMR Metabolomics at Natural ^{13}C Abundance, Anal. Chem., 92 (2020) 14867-14871. DOI:10.1021/acs.analchem.0c03510.

[23] M. H. Lerche, D. Yigit, A. B. Frahm, J-H Ardenkjær-Larsen, R. M. Malinowski, P. R. Jensen, Stable Isotope-Resolved Analysis with Quantitative Dissolution Dynamic Nuclear Polarization, Anal. Chem., 90 (2018) 674-678. DOI: 10.1021/acs.analchem.7b02779

[24] A. B. Frahm, P. R. Jensen, J-H. Ardenkjær-Larsen, D. Yigit, M. H. Lerche, Stable Isotope Resolved Metabolomics Classification of Prostate Cancer Cells using Hyperpolarized NMR Data, JMR, 316 (2020) 106750. DOI: 10.1016/j.jmr.2020.106750

[25] Clinicaltrials.gov

[26] H-Y. Chen, R. Aggarwal, R.A. Bok, M.A. Ohliger, Z.Zhu, P. Lee, J. W. Gordon, M. Van Criekinge, L. Carvajal, J.B. Slater, P.E.Z. Larson, E. J. Small, J. Kurhanewicz, D.B.Vigneron, Hyperpolarized ^{13}C-pyruvate MRI detects real-time metabolic flux in prostate cancer metastases to bone and liver: a clinical feasibility study, Prostate Cancer and prostatic Diseases, 23 (2020) 269-276. DOI: 10.1038/s41391-019-0180-z

[27] N. M. Greensberg, F. Demayo, M.J. Finegold, D. Medina, W.D. Tilley, J. O. Aspinalls, G.R. Cunha, A.A. Donjacour, R.J. Matusik, J. M. Rosen, Prostate cancer in a transgenic mouse, PNAS, 92 (1995) 3439-3443. DOI: 10.1073/pnas.92.8.3439

[28] J.R. Gingrich, R.J. Barrios, B.A. Foster, N.M. Greenberg, Pathologic progression of autochthonous prostate cancer in the TRAMP model, Prostate Cancer and Prostatic Diseases, 2 (1999) 70-75. DOI: 10.1038/sj.pcan.4500296

[29] A. A. Hurwitz, B. A. Foster, J.P. Allison, N. M. Greenberg, E. D. Kwon, Curr. The TRAMP Mouse as a Model for Prostate Cancer, Protocols in Immun., 20,5 (2001) 1-23. DOI: 10.1002/0471142735.im2005s45

[30] M. J. Albers, R. Bok, A. P. Chen, C. H. Cunninghamm M. L. Zierhus, V. Y. Zhang, S. J. Kohler, J. Tropp, R. E. Hurd, Y-F. Yen, S. J. Nelson, D. B. Vigneron, J. Kurhanewicz, Hyperpolarized ^{13}C Lactate, Pyruvate, and Alanine: Noninvasive Biomarkers for Prostate Cancer Detection and Grading, Cancer Res., 68, 20 (2008). DOI: 10.1158/0008-5472.CAN-08-0749

[31] R. Bok, J. Lee, R. Sriram, K. Keshari, S. Sukumar, S. Daneshmandi, D. E. Korenchan, R. R. Flavell, D. B. Vigneron, J. Kurhanewicz, The Role of Lactate Metabolism in Prostate Cancer Progression and Metastases Revealed by Dual-Agent Hyperpolarized ^{13}C MRSI, Cancers, 11 (2019) 257. DOI: 10.3390/cancers11020257

[32] D. K. Hill, E. Kim, J. R. Teruel, Y. Jamin, M. Widerøe, C D. Søgaard, Ø. Størkersen, D. N. Rodrigues, A. Heindl, Y. Yuan, T. F. Bathen, S. A. Moestue, Diffusion-Weighted MRI for Early Detection and Characterization of Prostate Cancer in the Transgenic Adenocarcinoma of the Mouse Prostate Model, J. magn. Reson. Imaging, 43 (2016) 1207-1217. DOI: 10.1002/jmri.25087

[33] S-M. T. Fagerland, D. K. Hill, A. v-Wamel, C. d-L. Davies, J. Kim, Ultrasound and magnetic resonance imaging for group stratification and treatment monitoring in the transgenic adenocarcinoma of the mouse prostate model, The Prostate, 80 (2020) 186-197. DOI: 10.1002/pros.23930

[34] T. Chiaverotti, S. S. Couto, A. Donjacour, J-H. Mao, H. Nagase, R. D. Cardiff, G. R. Cunha, A. Balmain, Dissociation of Epithelial and Neuroendocrine Carcinoma Lineages in the Transgenic Adenocarcinoma of Mouse Prostate Model of Prostate Cancer, Am J Pathol, 172 (2008) 236–246. DOI: 10.2353/ajpath.2008.070602

[35] Bergmeyer HU., editor. 1983. Methods of enzymatic analysis. Weinheim: Verlag Chemie.

[36] S. Katsikis, I. Marin-Montesinos, M. Pons, C. Ludwig, U. L. Günther, Improved Stability and Spectral Quality in Ex Situ Dissolution DNP Using an Improved Transfer Device, Applied Magnetic Reson., 46 (2015) 723-729. DOI: 10.1007/s00723-015-0680-5

[37] MNova version 11.0; MestreLab Research.

[38] MATLAB. (2019). version 9.6.0 (R2010a). Natick, Massachusetts: The MathWorks Inc.

[39] F. Savorani, G. Tomasi, S.B. Engelsen, Icoshift: a versatile tool for the rapid alignment of 1D NMR spectra, J. Magn. Reson, 202 (2010) 190-202. DOI: 10.1016/j.jmr.2009.11.012

[40] D.S. Wishart, Y.D. Feunang, A. Marcu, A.C. Guo, K. Liang, et al., The human metabolome database for 2018, Nucl. Acids Res. 46 (D1) (2018) D608–D617. DOI: 10.1093/nar/gkx1089

[41] Python Software Foundation. Python Language Reference, version 3. Available at http://www.python.org.

[42] Pedregosa, F., Varoquaux, G., Gramfort, A., Michel, V., Thirion, B., Grisel, O., … Duchesnay, E. (2011). Scikit-learn: Machine Learning in {P}ython. Journal of Machine Learning Research, 12, 2825–2830.

[43] Jones, E., Oliphant, T., Peterson, P., & others. (n.d.). {SciPy}: Open-source scientific tools for {Python}. Retrieved from http://www.scipy.org/.

[44] S. Meier, M. Karlsson, P. R. Jensen, M. H. Lerche, J. Ø. Duus, Metabolic pathway visualization in living yeast by DNP-NMR, Mol. BioSyst., 7 (2011) 2834–2836. DOI:10.1039/c1mb05202k

[45] S.P. Wang, D. Zhou, Z. Yao, S. Satapati, Y. Chen, N. A. Daurio, A. Petrov, X. Shen, D. Metz,…, D. E. Kelley, Quantifying rates of glucose production in vivo following an intraperitoneal tracer bolus, Am J Physiol Endocrinol Metab, 311 (2016) E911–E921. DOI: 10.1152/ajpendo.00182.2016

[46] A. Lane, J. Yan, T. W-M. Fan, ^{13}C Tracer Studies of Metabolism in Mouse Tumor Xenografts, Bio Protoc. 5 (2015) 22. DOI: 10.21769/bioprotoc.1650

[47] C. X. Hsu, B. D. Ross, C. E. Chrisp, S. Z. Derrow, L. G. Charlse, K. J. Pienta, N. M. Greenberg, Z. Zeng, M. G. Sanda, Longitudinal cohort analysis of lethal prostate cancer progression in transgenic mice, J. Urology,160 (1998) 1500-1505. DOI: 10.1016/S0022-5347(01)62603-X

[48] S. Bowen, C. Hilty, Phys. Rapid sample injection for hyperpolarized NMR spectroscopy, Chem. Chem. Phys., 12 (2010) 5766-5770. DOI: 10.1039/C002316G

[49] V. Gialleonardo, S. S. Tee, H. N. Aldeborgh, V. Z. Miloushev, L. S. Cunha, G. D. Sukenick, K. R. Keshari, High-Throughput Indirect Quantitation of ^{13}C Enriched Metabolites Using ^{1}H NMR, Anal. Chem., 88 (2016) 11147-11153. DOI: 10.1021/acs.analchem.6b03307

[50] N. Krause, A. Wegner, Fructose Metabolism in Cancer, Cells, 9 (2020) 2635. DOI: 10.3390/cells9122635

[51] A. Godoy, V. Ulloa, F. Rodriguez, K. Reinicke, A. J. Yanez, M. Garcia, R. A. Medina, M. Carrasco, S. Barberis,…, R. Nualart, Differential Subcellular Distribution of Glucose Transporters GLUT1–6 and GLUT9 in Human Cancer: Ultrastructural Localization of GLUT1 and GLUT5 in Breast Tumor Tissues, J. cell. Phys., 207 (2006) 614-627. DOI:10.1002/jcp.20606.

[52] A. Andres-Hernando, R. J. Johnson, M. A. Lanaspa, Endogenous fructose production: what do we know and how relevant is it?, Curr. OPin, Clin. Nutr. Metab. Care., 22,4 (2019) 289-294. DOI:10.1097/MCO.0000000000000573

[53] K. Reinicke, P. Sotomayor, P. Cisterna, C. Delgado, F. Nualart, A. Godoy, Cellular distribution of Glut-1 and Glut-5 in benign and malignant human prostate tissue, J. cell. Biochem., 113 (2012) 553-562. DOI: 10.1002/jcb.23379

[54] K. R. Keshari, D. M. Wilson, A. P. Chen, R. Bok, P. E. Z. Larson, S. Hu, M. V. Criekinge, J. M. Macdonald, D. B. Vigneron, J. Kurhanewicz, Hyperpolarized [2-^{13}C]-Fructose: A Hemiketal DNP Substrate for In Vivo Metabolic Imaging, JACS, 131 (2009) 17591-17596. DOI: 10.1021/ja9049355

Classification and biomarker identification of prostate tissue from TRAMP mice with hyperpolarized ^{13}C-SIRA

Anne B. Frahm[a], Deborah Hill[b], Sotirios Katsikis[a], Trygve Andreassen[b], Jan Henrik Ardenkjær-Larsen[a], Tone Frost Bathen[b], Siver Andreas Moestue[b,c], Pernille Rose Jensen[a], Mathilde Hauge Lerche[a,*]

a: Center for Hyperpolarization in Magnetic Resonance, Department of Health Technology, Ørsteds plads 349, 2800 Kongens Lyngby, Denmark.

b: Department of Circulation and Medical Imaging, Norwegian University of Science and Technology, Trondheim, Norway

c: Department of Pharmacy, Nord University, Bodø, Norway

*Corresponding author. E-mail: mhauler@dtu.dk

Table of contents

1. Pilot study

Two small pilot studies were performed to evaluate 1) if an intraperitoneal injection could efficiently distribute [U-^{13}C]glucose and 2) the needed distribution time for a reliable measurement of isotopical labelled metabolites.

Pilot 1

Two mice were injected with ^{13}C labelled glucose (with 150 mg/ml) one in the tail vein and one Intraperitoneal (in the abdominal cavity). The mice were kept under anesthesia and terminated after 15 minutes (i.v.) or 30 minutes (i.p.). Four types of tissue (prostate, brain, liver, kidney) was immediately harvested and placed in vials labelled with their empty weight and immediately frozen in liquid nitrogen and stored at -80 °C. The weight of tissue filled vials was measured and tissue weight was found by subtraction. Metabolites were extracted and freeze dried according to the protocol described in the main article. ^{1}H-^{13}C-HSQC and ^{1}H NMR spectra were acquired on all samples. Afterwards the samples were freeze dried and prepared for and measured with hyperpolarized 1D-^{13}C-NMR.

Administration of 150 mg/ml [U-^{13}C]glucose either intravenously (i.v.) or intraperitoneal (i.p.) into the abdominal cavity resulted in comparable amounts of isotopic labelling in prostate tissue of high concentration metabolites (lactate, alanine and glutamate), Figure S1.

A) B)

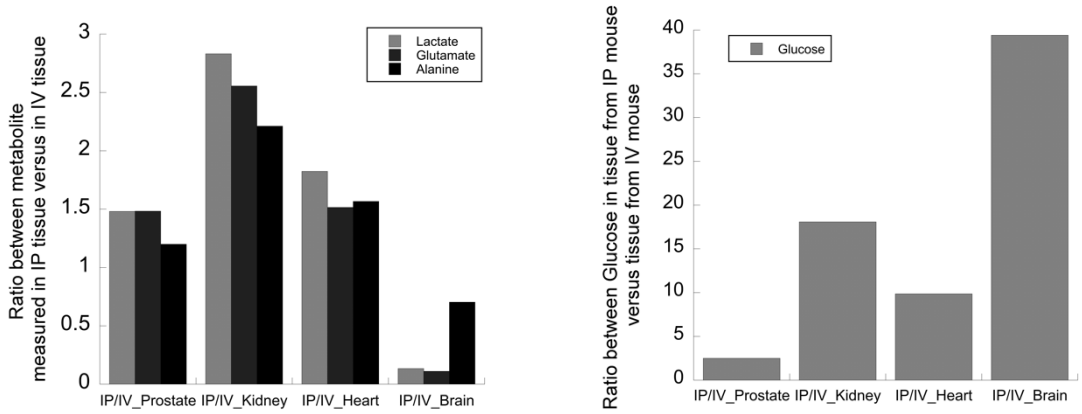

Figure S1. Amounts of metabolites in tissue from i.p. injected mice relative to i.v. injected mice. All data are extracted from ^{1}H-^{13}C-HSQC spectra collected for samples from the different tissue types and have been corrected for amount of tissue. A) Relative amounts of three ^{13}C-labelled metabolites (lactate, glutamate and alanine) in all analysed tissue types. B) Relative amounts of substrate (^{13}C-labelled glucose) in all analysed tissue types. All values, except for brain tissue are higher than 1 showing that i.p. injection is more effective (in the given concentration and time) than i.v. injection for most tissue types.

Availability of [U-^{13}C]glucose in the different tissue types was higher when injected i.p. but was generally low in prostate tissue, Figure S2.

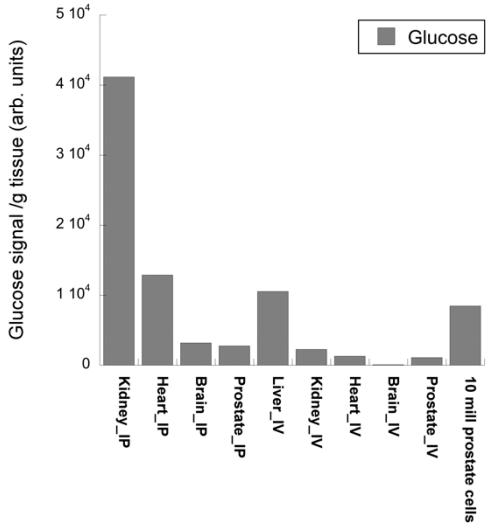

Figure S2. Glucose signal measured in the different types of tissue from the two mice injected with [U-^{13}C]glucose (i.p., 1666 µmol for 30 min or IV, 166 µmol for 15 min) compared to the glucose signal measured in an experiment using 10 mill prostate cancer cells in culture (120 µmol for 30

min). The latter were conditions used in a previously published study [1]. The available glucose in prostate tissue is relatively low.

Unless the low glucose signal in prostate tissue was due to low uptake in the prostate, we could expect to increase it by prolonging the waiting time between administration and sacrifice or by administrating a higher glucose concentration. These parameters were tested in a second pilot study.

Pilot 2
We tested different waiting times (15, 30 or 45 min) between i.p. administered [U-^{13}C]glucose and animal sacrifice for tissue excision. The isotopic labelling into high concentration metabolites increased from 15 to 30 minutes but was similar between 30 and 45 minutes.

Lastly, we investigated whether it was feasible first to collect thermal NMR data on tissue extracts and afterwards freeze dry the samples and reformulate them for dDNP NMR. Effects of re-formulation for dDNP NMR of samples which had been analysed with thermal NMR was assessed by comparing relative amounts of isotopic labelling in high concentration metabolites (lactate and glutamate) measured in three different excised tissue types from i.v. and i.p. administered U-^{13}C-glucose, respectively, Figure S3A. and by ratios between i.v. and i.p. administered U-^{13}C-glucose recovered as isotopic labelled lactate in four tissue types, Figure S3B.

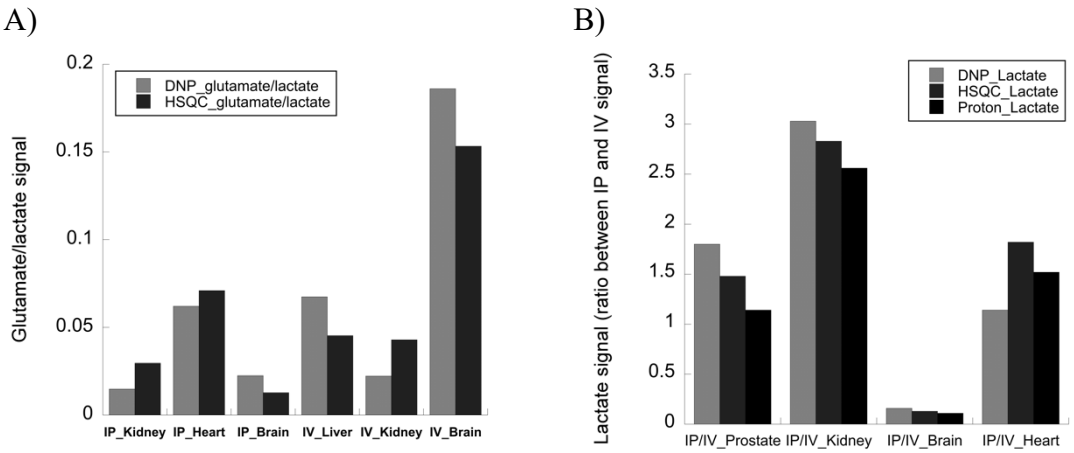

Figure S3. Measurement of isotopic labelling with thermal NMR and dDNP NMR of the same samples. A) Glutamate versus lactate signal measured by 1D-^{13}C dDNP NMR and ^{1}H-^{13}C-HSQC, respectively. B) Lactate signal given as the ratio between the i.p. and i.v. signal, measured by dDNP NMR, ^{1}H-^{13}C-HSQC and ^{1}H NMR. Differences between measured isotopic labelling with thermal NMR methods and dDNP NMR suggest that no notable effect could be detected of the re-formulation (average and standard error between samples measured with dDNP NMR 0.065±0.024 and those measured with ^{1}H-^{13}C-HSQC 0.061±0.022 were similar. There is no indication that the extra sample handling step included before the DNP analysis impact this analysis negatively.

To prolong T_1 usually deuterated glucose is applied in dDNP NMR studies [2] (T_1 increase from 0.6-1.2 s in protonated U-^{13}C-glucose to 10-14s in deuterated U-^{13}C-glucose at 37 °C and 9.4 T) however in order to be able to perform thermal NMR on the same samples protonated U-^{13}C-glucose was used as substrate. This choice affected the substrate signal in the dDNP NMR spectra (which was low for all samples), however the non-protonated carbons of the measured metabolites in the dDNP NMR spectra were detected in comparable amounts to the ^{1}H-^{13}C-HSQC and the ^{13}C-satelites in the proton spectrum.

2. Tissue sample collection and characterization

All samples were treated as belonging to one cohort based on no apparent correlations to mouse age nor sample weight, Figure S4.

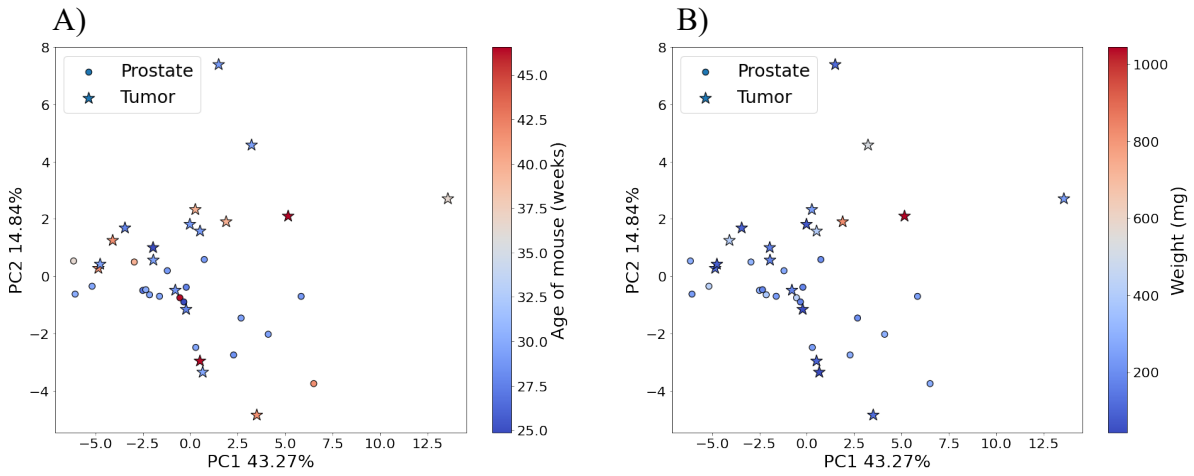

Figure S4. Sample correlation with mouse age (A) and tissue weight (B).

3. Analytical performance of hyperpolarized ^{13}C-SIRA of tissue extracts

Sample transfer system design

A custom-made sample transfer device was designed to work as an add-on to the Hypersense polarizer based on published principles [3]. The designed sample transfer system is sketched in Figure S5.

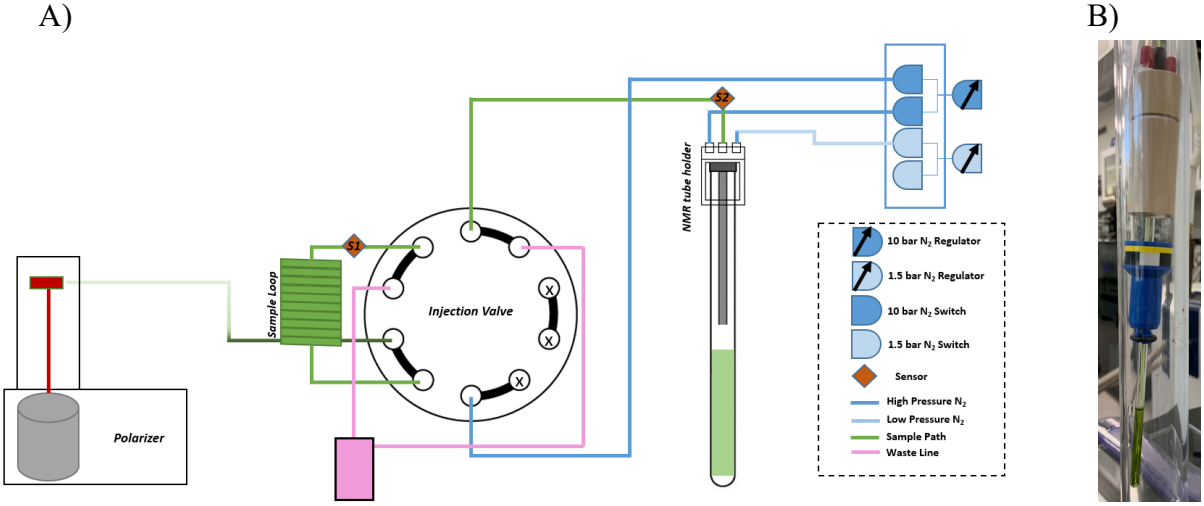

Figure S5. Automated Sample Transfer System A) Sample transfer system set-up. This custom-made device was designed to work as an add-on to a Hypersense polarizer type. The maximum driving and stabilization pressure was set to 10 bar, which made the system compatible with a conventional "thin wall" 5mm NMR tube and water injection. The main principle of operation is to collect the dissolved sample in a loop attached to an injection valve set to the load position, sense the presence

of the liquid using an optical sensor (sensor 1) and subsequently inject the "front" part of the loop in the NMR tube by switching the valve to injection position. The transfer is stopped by engaging the stabilization pressure after a preset injection delay following detection by sensor 2. B) Zoom on actual sample tube filled with sample.

Sequence of Events using the Automated Transfer System – The user sets up the system by assembling the NMR tube holder and initializing the transfer system. Initialization means that the NMR tube is pre-pressurized with 1 bar, the injection valve is in the LOAD position and the transfer system waits for the sensor 1 signal. Subsequently, the dissolution procedure on the polarizer is initiated. As the dissolved liquid exits the polarizer, it is collected in the sample loop and its presence is sensed by sensor 1, which triggers the switching of the injection valve from LOAD to INJECTION position. The content of the sample loop is then driven by a 10-bar pressure through the transfer line to the injector. Sensor 2, placed at the end of the transfer line, senses the position of the liquid and engages the stabilization pressure after a preset injection delay (305 ms for 50 mg of polarized sample, a loop size of 3.25 ml and a transfer line of approximately 4 m). For this study, the average travel time between the two sensors was found to be ca. 800 ms.

Sample transfer system performance and protocol adjustment

Metabolite relaxation was minimized by the faster transfer and a three times higher sample concentration was obtained with the automated sample transfer compared to a manual transfer. This translated into a total increase in carbonyl carbon signals of an approx. factor of 8, Figure S6. A side effect of concentrating the sample using the same solid state sample preparation protocol is the threefold increase of the radical concentration, which could increase paramagnetic relaxation. We therefore reformulated the solid-state extract sample and managed to reduce the amount of paramagnetics by a corresponding factor of three. Additionally, the glass former, glycerol, which was included in the sample formulation for optimal DNP, gave ringing artifacts in the NMR spectrum upon proton decoupling. We exchanged glycerol with deuterated glycerol to circumvent this problem and allowed proton decoupling during acquisition.

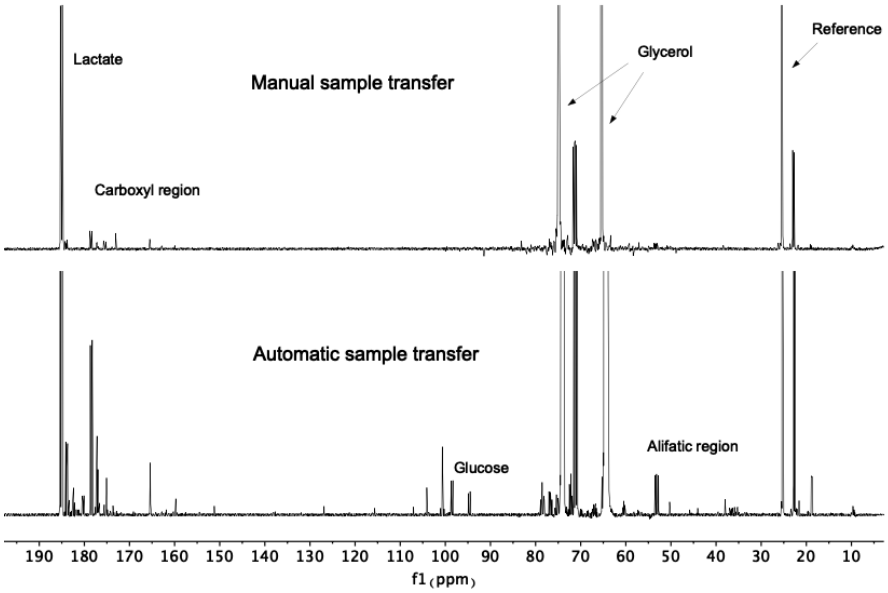

Figure S6. Comparison between 1D ^{13}C dDNP NMR spectrum of metabolite extracts from prostate tissue after a manual (A) and automatic transfer (B).

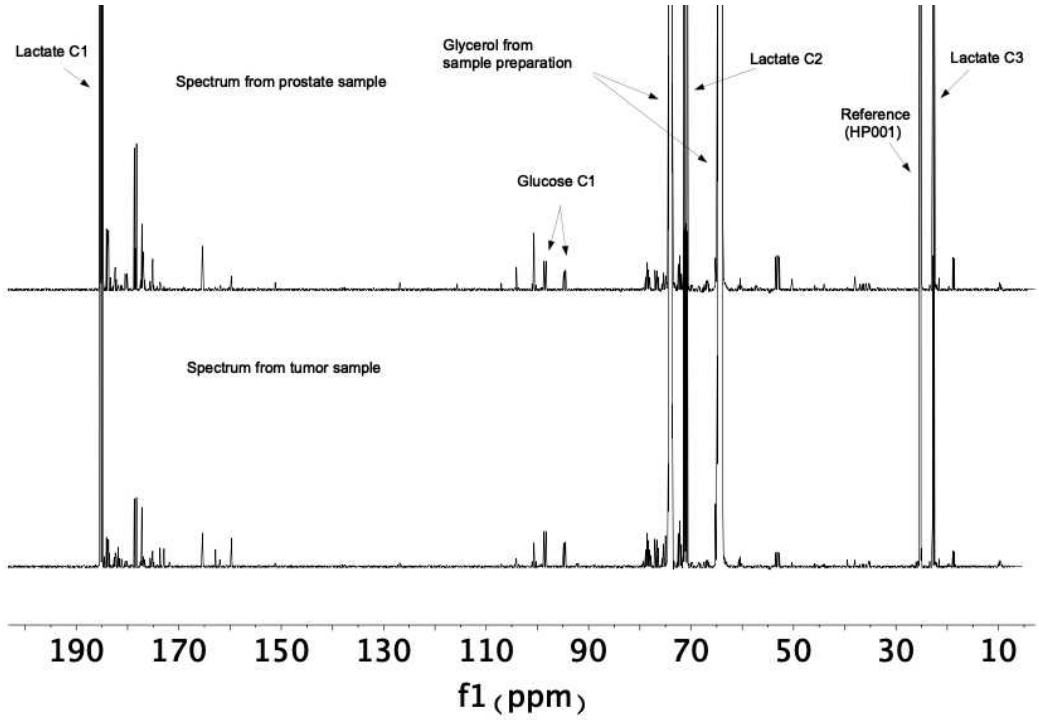

Figure S7. A full spectrum for each of the tissue classes. The spectra are sparse, with little overlap in signals. The largest signals, positioned as a triplet at 74 ppm and a quintet at 64.3 ppm, are from the deuterated glycerol, added to the samples to form the polarization matrix. The largest metabolite peaks are, by far, the ones produced by lactate, where all three signals are easily visible and identifiable.

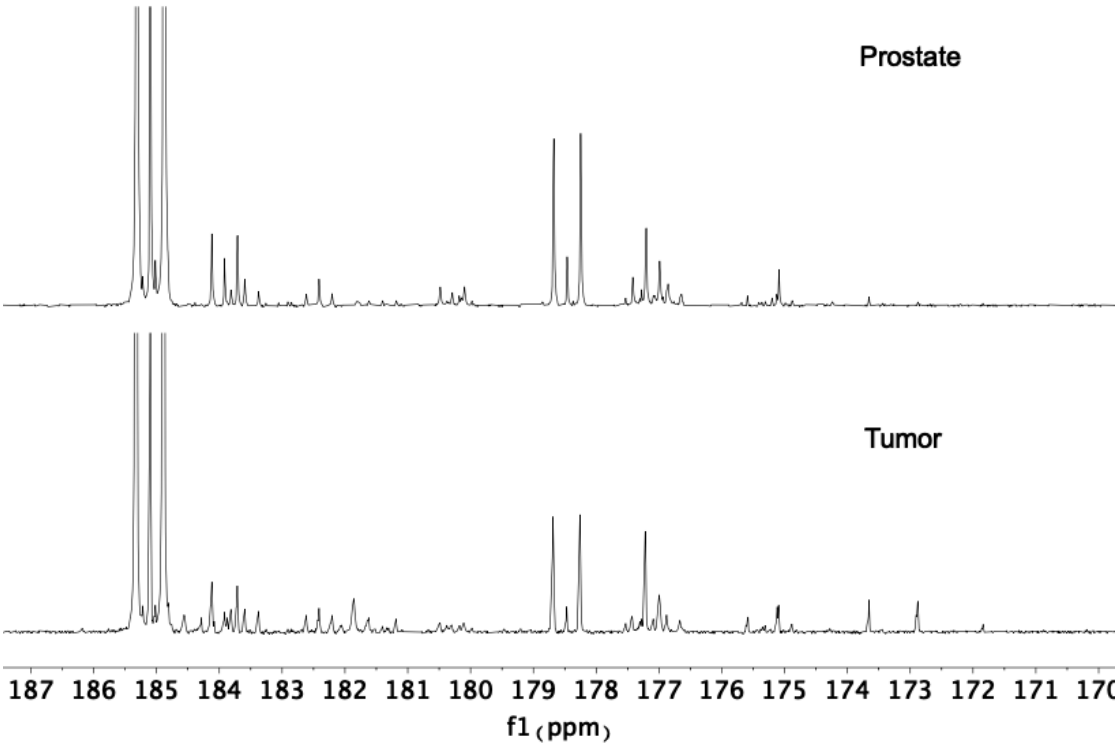

Figure S8. zoom in on carbonyl region for each of the tissue types.

4. Analysis and classification with proton NMR

A Principal Component Analysis (PCA) was used to investigate the separation between tumor and prostate samples. The plot of the two first components of the PCA on Pareto scaled NOESY data is shown in Figure S9A. It can be seen that, apart from two tumor samples, there is a separation between a loose cluster of tumor samples and a somewhat closer cluster of prostate samples. Still, the distance between the clusters is much smaller than the distance between points inside the clusters.

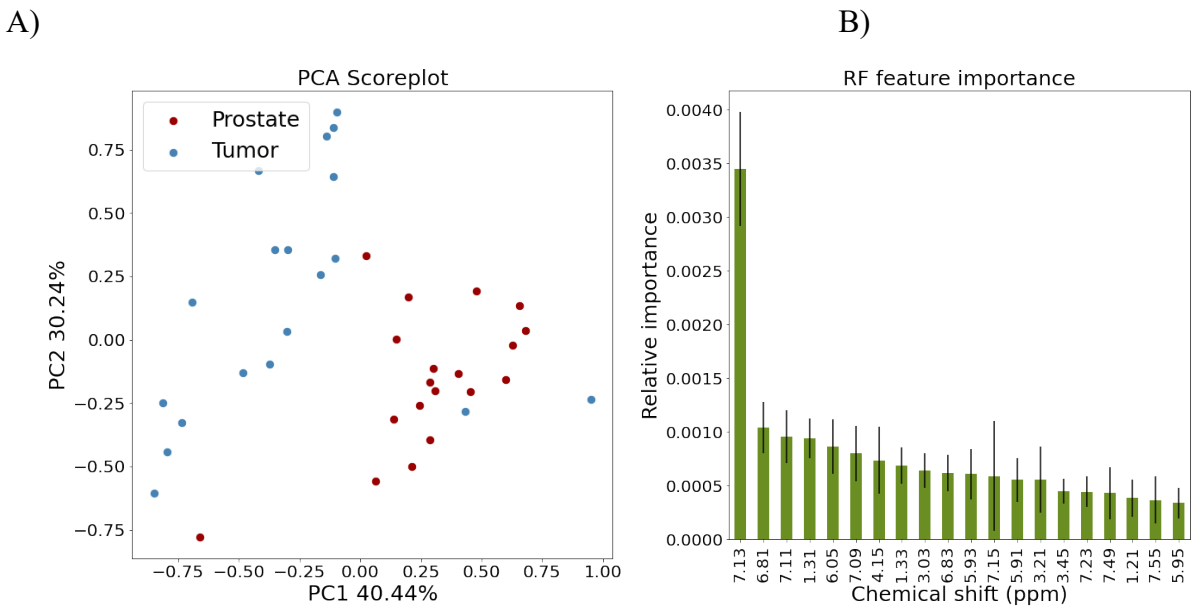

Figure S9. Results from analysis of the NOESY data. A) PCA plot, with 40.44 % of the variance in the data in the first component and 30.24 % in the second. B) Relative feature importance calculated with RF, for 20 features with positive mean importance. Black bars indicate Standard Error on the Mean (SEM).

Random Forest was applied as described for the dDNP data, except with 500 trees in each forest and repeated 3.000 times over.

The results of a feature ranking performed using Random Forest (RF) on un-scaled NOESY data is shown in figure S9B. The importance score is in arbitrary units, and a positive score for a feature indicates that the RF algorithm performs worse if the values for that feature are shuffled; thus, indicating that the feature is important for the separation between prostate and tumor samples. In the NOESY data, 20 features were found to have a significant, positive importance. The SVM algorithm was run on the data, using only a subset of the features of the full data: First with only the highest ranked feature found with RF, then the two highest rank data and so on. In this way we find that the best classification, with 100% correct, leave-one-out cross-validated, classification of prostate vs. tumor samples is made by using the top 3 features from RF: 7.13, 6.81 and 7.11 ppm.

5. Metabolite based analysis of hyperpolarized ^{13}C-SIRA spectra

We chose to combine tumors found in the prostate and in the seminal vesicles into one group - tumors. This was due to the number of available tumors and also due to uncertainty in characterization of the tumor origin in two mice. However, when making a separation based on identified molecular ^{13}C-tracer related metabolites it looked as though it could be possible to separate the tumors into more groups had we had more samples, Figure S10.

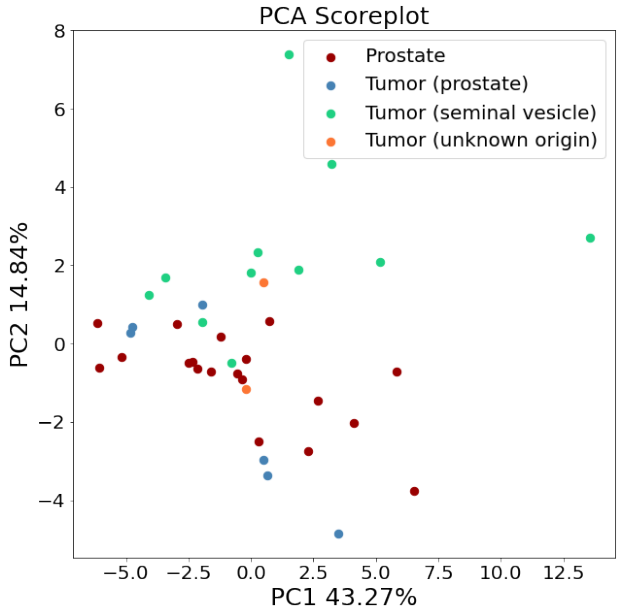

Figure S10. Metabolite analysis of hyperpolarized 1D-^{13}C-NMR spectra. Score plot of PCA analysis. Data was mean centered and unit variance scaled before PCA was applied. The PC1 x PC2 plan accounted for 58.1% of total variation among data points. Samples are colored according to tissue characterization. Red: Prostate tissue, blue: tumor tissue from tumors found in the prostate, green: tumor tissue from tumors found in the seminal vesicles and orange: tumors for which it was not possible to determine from where it originated.

6. Biomarker identification

A box-plot analysis of the 12 highest ranked metabolite isotopomers used to obtain a 95% discrimination of tumor and prostate tissue is shown in Figure S11.

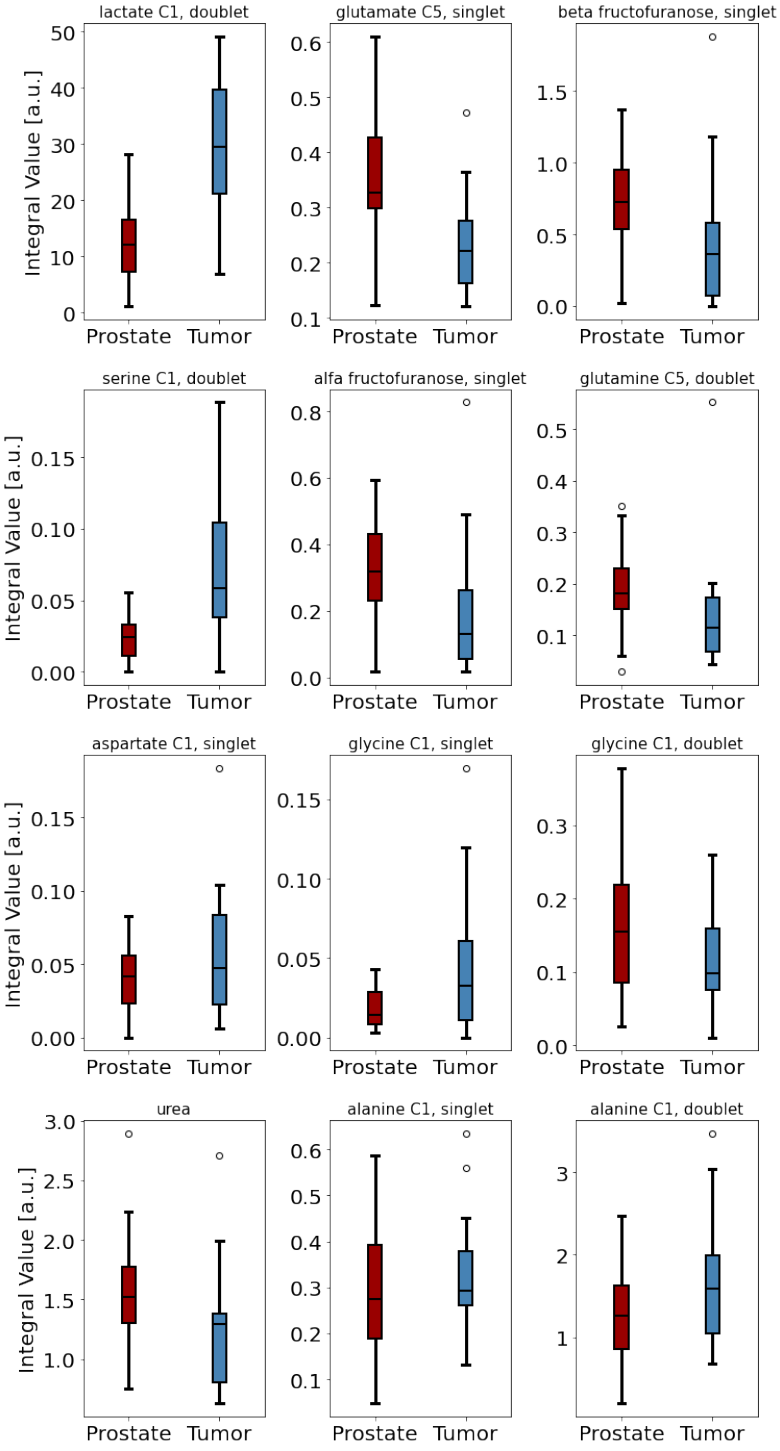

Figure S11. Box plot of 12 highest ranked features in RF analysis of metabolite dataset.

References:

[1] A. B. Frahm, P. R. Jensen, J-H. Ardenkjær-Larsen, D. Yigit, M. H. Lerche, JMR, 316 (2020) 106750.

[2] S. Meier, M. Karlsson, P. R. Jensen, M. H. Lerche, J. Ø. Duus, Mol. BioSyst., 7 (2011) 2834–2836.

[3] S. Katsikis, I. Marin-Montesinos, M. Pons, C. Ludwig, U. L. Günther, Applied Magnetic Reson., 46 (2015) 723-729.